Ana Filipa Patrício Amendoeira

Licenciada em Bioquímica

Steroid-BODIPY theranostics: Receptor-mediated cell uptake and applications in cancer Diagnostics and therapy

Dissertação para obtenção do Grau de Mestre em Bioquímica para a Saúde

Orientador: Maria Alexandra Núncio de Carvalho Ramos Fernandes, Professora Doutora, FCT/UNL

Co-orientador: Fernanda Marujo Marques, Doutora, CTN/IST

Março, 2020

Ana Filipa Patrício Amendoeira

Licenciada em Bioquímica

Steroid-BODIPY theranostics: Receptor-mediated cell uptake and applications in cancer Diagnostics and therapy

Dissertação para obtenção do Grau de Mestre em Bioquímica para a Saúde

Orientador: Maria Alexandra Núncio de Carvalho Ramos Fernandes, Professora Doutora, FCT/UNL

Co-orientador: Fernanda Marujo Marques, Doutora, CTN/IST

Júri:

Presidente: Professora Doutora Maria Teresa Nunes Mangas Catarino

Arguente: Doutora Maria Cristina das Neves Oliveira

Vogal: Professora Doutora Maria Alexandra Núncio de Carvalho Ramos Fernandes

Faculdade de Ciências e Tecnologia, Universidade Nova de Lisboa

Março, 2020

Steroid-BODIPY theranostics: Receptor-mediated cell uptake and applications in cancer Diagnostics and therapy

Acknolowdgements

Firstly, I would like to specially thank to my supervisor Professor Alexandra Fernandes which was a patient mentor, contributing to my development in the world of science and helping me whenever possible. To Professor Pedro Baptista which always contributes with his ideas and calmed his students. Both have given me the opportunity to develop as a scientist and as human being. Thank you both for all your support and opportunities. To Dr. Fernanda Marques, my co-supervisor, for all support and availability. I would also like to thank my professor Teresa Catarino for her patience and support during these years of master degree.

All members of 319 and 315 laboratories, specially to my master student colleagues Inês Pombo, Diogo Sequeira and Beatriz Oliveira, and Daniela Ferreira. Without them it would have been impossible to do this work. Thank you for your help, inspiration and motivation.

My friends, for always being there, for the support, advices and motivation that gave me. They are too many and those who are special know it. However, there is a small group of special friends who have supported me recently in difficulty times. They know who that and they will always be in my heart.

To my parents, for trusting me and understanding for the missing moments. To my sister for your patience and for listening to my good and bad emotions. To my little nieces for giving me such joy.

Thank you all!

Ana Filipa Amendoeira
(Pipa)

Resumo

O cancro continua a ser uma das principais causas de morte a nível mundial, apesar da investigação intensiva dos mecanismos da patologia e o desenvolvimento de novas abordagens terapêuticas. Por conseguinte, é urgente incrementar o desenvolvimento de novas plataformas de diagnóstico e tratamento, que sejam mais seletivas, poupando as células saudáveis, e que suplantem a resistência das células cancerígenas. Reporta este a um estudo de derivados de estradiol – testosterona -, e de nortestosterona conjugados ao corante BODIPY como potenciais agentes de teranóstico multimodal (tomografia por emissão de positrões (PET) / fluorescência e terapia fotodinâmica (PDT).

Foram realizados ensaios de captação celular em células relevantes do cancro da mama e da próstata, assim como em fibroblastos normais, utilizando microscopia de fluorescência de forma a avaliar as respetivas vias de tráfego celular. Os resultados mostraram uma internalização inespecífica dos conjugados em ambas as células normais e cancerígenas, sugerindo uma captação celular dependente de energia, através de endocitose mediada por cavéolas. Co-culturas 2D indicaram ainda que os conjugados são mais específicos para as células cancerígenas.

Os ensaios de viabilidade celular mostraram que os conjugados BODIPY não são tóxicos para ambas as células normais e cancerígenas. Em contraste, e em consequência da irradiação de luz visível, foi observado um efeito intenso de morte celular. Os resultados demonstraram que os conjugados de esteroides-BODIPY (EE2-C8 e HA-4198) são potenciais fotossensibilizadores para PDT contra as células do cancro da mama e da próstata. Será necessária investigação adicional para auferir mais pistas sobre o mecanismo de ação induzido por estas plataformas após a PDT.

Palavras-Chave: Cancro, Conjugados esteroides-BODIPY, Captação celular, Terapia Fotodinâmica

Abstract

Cancer is still one of the leading cause of death worldwide despite the intensive investigation of the disease mechanisms and the development of new therapeutic approaches. Therefore, it is urgent to develop novel diagnostic and treatment platforms more selective and sparing healthy cells and overcoming resistance of cancer cells. Here, we report the study of estradiol-, testosterone- and nortestosterone derivates conjugated to BODIPY dye as a potential multi-modality theranostic agents (positron emission tomography (PET)/ fluorescence and photodynamic therapy (PDT)).

Cellular uptake assays were performed in relevant breast and prostate cancer cells, as well as in normal fibroblasts, using fluorescence microscopy, in order to evaluate the trafficking pathways. Results showed a non-specific internalization of conjugates in cancer and normal cells, suggesting an energy-dependent cellular uptake through caveolae-mediated endocytosis. 2D co-cultures demonstrated that the conjugates are more specific for cancer cells.

Cell viability assays showed that BODIPY conjugates are non-toxic for cancer and normal cells. In contrast, upon visible light irradiation a severe cell death effect was observed. Results demonstrated that EE2-C8 and HA-4198 steroid-BODIPY conjugates are potential photosensitizers for PDT against breast and prostate cancer cells. Future work are needed to gain more clues into the mechanism of action induced by these platforms after PDT.

Keywords: Cancer; steroid-BODIPY conjugates, cellular uptake, Photodynamic Therapy

Table of contents

Figure Index

Table Index

Acronyms and List of Abbreviations

AF1	Transactivation function 1 domain
AF2	Transactivation function 2 domain
AR	Androgen Receptor
ATCC	American Type Culture Collection
ATP	Adenosine triphosphate
BODIPY	4,4-difluoro-4-bora-3a,4a-diaza-s-indacene
BRCA1	Breast cancer 1 susceptibility gene
BRCA2	Breast cancer 2 susceptibility gene
BSA	Bovine Serum Albumin
CAV1	Caveolin-1
CCP	Clathrin coated pits
CCV	Clathrin coated vesicles
CIE	Clathrin-independent endocytosis
CME	Clathrin-mediated endocytosis
CTCF	Corrected Total Cell Fluorescence
DHEA	dehydroepiandrosterone
DHEAS	Dehydroepiandrosterone sulfate
DHT	dihydrotestosterone
DMEM	Dulbecco's Modified Eagle Medium
DMEM/F-12	Dulbecco's Modified Eagle Medium/ Nutrient Mixture F-12)
DMSO	Dimethyl sulfoxide
DNA	Deoxyribonucleic acid
DTT	1,4-Dithiothreitol
E2	Estradiol
ECL	Enhanced chemiluminescence
EDTA	Ethylenediamine tetraacetic acid
EE2	Ethynylestradiol
EIPA	5-(N-ethyl-N-isopropyl)-Amiloride
ER	Estrogen Receptor
ESR1	Estrogen Receptor 1 gene
ESR2	Estrogen Receptor 2 gene
FBS	Fetal bovine serum
FITC	Fluorescein isothiocyanate
HER2R	Human Epidermal Growth Factor Receptor 2

Hoechst	Phenol,4-[5-(4-methyl-1-piperazinyl)[2,5'-bi-1H-benzimidazol]-2'-yl]-trihydrochloride
HPR	Horseradish peroxidase
LAMP-2	Lysosome-associated membrane glycoprotein 2
LAMP2A	Lysosome-associated membrane glycoprotein 2 A
LDI	Laser diode intensity
LNCaP	Human metastatic prostate carcinoma cell line
MCF-7	Human metastatic breast adenocarcinoma cell line
MDA-MB-231	Human metastatic breast adenocarcinoma cell line
MEM	Non-essential amino acid
MTS	3-(4,5-dimethylthiazol-2- yl)-5-(3 carboxymethoxyphenyl)-2-(4-sulfophenyl)-2H-tetrazolium
NADH	Nicotinamide adenine dinucleotide
NADPH	Nicotinamide adenine dinucleotide phosphate
PBS	Phosphate Buffered Saline
PC-3	Human metastatic prostate adenocarcinoma cell line
PCR	Polymerase Chain Reaction
PDT	Phorodynamic therapy
Pen/Strep	Penicillin/Streptomycin
PET	Positron emission tomography
PMS	Phenylmethylsulfonyl fluoride
PR	Progesterone receptor
PS	Photosensitizer
PVDF	Polyvinylidene fluoride
ROS	Reactive Oxygen species
RPMI	Roswell Park Memorial Institute medium
RT	Room Temperature
SDS	Sodium dodecyl sulfate
SDS-PAGE	Sodium dodecyl sulfate Polyacrylamide gel electrophoresis
SPECT	single photon emission computed tomography
T	Testosterone
TBST	Tris Buffered Saline with Tween
TNBC	Triple Negative Breast Cancer

TRICT	Tetramethylrhodamine
UV	Ultraviolet
WHO	World Health Organization

1. Introduction

1.1. Cancer: an overview

The human body has approximately $3x10^{13}$ cells and the average human lifespan includes 10^{16} cell divisions (1). A precise control of cellular division and differentiation through a network of complementary mechanisms that regulate cell proliferation and death are of most importance. Thus, the uncontrolled multiplication of cells in a specific location it would be clinically described as neoplasia (2,3).

Cancer is a large group of diseases of higher multicellular organisms. It is characterized by alterations in the expression of a variety of genes resulting in the uncontrolled growth and division of abnormal cells. Usually, can invade surrounding tissue and can metastasize to other organs. Metastases are the leading cause of death from cancer (4). Cancer can be caused by a variety of changes in gene expression resulting in dysregulated balance of cell proliferation and cell death (5). These alterations are the consequence of the interaction between genetic factors, lifestyle and three types of external agents, such as: chemical carcinogens (tobacco-smoking, food and drinking water contamination); physical carcinogen (UV and ionizing radiation); and biological carcinogens (infections caused by viruses, bacteria or parasites) (1,5).

Some types of cancers can be cured by conventional therapies such as surgery, radiotherapy, or chemotherapy if they are detected early. Additionally, avoiding the exposure to common risk factors, a significant proportion of cancers could be prevented (4).

1.1.1 Incidence and Mortality

Cancer is a major public health problem worldwide and the second leading cause of mortality. According to the World Health Organization (WHO), cancer was responsible for an estimated 9.6 million deaths in 2018. Globally, about 1 in 6 deaths is due to cancer (4). Approximately 70% of cancer deaths occur in low- and middle-income countries. Cancer incidence and mortality are rapidly growing worldwide due to the growth and aging of the population, particularly in less developed countries (6). The incidence of cancer is also due to an increase of established risk factors such as overweight, smoking, absence of physical activity, and altered reproductive patterns related to economic development and urbanization.

A significant proportion of cancer deaths is caused by lung, colorectal, stomach, liver and breast cancers. The most recurrent types of cancer vary between different global regions and among men and woman (6).

In Europe, the total number of cancer cases and cancer deaths in 2018 are approximately 23% and 20%, respectively. These estimated numbers represent only 9% of the global population.

Figure 1.1 presents the distribution of all new cancer cases and deaths in Europe in 2018 for both sexes in all ages. For both sexes combined, female breast cancer is the most commonly diagnosed cancer (12.4% of the total cancer cases) in Europe followed by colorectal cancer (11.8%), lung cancer (11.1%) and prostate cancer (10.6%). Lung cancer is the leading cause of cancer death (20% of the total deaths) in Europe following by colorectal cancer (12.5%), breast cancer (7.1%), pancreas (6.6%) and prostate cancer (5.5%). In females, breast cancer is the most commonly diagnosed cancer and the leading cause of death. In contrast, the most frequently diagnosed cancer in males is prostate cancer and lung cancer for mortality (6).

In Portugal, cancer incidence is similar to Europe. This disease was the cause of death of 27,900 patients in 2016, 3% more than the previous year (7).

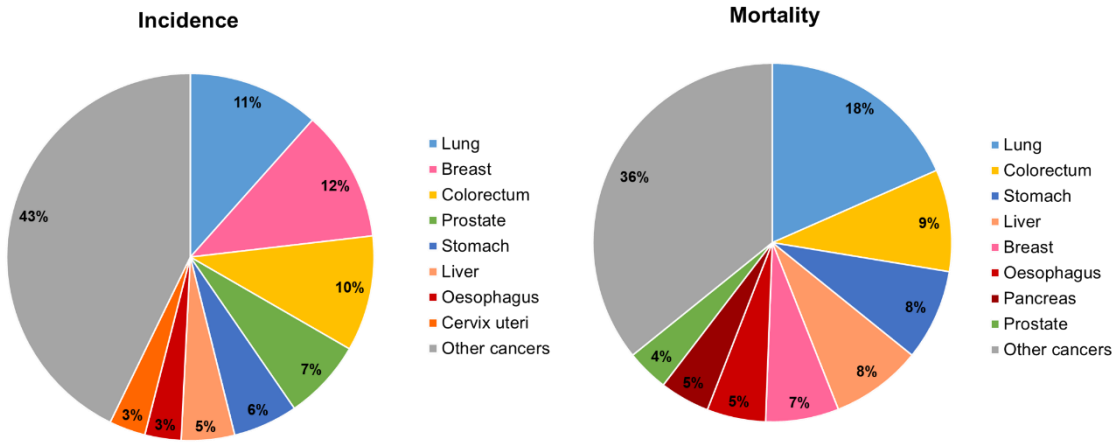

Figure 1.1 - Distribution of estimated number of new cases and mortality by Europe in 2018 of all cancer types in both sexes, all ages. Adapted from GLOBOCAN 2018.

In the last decade, cancer has been extensively investigated at various levels, such as physiological, cellular and molecular levels promoting the remarkable development of new approaches for cancer treatment (8).

1.1.2 Breast and Prostate Cancers

Breast and Prostate cancers are two malignant diseases that have some remarkable similarities namely they are tumours of female and male accessory sex organs, respectively and are both characterized by hormone-sensitive cancers, which could respond to hormone therapy (9). These tumours constitute one of the most commonly diagnosed cancers in Europe as well as the leading causes of cancer-related mortality for women and men, respectively (9).

Breast cancer is a complex disease and the second cause of cancer-associated death among various women (10). Worldwide, there are about 2.1 million new breast cancer cases diagnosed

in 2018. In the majority of the countries (154 of 185), this condition is the most diagnosed cancer and is also the leading cause of cancer death in over 100 countries (6).

In addition, almost 1.3 million new cases and 359,000 related deaths of prostate cancer were estimated worldwide in 2018. This type of cancer is considered the second most frequent cancer and the fifth leading cause of cancer death in men (6).

Several factors such as genetical susceptibility and environmental factors, could be related with initiation and development of breast and prostate cancers (10). In breast cancer, family and thus genetic predisposition are the most important risk factors (9). The majority of inherited breast cancer cases are due to mutations in tumour suppressor genes *BRCA1* and *BRCA2*. Additionally, prolonged and unopposed exposure to estrogen is another significant risk factor for breast cancer. Other risk factors associated to this malignancy, include age, race, radiation exposure, weight, exercise, alcohol consumption, smoking and previous breast disease. As with breast cancer, a genetic predisposition is also an important risk factor in prostate cancer. In fact, prostate cancer has many risk factors in common with breast cancer. Prolonged exposure to steroid hormones, like breast cancer but in this case androgens, is also an important risk factor for prostate cancer. This hormone-dependent fact is supported by the elimination of prostate cancer risk in men that have genetic anomalies blocking androgen production or suffer early castration. Prostate cancer has other risk factors similar to breast cancer as age, obesity, low-fiber and high-fat diet, and prostate inflammation (9).

A better understanding of the cellular and molecular mechanisms associated to breast and prostate cancers, and the identification of new biomarkers for early diagnostics and prognosis could contribute to design effective cancer therapeutic approaches (10). An example of these biomarkers in hormone-dependent cancers are steroid hormones receptors.

1.2. Steroid Hormones

Steroids are a class of organic compounds with a four-ring skeleton composed by 17 carbon atoms. They can differ significantly by modifications in functional groups attached to the core, the oxidation state of the individual rings, alterations to the ring structures and degree of unsaturation. Steroids include, for example, some anti-inflammatory drugs, dietary lipids (cholesterol) and, especially sex hormones such as estradiol and testosterone. These molecules have two fundamental biological functions: (1) several steroids are signalling molecules that activate steroid hormone receptors, and (2) are important components of cell membrane structures, such as cholesterol, controlling membrane fluidity (11).

Steroid hormones are a class of hormones synthetized from a common precursor molecule, cholesterol. These hormones act as chemical messengers in the body and control several

physiologic mechanisms such as the development and function of the reproductive system (12). They are grouped depending on their biological function: estrogens (female sex steroids), androgens (male sex steroids), progestins, glucocorticoids and others **(Figure 1.2)** (11). These molecules are small lipophilic ligands that bind with high affinity to their respective receptors, intracellular proteins which are included in the nuclear family of transcription factors (12). Signal transduction is mediated by these receptors through genomic and nongenomic actions (12). Steroid hormone receptors are present in many cells but that levels are elevated in premalignant and malignant cells (11). The development and growth of numerous human cancers are influenced by these molecules (13).

Steroids and steroid receptors played an important role in the occurrence of cancer as well as target for this condition therapeutics. Thus, currently, this is a promising area of research (13).

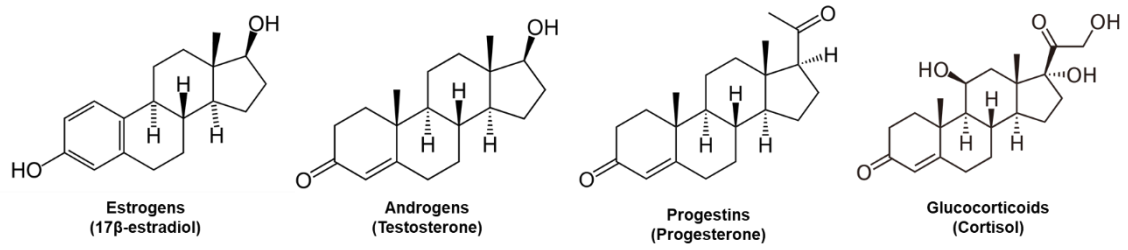

Figure 1.2 - Structures of representative examples of steroid hormones.

1.2.1. Estrogens

Estrogens, known as female hormones, are organic compounds with a core structure composed of 17 carbon-carbon bonds arranged as four fused rings. All estrogens have 18 carbons being known as C18 steroids with identical chemical structures and function (14). Estrogens are small lipophilic molecules essential to the function of the female reproductive system (13). These molecules are mainly produced by the ovary and transported via blood stream to specific target tissues. The most important and potent form of natural estrogen is 17β-estradiol (E2) followed by less effective estrogens, estrone and estriol (15). E2 is an important regulator of growth, differentiation and function in a variety of target tissues, including the female and male reproductive systems, mammary gland, and cardiovascular and skeletal systems (11,16). The principal biological effects of E2 are triggered through the estrogen receptors (ER) (16).

The ER is classified as two distinct forms, ERα and ERβ, which are encoded by different genes (*ESR1* and *ESR2*, respectively). However, these proteins are members of the nuclear hormone receptors superfamily of transcription factors sharing high degree of homology (14,16). The major difference between the two ER forms is the amino terminal domain, ERβ has a shorter than ERα – see **Figure 1. 3.** The full length size of human ERα has 595 amino acids and 66 kDa while human ERβ protein has 530 amino acids and 54 kDa. Besides full-length ERα isoform (66 kDa), two shorter isoforms (36 kDa and 46 kDa) have been described as consequence of products of

alternative splicing, or the presence of alternate start codons. Additionally, ERβ has five well-known isoforms (14,17).

1.2.2. Androgens

Androgens are a class of steroid hormones that are synthesized by the testis and adrenal glands consisting of cholesterol 19-carbon derivates. Androgens play a key role in the development and survival of male reproductive tissues, as prostate, by influencing gene expression levels. They are also precursors for estrogens, female sex hormones. The most abundant androgen in men is testosterone (16). However, there are other forms of androgens, including dihydrotestosterone (DHT), androstenedione, and dehydroepiandrosterone (DHEA) and its sulfonylated derivate (DHEAS). Testosterone or DHT are more potent than Androstenedione and DHEAS. In addition, weakly activating androgen receptors can also be metabolized into the more potent androgens (18). These steroid hormones primarily perform their functions through their respective receptor (androgen receptor) (19) .

Androgen receptor (AR) is a ligand-dependent transcription factor which is activated in the presence of androgens (20,21). This receptor is a member of the superfamily of nuclear hormone receptors sharing several structural and functional characteristics with other receptors (22–24). The AR protein consists of 910-919 amino acids and has 110 kDa (**Figure 1.3**) (19,25) . In the absence of androgens, the AR is stabilized in an inactive state, in the cytoplasm, by a complex of chaperone proteins (heat-shock proteins) (18,19). Upon androgen binding AR is translocated into the nucleus and subsequently can initiate expression of genes by binding to a specific DNA sequence which are recognized by the AR (21,26).

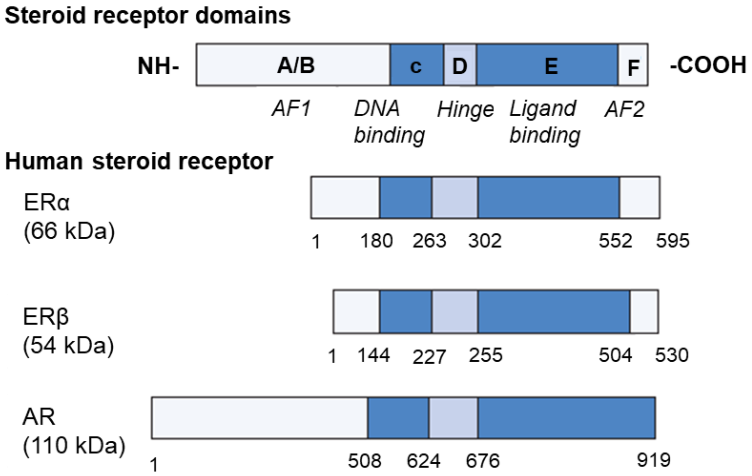

Figure 1.3 - Schematic illustration of the primary structure of steroid receptors and its functional domains. The primary structure of human steroid receptors: ER – estrogen receptor; AR – androgen receptor. Region A/B contains transactivation function 1 domain (AF1); Region C the DNA-binding domain; Region D is the hinge region; Region E consist of ligand-binding domain; and Region F the transactivation function 2 (AF2) domain. Adapted from (12).

1.2.3. Hormone Receptors Signaling Pathways

There are two distinct types of hormone receptors signaling, usually named as genomic and non-genomic pathways (12,14). Generally, in the genomic pathway, upon hormones binding to the respective hormone receptor in the cytoplasm, a conformational change occurs and the ligand-receptor complex translocates into the nucleus. In the nucleus, the receptor binds to the chromatin at specific response elements sequences or transcription initiation complexes on the DNA, activating or repressing transcription (**Figure 1.4**) (14,25,27–29). Despite hormone-dependent transcription, the principal mechanism of action for hormone receptors, hormones can also signal without direct binding of the hormone receptors to the DNA (14,18,27). These non-genomic pathway occurs rapidly (in seconds to minutes) and includes the activation of second messenger signaling cascades that involve kinases, calcium flux, phospholipases, among others secondary messengers (18). This rapid signaling results from binding to specific extranuclear receptors, which is localized mostly in the cell membrane (28).

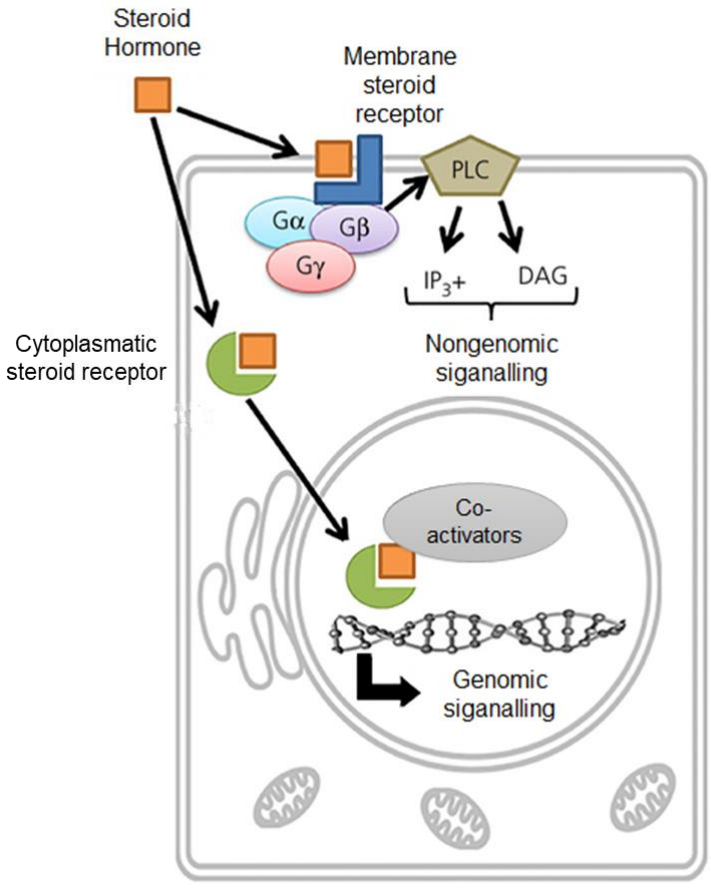

Figure 1.4 - General schematic illustration of steroid hormones signalling at cellular level. Steroid Hormones can bind to cytoplasmatic receptors or membrane-associated receptors. When the hormones bind to cytoplasmatic recepors, the complex hormone-receptor is translocated to the nucleus activating transcription (genomic pathway). On the other hand, when the hormones bind to membrane receptors activates second messengers signalling cascades. Adapted from (29).

1.2.4. Hormone Receptors and Cancer

There is evidence that steroid hormones, as estrogens and androgens, influence many human hormone-dependent cancers, such as breast and prostate cancers, through diverse mechanisms mediated by respective steroid hormone receptors (30). Breast and prostate cancers shares a diversity of molecular similarities.

For breast cancer, estrogens represents a role in tumour development and progression. Approximately 80% of all breast cancers express estrogen receptors (ER) (16,31). Thus, these receptors are a potential biological target for diagnosis and therapy in hormone-dependent breast cancers (30). Usually, ER are overexpressed on the membrane and nucleus of breast cancer cells providing a possible mechanism for targeted drug delivery (11). Furthermore, the case is similar for prostate cancer diagnostic and therapy. High levels of testosterone have been linked with a diversity of diseases, namely prostate cancer (16). The progression of this cancer, however, have been associated to elevated AR expression in malignant tissue indicating that AR plays an important therapeutic target for prostate cancer treatment (16,19,21).

Therefore, the study of steroid hormones, as well as, their respective steroid receptors have a great potential as diagnostic or prognostic biomarkers during tumour development and progression (30).

1.3. Cellular uptake mechanisms

Cellular trafficking of substances and signaling are the most important mechanisms for biological activity, which is regulated by cellular membrane. Cells may internalize steroid via various mechanisms, including passive diffusion (metabolic energy-independent) and transporter-mediated mechanisms as facilitated diffusion and active transport (metabolic energy-dependent) (32–34). Conventionally, steroid hormones cross the cell membrane bi-phospholipid layer through passive diffusion, due to their hydrophobicity. Alternatively, are known that sex hormones, namely estrogens and androgens, binds with cell membrane-bound G-protein coupled receptors to perform their genomic or non-genomic functions (28,33).

Endocytosis mediated by membrane receptor also may be involved in cellular uptake of steroid hormones. However, the purpose of the steroids endocytosis in nuclear receptor-mediated functions it is still unclear (32,33). In all mammalian cells, endocytosis is a fundamental used to communicate with the extracellular environment. This is an energy-dependent process whereby cells internalize portions of cell membrane, cell-surface receptors, and a diversity of soluble molecules and ions, such as nutrients, from the extracellular environment (34,35). However, small cells can also be internalized forming vesicles that carry its contents into the cells.

Cells have numerous mechanisms for endocytosis. The traditional classification of endocytosis mechanisms is divided by size into two categories: phagocytosis, the uptake of large particulates (“cell eating”), and pinocytosis, the uptake of fluids and solutes (“cell drinking”) (36–38) . The latest category is sub-categorized in other mechanisms based on the proteins and lipids involved in endocytic processes. Accordingly, pinocytosis is divided into clathrin-mediated endocytosis (CME) and clathrin-independent endocytosis (CIE) (36,37). This last category is still sub-divided in caveolae- mediated endocytosis, clathrin- and caveolae-independent endocytosis and macropinocytosis (37). **Figure 1.5** illustrated a schematic representation of the different endocytosis pathways.

Nonetheless, these mentioned endocytic pathways are focused in four essential steps: (1) specific binding at the cell surface; (2) plasma membrane pinching and budding off; (3) roping of the trafficking vesicle obtained and (4) trafficking of the vesicle to cytoplasm (36,37).

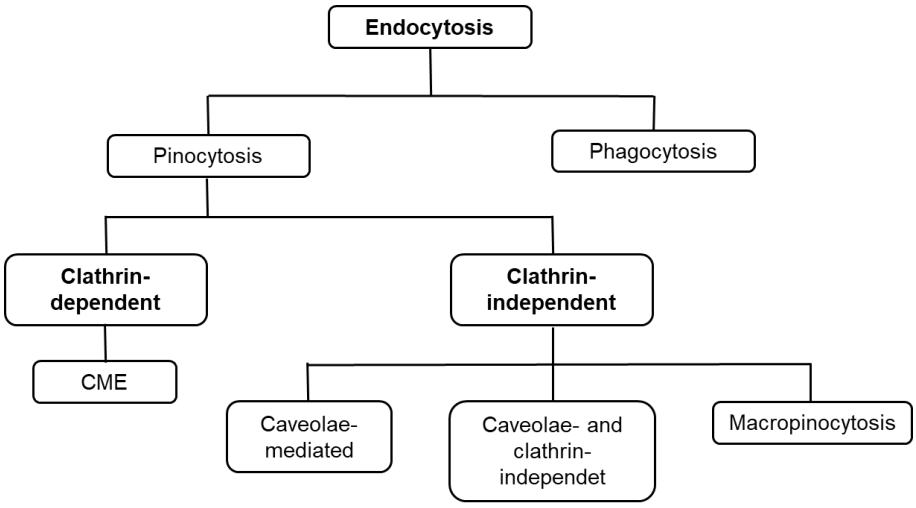

Figure 1.5 - Classification of endocytosis pathways based on the proteins that are involved in the internalization of particles and solutes. Adapted from (36).

1.3.1. Phagocytosis

Phagocytosis is an endocytosis pathway and consists in the ingestion of large particles by an actin-dependent mechanism. This process is typical of specialized cells, including immune cells, as dendritic cells, macrophages, monocytes, neutrophils, and mast cells. Nevertheless, it is also associated to the nutrient, pathogens, dead cells and cell debris uptake (37,39). Primarily, the phagocytic pathway requires a specific recognition of the particles through receptors at surface of cell membrane. This recognition leads to a membrane distortion that surrounds the particle, engulfs it, and ends with the formation of a phagosome (36,37,40). Thereafter, the phagosome undergo maturation, fuses with lysosomes for degradation (36).

1.3.2. Pinocytosis

1.3.2.1. Clathrin-mediated Endocytosis (CME)

CME is one of the most studied and important pathways of cellular entry in all mammalian cells. This route is responsible for uptake of essential nutrients, efficient receptors signalling and synaptic vesicle recycle in neurons (36,37). CME is initiated by the attachment of particles at the cell membrane surface, forming clathrin coated pits (CCP). After invagination, CCP are pinched off from the plasma membrane by dynamin (a small GTPase), triggered the formation of clathrin coated vesicles (CCV). Then, clathrin coat is discarded and the vesicles fuse with endosomes and subsequently with lysosomes initiating a degradation process. Alternatively, endosomes containing particles can be transported back to cell membrane for endosomes recycling – see **Figure 1.6**. Clathrin, a cytosolic protein, together with adaptor proteins (APs), constitute the coated pits (36,37,41).

1.3.2.2. Clathrin-independent Endocytosis

The most studied clathrin-independent internalization mechanisms is the caveolae-mediated endocytosis. This endocytic pathway is responsible for diverse biological functions, including lipid regulation, vesicular transport, and cell signalling (37,42). Caveolae are cholesterol-rich cell membrane microdomains composed mainly of caveolin proteins (caveolin-1 and caveolin-2). Endocytosis via caveolae is initiated by the formation of plasma membrane flask-shaped invagination that contains a striated coat of caveolin. After internalization, the vesicles are transformed into caveossomes and finally the particles can be released to the cytoplasm or fused with lysosomes for degradation – see **Figure 1.6** (36,37,41–43). Caveolae have been associated to several disease conditions, namely cancer, making their mechanisms investigation of potential biomedical relevance (42).

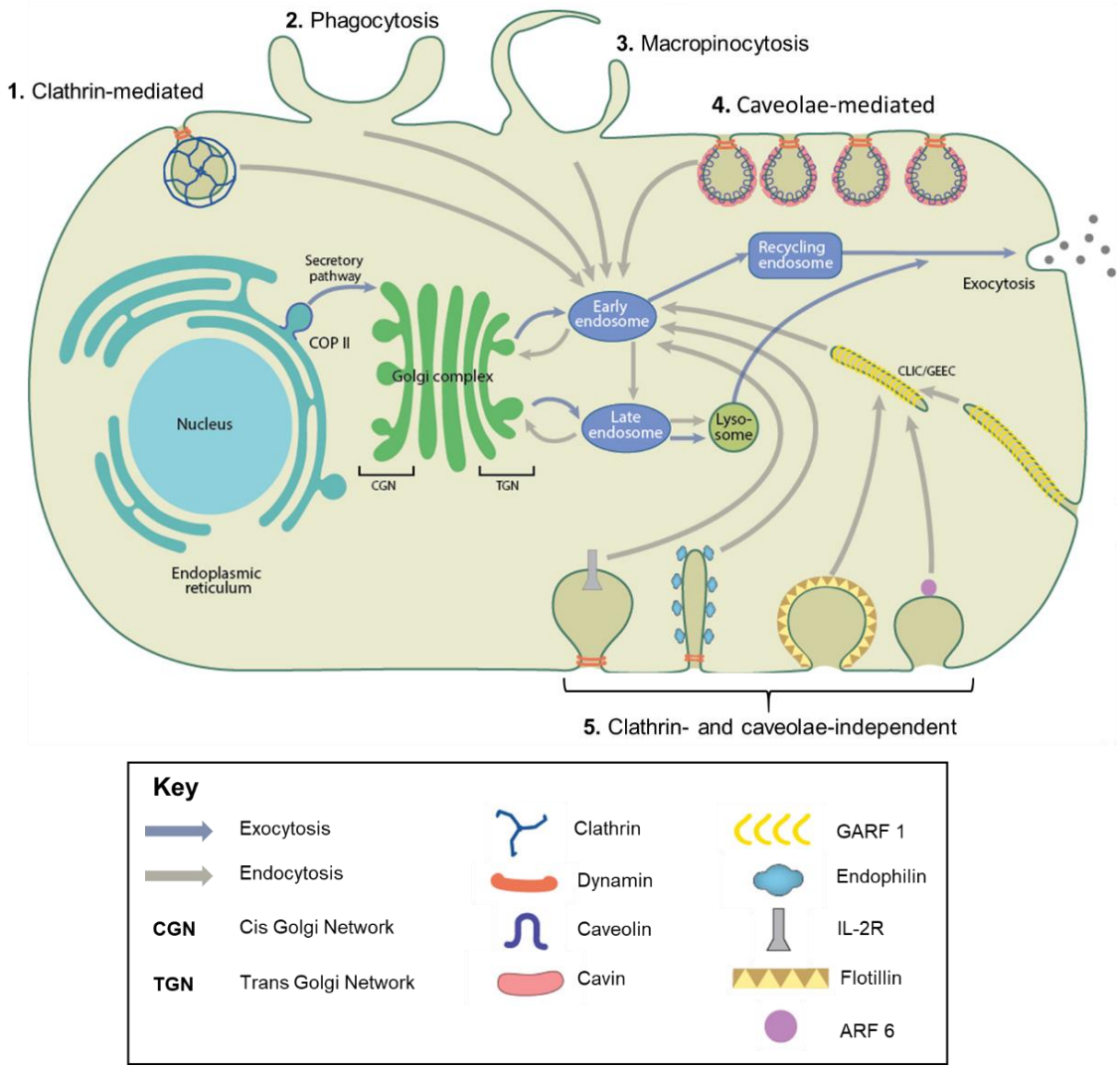

Figure 1.6 - Schematic representation of different endocytosis pathways. (1) Clatherin-mediated endocytosis; (2) Phagocytosis; (3) Macropinocytosis; (4) Claveolae-mediated endocytosis; and (5) Clathrin- and caveolae-independent endocytosis. Adapted from: What is membrane trafficking . 2018. Available from: https://www.mechanobio.info/what-is-the-plasma-membrane/what-is-membrane-trafficking/#ITEM-1574-0). Acecessed February 2020.

1.4. Cancer Theranostics

There are several therapies for cancer treatment. Currently, the most common conventional therapies used for cancer treatment are surgery, chemotherapy and radiotherapy. The method of treatment is chosen depending mainly on the type and stage of cancer. There is no general methodology to treat all types of cancer due to the heterogeneity and the complexity between different patients with the same cancer and different types of cancer. Conventional therapies for cancer treatment have some significant restrictions because of side effects, incomplete tumour eradication, lack of selectivity, and the variable tumour response to treatment and clinical behaviour. Another problem of these conventional therapies is the increased resistance to treatment. Although these disadvantages they are still used for cancer treatment (44–46). Despite the recent biomedical advancements of these conventional therapies for cancer treatment, it is important the investigation and development of new diagnostic and treatment approaches. Recently, has been developed new technologies which could clinically advantageous for cancer diagnostic and treatment (47).

Cancer theranostics is a new technology that combines diagnosis and therapy. This new approach has a great potential for personalized cancer treatment. Therefore, personalized medicine has the capacity to optimize targeted delivery and dosing of treatments having purpose to decrease delays in treatment and facilitate patient care (46,48).

Molecular imaging is a technique diagnostic system which allowed to visualize, measure and characterize biological mechanisms at the cellular and molecular levels in humans. Molecular imaging of cancer is a growing area and it can be executed with several imaging tools providing sensitive non-invasive information of tumour properties. Ligands used can be labelled with a fluorescent dye for optical imaging, a positron emitting radionucleotide for positron emission tomography (PET), a contrast agent for magnetic resonance imaging (MRI) or a gamma emitting radionucleotide for single photon emission computed tomography (SPECT) imaging (46,49).

There are many tools that can combine imaging and therapy. The use of light as an activation mechanism had a marked development in cancer treatment. It can be used directly, triggering physiological changes in cells and tissues, or indirectly, inducing the formation of by-products (effector molecules). These types of light-induced therapies include particularly photodynamic therapy (PDT) (46,50).

A theranostic approach requires agents that simultaneously have the capacity of targeting, imaging, and treatment (46). An example are the receptor based fluorescence ligands, specifically a series of estrogen-, testosterone- and 19-nortestosterone conjugates linked to a BODIPY dye (16).

1.4.1. Photodynamic Therapy (PDT)

PDT is widely used in the treatment of several types of tumours, such as breast and prostate cancers (51,52). PDT is an alternative method for cancer treatment and combines three principal components, a light-activated chemical known as a photosensitizer (PS), light irradiation at an appropriate wavelength, and molecular oxygen from tissues to induce cell death through oxidative damage (53–55). Individually, each of these components do not develop a biological response. However, a mixture of the three factors promotes the formation of reactive oxygen species (ROS), as singlet oxygen ($^1O_2$), hydrogen peroxide (H_2O_2), superoxide anions ($O_2^{\bullet-}$) and hydroxyl radicals ($OH^{\bullet}$) (52). These ROS produced intracellularly have short lifetimes and can provoke irreversible damage to crucial cellular macromolecules such as DNA, amino acids, proteins, phospholipids, leading to ablation of the tumour cells(56).

Clinically, the treatment is dependent on the uptake of the PS into malignant tissue. PSs are usually administered by systemic or topical application but normally it is executed by intravenous injection (57). Once the optimal tissue concentration is optimized, the malignant tissue can then be exposed to light with a convenient wavelength for a pre-determined time triggering the selective activation of the PS. Subsequently, this PS activation produces highly reactive ROS and can induce cell apoptosis and/or necrosis, immune response and microvasculature shutdown in the tumour – see **Figure 1.7** (52,55). This alternative approach is a clinically approved therapy and has several of advantages over other cancer therapies. These advantages include low toxic, good selectivity, side effects, minimal invasiveness, and it can be combined with other cancer therapies (51,58). Despite these advantages, PDT has various drawbacks such as lack of tumour selectivity; photobleaching of PS; photosensitization; the need of an oxygen-rich environment and absence of accepted light dosimetry; short tissue penetration depth; as a local treatment, cannot be used to treat metastasized cancers (50,59,60). Therefore, these limitations make the development of PDT a challenge by increasing the interest of theranostics approaches.

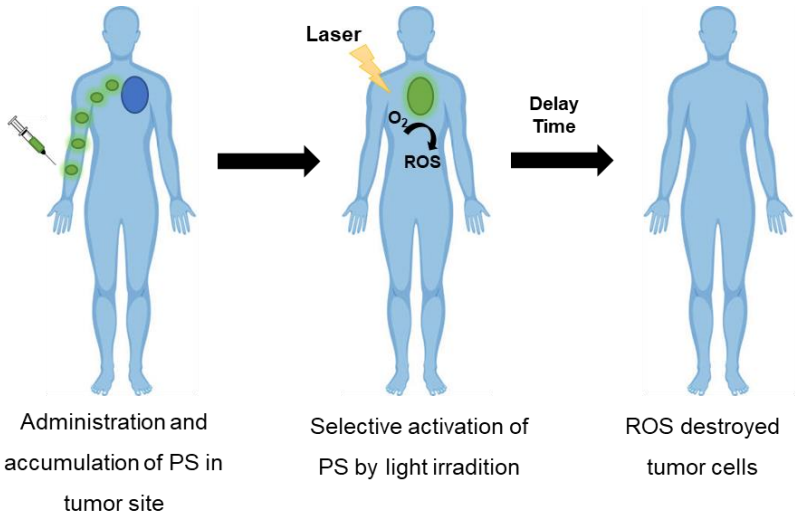

Figure 1.7 - Schematic illustration of general clinical procedure in a clinical of PDT.

1.4.1.1. BODIPY-based photosensitizers

Photosensitizers are compounds which have been used in the treatment of various medical conditions. These class of compounds is a key factor in PDT. A PS is considered to be an ideal drug for cancer PDT if it has the subsequent characteristics: (1) selectivity to tumor cells and rapidly clear from the normal tissues; (2) rapid body clearance; (3) capacity to be delivered via several administration routes; (4) good water solubility; (5) chemical and physical stability; (6) dark biological stability with no cytotoxicity; (7) high molar extinction coefficients; (8) photostability; (9) activation at visible/near-infrared wavelengths for good tissue penetration (53,56,57).

The PS classification is based on its functional capabilities and the structural characteristics have an important position. These type of compounds are divided into three groups: first, second and third generation. First generation PS are porphyrin-based drugs which are aromatic tetrapyrrolic structures. Due to the disadvantages of the first generation PSs, the clinical use of these photosensitizing drugs is limited and an extensive investigation was required in order to improve the efficiency of PSs (45,55,56,61,62). The second generation PSs, such as chlorin, phthalocyanines, and porphyrins, were designed to reduce side effects, increase tumour selectivity, and to increase depth penetration of light with longer wavelength (600 nm - 800 nm) (61,63). These type of PSs include a broad group of compounds that can be applied in numerous therapeutic applications. Because of solubility problems of a multiple PS in aqueous medium, the development of delivery models could be advantageous for PS transportation to the tumour site improving the cellular uptake. Second generation PSs have been bound to drug carrier molecules, such as steroid hormones, originating third generation PSs. Thus, with the rapid advancements in this study area, a variety of new and more specific PSs has revealed potential for cancer therapy (62,64).

Among a wide range of chromophores, Boro-dipyrromethene (BODIPY) is one of the most commonly used fluorescent dye (31). BODIPY is a fluorescent dyes and structural analogs of porphyrins (**Figure 1.8**). These molecules have several attractive properties, including facile synthesis and structural flexibility, good solubility, peculiar spectroscopic properties (narrow absorption and emission bands), strong absorption coefficients in the visible range, high fluorescence quantum yields, good photostability, and others (31,65). In addition to these greater chemical and physical properties, BODIPY is cell membrane-permeable, and thus used in a variety of biological applications, such as helping to monitor mechanisms of action in living systems as well as to guide surgery (11,31). The potential use of BODIPY dye in PDT has been suggested because of its capacity to generate singlet oxygen. However, in recent times, techniques to introduce 18F radioisotopes into BODIPY has been recently described, in order to provide a potential development of dual fluorescence/PET imaging probes (16). BODIPY dyes have also been used to label several ligands including DNA, proteins, peptides, carbohydrates lipids, and in particular, steroid hormones (65,66).

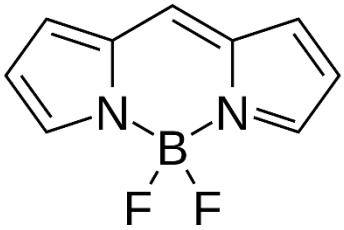

Figure 1.8 - Structure of BODIPY dye core.

1.4.1.2. Steroid-BODIPY conjugates

Nowadays, a major problem of chemotherapeutic agents clinically is the lack of selectivity. Therefore, the development of selective and potent therapeutic agents is under continuous investigation in order to target tumour tissue without affecting cell viability of normal cells (16).

Around 80% of all breast cancers express estrogen receptors (ER-positive). Thus, the first line of treatment for hormone-dependent breast cancer is hormone therapy and drugs that target and block ER. Hormone steroid receptors have also become attractive targets for molecular imaging due to their implication in the growth hormone-dependent cancer types, such as breast and prostate cancers. Testosterone is the most hormone in men. In case of prostate cancer, low levels of testosterone led to this condition. As well as in breast cancer, hormone receptors, as androgen receptor, also provide significant prognostic information for the diagnosis and treatment of hormone-dependent tumours. Therefore, hormone receptor-imaging has a great potential for breast and prostate cancers screening, staging, response assessment and guiding therapies (11,16,31).

Recently, has been reported the development of multimodality theranostics agents as BODIPY dyes conjugated to estradiol-, testosterone- and 19-nortestosterone. 17α-ethynylestradiol (EE2)-BODIPY conjugate, with a linear eight carbon spacer chain, presents the highest relative binding affinity (RBA) for the ERα. However, the 11β-methoxy derivate of EE2-C8-BODIPY conjugate improve *in vivo* localization. Additionally, four androgen-BODIPY conjugates shown significant RBA for the AR and thus, cellular uptake studies and continuous investigation of these conjugates are important for the improvement of cancer diagnostic and therapy strategies (16,67,68).

In summary, these conjugates provide a potential platform as a receptor-based fluorescence probes for imaging breast and prostate cancers, PSs for PDT, and also as a PET imaging agents upon 18F radioisotope substitution (16).

1.5. Objectives

Steroid receptors studies have shown their potential use as biological targets for hormone responsive cancers. Receptors overexpression in human cancer cells and their binding properties provides an important role for malignant tumours localization.
The main goal of this work was to evaluate the cellular uptake of estradiol-, testosterone- and nortestosterone-derivates conjugated to BODIPY as potential multi-modality theranostic agents (PET/fluorescence and PDT) in relevant breast and prostate cancer cells by fluorescence microscopy. To assess conjugates potential for photodynamic therapy (PDT), irradiation studies were also done.

In order to reach this main goal, various tasks were set:

i. Effects of conjugates in tumour and normal cells uptake;
ii. Steroid receptor blocking with specific inhibitor;
iii. Understand the mechanism of cellular uptake of conjugates;
iv. Localization of conjugates in tumour cells;
v. Interaction of conjugates with tumor and normal cells in co-culture;
vi. Irradiation studies in tumour and normal cells in order to assess conjugates potential for PDT.

2. Methods and Materials

2.1. Compounds

Steroid-BODIPY conjugates studied were synthesized in the Faculty of Medicine and Health Sciences (Université de Sherbrooke, Canada). These compounds are estradiol-, testosterone- and nortestosterone derivates conjugated to BODIPY dye (as fluorescent probe) (**Figures 2.1 and 2.2)**. The characteristics of the conjugates are described in **Table 2.1**. Solid compounds were stored at 4°C protected from light.

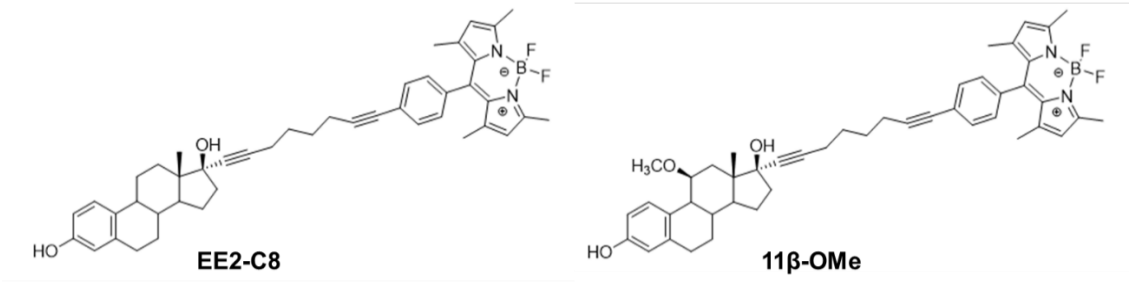

Figure 2.1 - Structures of estradiol-BODIPY conjugates: **EE2-C8** (17α-[1-heptyne-7-(4-ethynylphenyl)-(4,4-difluoro-8-(1,3,5,7-tetramethyl-4-bora-3a,4a-diaza-s-indacen)]-3,17β-estradiol); and **11β-OMe** - 11β-methoxy-3,17β-estradiol).

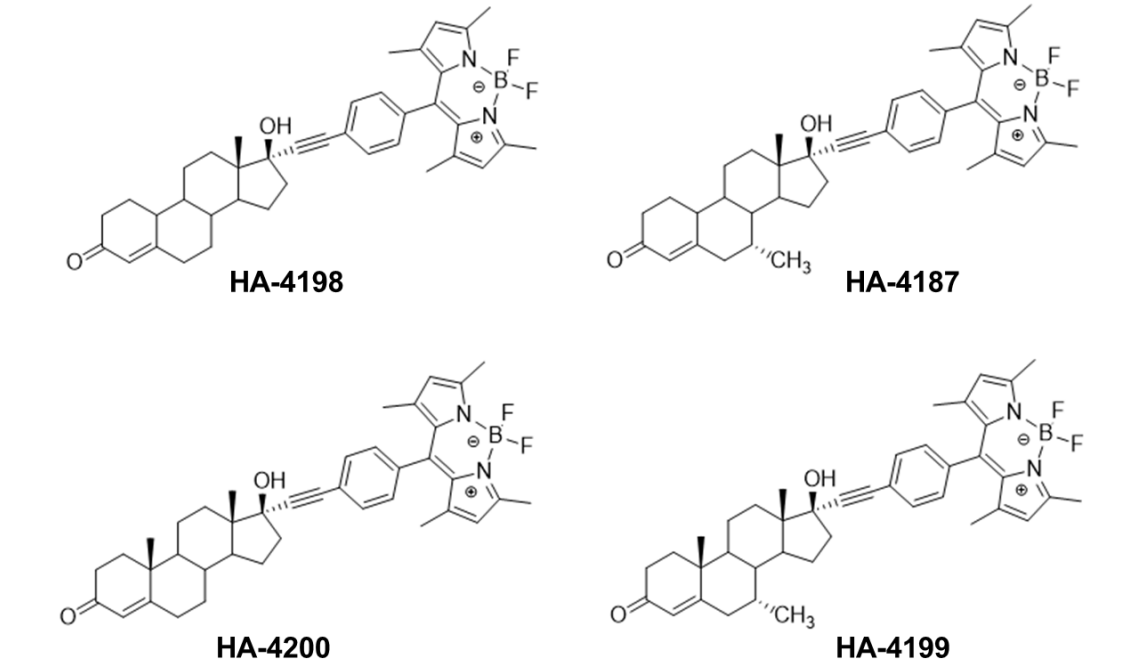

Figure 2.2 - Structures of androgen-BODIPY conjugates: HA-4198 (17α-[4,4-difluoro-8-(4/-ethynylphenyl)-1,3,5,7-tetramethyl-4-bora-3a,4a-diaza-s-indacene]-19-nortestosterone); **HÁ-4187** -7α-methyl-19-nortestosterone); **HÁ-4200** -testosterone); and **HÁ-4199** -7α-methyl-nortestosterone).

Table 2.1 - Characteristics of the steroid-BODIPY conjugates studied.

Name/Code	Molecular Formula	Molecular Weight ($g.mol^{-1}$)
EE2-C8 (-3,17β-estradiol)	$C_{44}H_{46}BF_2N_2O_2$	699.0
11β-OMe (-11β-methoxy-3,17β-estradiol)	$C_{45}H_{49}BF_2N_2O_3$	714.7
HA-4198 (-19-nortestosterone)	$C_{39}H_{43}BF_2N_2O_2$	620.6
HA-4187 (-7α-methyl-19-nortestosterone)	$C_{40}H_{45}BF_2N_2O_2$	634.6
HA-4199 (-7α-methyl-nortestosterone)	$C_{41}H_{47}BF_2N_2O_2$	648.6
HA-4200 (-testosterone)	$C_{40}H_{45}BF_2N_2O_2$	634.6

Due to the low solubility of the conjugates in water, dimethyl sulfoxide (DMSO) (Sigma, St. Louis, USA) was used to solubilize the steroid-BODIPY conjugates. DMSO is an organic, polar and aprotic solvent commonly used to solubilize several nonpolar or poorly soluble drugs due to their amphipathic properties (69). The stock solutions of each conjugate were prepared at a concentration of 10 mM in DMSO and stored at -20°C protected from light. The concentrations of compounds used to perform the biological assays were prepared by diluting each stock solution in complete medium.

2.2. Human Cell Lines

In this work, four types of adherent human cancer cell lines were used to evaluate the effect of the steroid-BODIPY conjugates after green light irradiation, two from breast adenocarcinoma cells (MCF-7 and MDA-MB-231) and two from prostate cancer cells (PC-3 and LNCaP). **Table 2.2** summarizes details and cancer cell lines general characteristics, such as origin, morphology, steroid receptors (estrogen receptor and androgen receptor) and culture medium.

Table 2.2 - Human cancer cell lines used in this work and its general characteristics such as origin, morphology, steroid receptors and culture medium used.

Cancer Cell Line	Origin	Morphology	Steroid Receptors	Culture Medium % (v/v)
PC-3	Metastatic prostate adenocarcinoma	Epithelial	ER(+); AR(-)	RPMI 1640; 10% FBS; 1% Pen/StreP
LNCaP	Metastatic prostate carcinoma	Epithelial	ER(-); AR(+)	RPMI 1640; 10% FBS; 1% Pen/StreP
MCF-7	Metastatic breast adenocarcinoma	Epithelial	ER(+); AR(+)	DMEM; 10% FBS; 1% Pen/Strep; 1x MEM
MDA-MB-231	Metastatic breast adenocarcinoma (triple negative breast cancer cell model)	Epithelial	ER(-); AR(+)	DMEM; 10% FBS; 1% Pen/Strep; 1x MEM

Abbreviations: (ER – Estrogen Receptor; AR – Androgen Receptor; (+) – positive; (-) – negative; RPMI 1640 - Roswell Park Memorial Institute 1640 Medium (Gibco™ by Life Technologies, Invitrogen, California, USA); DMEM – Dulbecco's Modified Eagle Medium (Gibco™ by Life Technologies, Invitrogen, California, USA); FBS – Fetal Bovine Serum (Gibco™ by Life Technologies, Invitrogen, California, USA); Pen/Strep – Penicillin/Streptomycin solution (GibcoTM by Life Technologies, Invitrogen, California, USA); MEM - non-essential amino acid (Sigma, St. Louis, USA).

Additionally, as a normal cell line, primary dermal fibroblasts from foreskin of a neonatal African American was also used in this work. Fibroblasts were cultured in DMEM culture medium supplemented with 10% of FBS and 1% Pen/Strep. Fibroblasts morphology is spindle-shaped, and the cells are bipolar and refractile.

All cell types used in this work were obtained from American Type Culture Collection (ATCC®, Virginia, USA).

2.2.1. Maintenance of Cell Cultures

Cell lines were cultured in RPMI 1640 medium or Complete Culture Medium constituted by DMEM medium (see **Table 2.2**) supplemented with 10% (v/v) FBS, 1% (v/v) Pen/Strep solution (solution with 10000 U/mL penicillin, 10000 µg/mL streptomycin) in culture flasks of 25 and 75 cm^2 (SPL

Life Sciences, South Korea). Cell cultures were maintained in a CO_2 incubator (Sanyo, Osaka, Japan) at 37°C in a humidified atmosphere (99%) and 5% (v/v) of CO_2. For breast cancer cell lines, MCF-7 and MDA-MB-231, 1% (v/v) of MEM were added to the DMEM medium.

Cell cultures were subcultured routinely to maintain exponential growth. Upon reaching approximately 80% of confluence (Nikon TMS, Nikon Instruments, Tokyo, Japan), cells were subcultured to avoid loss of growth due to contact inhibition and lack of nutrients. To this end, the culture medium was removed and discarded and 2 or 3 mL of TrypLE™ Express (Gibco™ by Life Technologies, Invitrogen, California, USA) was added to help cell detachment. After approximately 5 min of incubation in the CO_2 incubator, 1 or 1.5 mL of fresh culture medium was added to block trypsin activity. Then, the cell suspension was transferred to 15 mL falcon tubes (SPL Life Sciences, South Korea) and centrifuged for 5 min at 300 x g and 15°C (Sigma 3-16K 10280, Osterode am Harz, Germany). The supernatant was discarded and the pellet was resuspended in 1 mL of fresh medium.

Cells were counted by the Trypan blue exclusion method in a hemocytometer (Hirschmann, Eberstadt, Germany). For that, 350 µL of culture medium were mixed with 50 µL of cellular suspension obtained during the subculturing procedure and 100 µL of 0.4% (v/v) Trypan blue solution (Gibco™ by Life Technologies, Invitrogen, California, USA). Viable cells were immediately visualized through an optical inverted microscope (Nikon TMS, Nikon Instruments, Tokyo, Japan) and cell density (cells/mL) determined by multiplying the number of total cells, the volume of the hemocytometer chamber (10^4 mL^{-1}) and the dilution factor (10) divided by the number of squares counted - **Equation 1**.

Equation 1.

$$Cell\ density\ (cells/mL) = \frac{Total\ cells\ counted}{Number\ of\ squares} \times 10^4\ (chamber\ volume) \times 10\ (dilution\ factor)$$

For each 25 and 75 cm^2 culture flask, the volume of cell suspension (estimated by equation 1) was added to fresh culture medium to perform a final volume of 5 and 15 mL, respectively. Subsequently, cell cultures were incubated at 37°C in a humidified atmosphere of 99% and 5% (v/v) of CO_2.

Cell cultures were periodically analyzed for possible mycoplasma contamination. This quality control assessment was performed by Polymerase Chain Reaction (PCR) detection on total genomic DNA extracted from the studied cultures (quality control is routinely performed by lab members).

2.3. Expression of steroid receptors by Western-Blot

Expression of estrogen α and androgen receptors was quantified by Western-Blot and performed for every cell line mentioned in section 2.2.

2.3.1. Sample preparation

For protein extraction, cell lines were seeded as described in section 2.2.1.At 80% of confluence, cells were washed three times with PBS 1x and harvested with a scrapper in 1 mL of PBS 1x for microfuge tube on ice. Samples were centrifuged for 5 min at 700 x g at 4°C (Sigma 3-16K 10280) and the supernatant was discarded. A final spin was done to remove all supernatant. The pellet was resuspended in 30 µL of cell lysis solution 4x NaCl-Tris-EDTA buffer (150 mM NaCl; 50 mM Tris, pH=8; 5 mM EDTA), 1x protease inhibitor (complete ULTRA Tablets, Mini, EASYpack, Roche, Switzerland), 1x phosphatase inhibitor (PhosStop, Roche), 0.1% (w/v) 1,4-Dithiothreitol (DTT; AMRESCO, USA), 2% (w/v) NP-40 (Thermo Scientific, MA, USA) and 1 mM phenylmethylsulfonyl fluoride (PMSF; Sigma, St. Louis, USA) and samples stored at -80 °C, until further processing.

All samples were thawed and submitted to 2 min 30 s of continue pulses at ultrasonic bath in ice and preserved on ice for 1 min to avoid sample heating and the denaturation of proteins. Cell lysates were centrifuged for 5 min at 700 x g at 4°C and supernatants were used for protein quantification.

Protein concentrations were determined using the Pierce Protein Assay (Thermo Scientific, MA, USA). A calibration curve was performed with standard BSA solutions with different concentrations (0-2000 µg/mL) and protein samples were diluted 1:10 in ultrapure water (18.2 $M\Omega.cm^{-1}$ at 25 °C). Thereafter, 150 µL of Pierce reagent was added and samples incubated for 5 min at room temperature (RT). Absorbances were measured at 660 nm with a Tecan Infinite F200 microplate reader (Tecan, Männedorf, Switzerland). For western blot analysis, 20 or 50 µg of total protein extracts were transferred to another Eppendorf tube with Sodium Dodecyl Sulfate (SDS) Loading Buffer 4x and 3% (w/v) DTT and incubated overnight at RT.

2.3.2. SDS-PAGE and transfer to PVDF membrane

A 10% acrylamide-bisacrylamide gel (SDS-PAGE) was prepared and samples were loaded in the gel (120 V for approximately 1 h). The transfer of proteins from the gel to the PVDF membrane (Amersham™ Hybond™ 0.45 PVDF, GE Healthcare, Life Sciences, Little Chalfont, UK) was performed using a semi-dry system transfer to provide a faster and more efficient transfer. For that, a specific semi-dry transfer device with the anode plate as the base and three-buffer system to achieve efficient transfer of proteins (see **Table 2.3**) were used. The semi-dry transfer system

is represented in **Figure 2.3**, in which the membrane is in contact with the SDS-PAGE gel. The transfer process was run at 130 mV for 45 min.

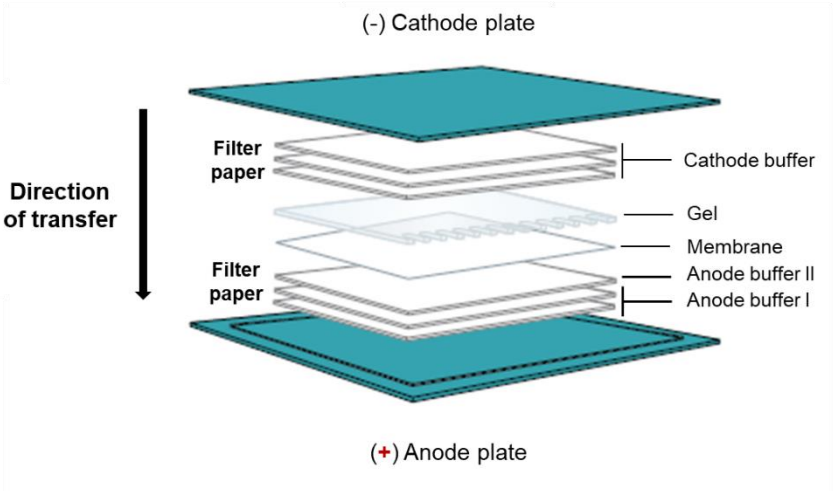

Figure 2.3 - Semi-dry transfer system. Adapted from *Protein Blotting Handbook Tips and Tricks* (Millipore).

Table 2.3 - Three buffer system of semi-dry transfer.

Buffer	Composition
Anode I	0.3 M Tris, pH 10.4, 10 % (v/v) methanol
Anode II	25 mM Tris, pH 10.4, 10 % (v/v) methanol
Cathode	25 mM Tris, 40 mM 6-amino-n-caproic-acid, 10 % (v/v) metanol, pH 9.4

The efficiency of the protein transfer process was analysed by staining the membrane with a Ponceau S solution for 5 min. Thereafter, the membrane was washed with ultrapure water (18.2 $M\Omega.cm^{-1}$ at 25 °C) in order to observe the protein bands.

2.3.3. Primary and secondary antibodies incubation

To quantify estrogen and androgen receptors, specific antibodies against these proteins were used. Following transfer process, membrane was blocked with 5% (w/v) non-fat milk solution in TBST (50 mM Tris, 150 mM NaCl and 0.1% (v/v) Tween 20, pH 7.5) during 1 h at RT with agitation. This blocking step was done for possible non-specific binding because of the high protein affinity of membrane. Then, each PVDF membrane was incubated with a primary antibody in 5% non-fat milk in TBST, anti-androgen receptor (1:5000) (Abcam, Cambridge, UK) or anti-estrogen receptor α (1:500) (Sigma, St. Louis, USA), for 1h at RT with agitation or overnight at 4 °C, respectively. After primary antibody incubation, the membrane was washed three times with TBST 1x during 5

min with agitation and incubated with the appropriate secondary antibody, anti-rabbit IgG HPR-linked antibody (1:2000) (Cell Signalling Technology, Massachusetts, USA) for 1 h with agitation. Protein bands in the membrane were detected as described in section 2.3.4.

Actin levels were used as a control to normalize the results. Consequently, the membrane was incubated with stripping buffer (0.1 M glycine, 20 mM magnesium acetate and 50 mM potassium chloride) three times for 10 min with agitation to remove specific antibody binding. The same procedure of blocking and antibodies incubation described previously was done with anti-β-actin (1:5000) (Sigma, St. Louis, USA) primary antibody, and anti-mouse IgG HPR-linked antibody (1:3000) (Sigma, St. Louis, USA) as secondary antibody.

2.3.4. Film Exposition

In order to detect protein bands in the membrane, a WesternBright ECL substrate (Advansta, Menlo Park, California, USA) was applied to the membrane and incubated for 5 min. ECL is a chemiluminescent HRP substrate for western blots imaging. After ECL incubation, the film was exposed to the membrane in light absence. Densitometric analysis was performed by using Image J software to determined protein band quantification.

2.4. Intracellular tracking of steroid-BODIPY conjugates in cancer and normal cells

Taking advantage of BODIPY fluorescence, the internalization of steroid-BODIPY conjugates in breast and prostate tumor cell lines and in normal cells was investigated by fluorescence microscopy.

All cell lines mentioned in section 1.2 were seeded on a 24-well plate (SPL Life Sciences, South Korea) with a cell density of $1x10^5$ cells/well and incubated for 24 h at 37 °C in a 99% humidified atmosphere and 5% (v/v) CO_2. After this time, the medium was replaced by fresh media (without phenol red) supplemented with 50 μM of conjugate or 0.5% (v/v) DMSO (vector control). Cells were visualized at 0 h, 45 min, 2 h and 6 h using a Ti-U Eclipse inverted microscope (Nikon, Tokyo, Japan). Images of BODIPY-conjugates fluorescence were acquired using a FITC filter (excitation at 480/30 nm in the blue region and emission at 535/45 nm). Before visualizing the fluorescence, the culture medium was replaced by fresh medium (without phenol red). The images were treated and analyzed with Image J software allowing the quantification of the Corrected Total Cell Fluorescence (CTCF) for each cell according with **Equation 2.** CTCF was quantified for five cells analyzed per image in three random microscopic fields in duplicate for each cell line.

Equation 2.

$$CTCF = Integrated\ density - (Area\ of\ cell \times Background\ mean\ fluorescence)$$

2.5. Internalization of Steroid-BODIPY with specific inhibitors

The internalization of steroid-BODIPY conjugates in breast and prostate tumor cell lines was also studied in the presence of inhibitors of the steroid receptors. And fluorescence quantified by fluorescence microscopy.

All cell lines were seeded in the same conditions described in section 2.4. After 24 h of incubation in DMEM/F-12 medium (Dulbecco's Modified Eagle Medium/Nutrient Mixture F-12) (Gibco™ by Life Technologies, Invitrogen, California, USA) without phenol red supplemented with charcoal stripped FBS (medium without hormones) (Gibco™ by Life Technologies, Invitrogen, California, USA) or DMEM/F-12 medium supplemented with normal FBS (medium with hormones), the medium was replaced by fresh DMEM/F-12 media (with or without hormones) and cells incubated overnight at 37 °C in a 99% humidified atmosphere and 5% (V/V) CO_2. Then, the medium was replaced by fresh DMEM/F-12 media (with or without hormones) supplemented with 10 μM of inhibitor – testosterone (Sigma, St. Louis, USA) or 17α-ethynylestradiol (EE2) (Sigma Aldrich, St. Louis, USA) - or without inhibitor and incubated for 1 h at the same conditions of previous incubations. After this period of incubation, the medium was again replaced by fresh DMEM/F-12 media (with or without hormones) supplemented with 25 μM of compound or 0.25% DMSO (vector control) and incubated for an additional 6 h (same conditions detailed in section 2.4). Cells were visualized at 0h and 6h using a Ti-U Eclipse inverted microscope. Before visualizing the fluorescence, the culture medium was replaced by fresh FluoroBrite™ DMEM media (with or without hormones) (Gibco™ by Life Technologies, Invitrogen, California, USA), a DMEM-based formulation with reduced background fluorescence. Images treatment and fluorescence quantification were performed as described in section 2.4.

2.6. Assessment of cell uptake and trafficking of steroid-BODIPY conjugates

2.6.1. Active vs. passive transport

In order to better understand the energy dependence of the transport mechanism of steroid-BODIPY conjugates through cell membrane, it is important to study the difference between internalization of conjugates at 37 °C and 4 °C. PC-3 cells (used in this assay as a model) seeding and conjugates application in cells were performed as described in section 2.4. The incubation of

conjugates was done for 6 h at 4 °C. Cells were visualized under Ti-U Eclipse inverted microscope at 6h. Images treatment and CTCF quantification were done as described in section 2.4.

2.6.2. Inhibition of endocytosis of steroid-BODIPY conjugates in the triple negative breast cell line (MDA-MB-231)

MDA-MB-231 cells were seeded at the same density and conditions as described in section 2.4. After 24 h, cells were pre-treated with or without endocytic inhibitors for 2h at 37°C in a 99% humidified atmosphere and 5% (v/v) CO_2. The following endocytic inhibitors (diluted in DMEM/F-12 medium without hormones) were used: 5 µM filipin III (Sigma, St. Louis, USA), 30 µM chlorpromazine hydrochloride (Sigma, St. Louis, USA), 12.5 µM amiloride hydrochloride (Sigma, St. Louis, USA) and 0.3 µM wortmannin (Sigma, St. Louis, USA). Subsequently, culture medium was replaced by fresh culture medium supplemented with EE2-C8 estradiol-BODIPY conjugate. The internalization assay was performed at the same conditions as described in section 2.4. Cells were visualized at 6h using a Ti-U Eclipse inverted microscope. Images treatment and CTCF quantification were also done as mentioned in section 2.4.

2.6.3. Intracellular localization of Steroid-BODIPY in Breast and Prostate cancer cell lines

In order to understand the intracellular localization of steroid-BODIPY conjugates in cancer cells, the nucleus and lysosomes were stained. To this purpose, a fluorescence microscopy assay was performed using Hoechst 33258 dye (Phenol, 4-[5-(4-methyl-1-piperazinyl)[2,5'-bi-1H-benzimidazol]-2'-yl]-, trihydrochloride 23491-45-4) (Molecular Probes® by Life Technologies, Invitrogen, California, USA) for nucleus staining and anti-LAMP-2A antibody (Abcam, Cambridge, UK) to stain lysosomes. Hoechst 33258 is a nuclear dye that binds to DNA and emits blue fluorescence (excitation at 352 nm and emission at 461 nm) (70). On the other hand, LAMP-2A (lysosome-associated membrane glycoprotein 2A) is located at the membrane of lysosomes and is labelled with a secondary antibody Goat anti-rabbit IgG (TRITC - Tetramethylrhodamine isothiocyanante) which emits red fluorescence (excitation at 574 nm and emission at 572 nm) (71,72).

2.6.3.1. Hoechst 33258 and LAMP-2 Staining

Cells seeding and the internalization procedure was done as described previously in section 2.4. Before Hoechst and LAMP-2 staining, cells were fixed with 4% (v/v) paraformaldehyde in PBS 1x solution for 20 min at RT. After that, cells were washed three times with PBS 1x. Permeabilization was done to allow antibodies to enter the cell by using a non-ionic detergent, Triton-X 100 (0.1%) in PBS for 5 min. Cells were washed again three times with PBS 1x.

To stain the nucleus, cells were incubated 15 minutes with 0.0075 mg/mL Hoechst 33258 dye at RT and washed three times with PBS 1x. Then, cells were incubated with bovine serum albumin (BSA) (1%) for 30 min at RT to prevent nonspecific antibody binding. After blocking step, cells were stained with anti-LAMP2A antibody (1:200) for 1h at RT to staining lysosomes. Cells were washed again three times with PBS 1x. Before visualizing at the microscope, cells were incubated with respective secondary antibody Goat anti-rabbit IgG (TRITC) (1:2000) (Abcam, Cambridge, UK) for 30 min at RT and washed three times with PBS 1x. Finally, cells were visualized in PBS 1x using a Ti-U Eclipse inverted microscope. Images of the nucleus were acquired with a DAPI filter (excitation at 375/60 nm in the UV region and emission at 469/60 nm in the blue region), LAMP-2 images with G2A filter (excitation at 535/50 nm in blue region and emission >580 nm) and images of steroid-BODIPY conjugates fluorescence were acquired using a FITC filter (excitation at 480/30 nm in the blue region and emission at 535/45 nm). Fluorescence images were treated with Image J software.

2.7. Internalization of steroid-BODIPY conjugates in a 2D Co-culture

MDA-MB-231, PC-3 cells or Fibroblasts were seeded on 24-well plate in a 1:1 proportion and incubated for 24 h at 37 °C in a 99% humidified atmosphere and 5% (v/v) CO_2. After 24h, the medium was replaced by fresh media (without phenol red) supplemented with 5 µM and 25 µM of compound or 0.05% (v/v) and 0.25% (v/v) DMSO (vector control) for 6 h in same conditions of incubation described before. After 6 h, the culture medium was replaced by fresh medium (without phenol red) and without compound. Cells were visualized at 0 h and 6 h using a Ti-U Eclipse inverted microscope as detailed in section 2.4, as well as images treatment and fluorescence quantification.

2.8. Cell Viability Assays

Cell viability was evaluated by a CellTiter 96 Aqueous One Solution Cell Proliferation Assay (Promega, Madison, USA), a colorimetric method for determining the number of viable cells. In this method, an inner salt, 3-(4,5-dimethylthiazol-2- yl)-5-(3 carboxymethoxyphenyl)-2-(4-sulfophenyl)-2H-tetrazolium (MTS) is bio-reduced into a coloured formazan product that is soluble in culture medium. This conversion is achieved by mitochondrial dehydrogenases (NADPH or NADH) present in metabolically active cells in the presence of the phenazine methosulfate (PMS) that is used as electron coupling reagent. Formazan product amount, measured by absorbance at 490 nm, is directly proportional to the number of living cells in culture medium (73–75).

Cells were harvested and centrifuged as mentioned in section 2.3 when 80% of confluence is reached. For cell viability assays, cells were seeded on a 96-well plate (SPL Life Sciences, South Korea) with a density of $0.75X10^4$ cells/well and incubated for 24 h at 37 °C in a 99% humidified atmosphere and 5% (v/v) CO_2. After 24 h, the medium was replaced by fresh media supplemented

with 50 µM of compound, 0.5% (v/v) DMSO (vector control), or 0.4 µM of doxorubicin (positive control) and incubated for 6 h and 24 h at 37 °C in a 99% humidified atmosphere of 5% (v/v) CO_2. Additional wells were prepared to evaluate compounds sensitivity to the MTS (compounds incubated without cells). After 6 h and 24 h, the compounds were replaced by a reaction mixture of MTS and PMS diluted in fresh medium in a proportion of 100:19:1. After approximately 1 h of incubation, under previously incubation conditions, absorbance at 490 nm was measured directly from 96-well assay plates with a Tecan Infinite F200 microplate reader. Cell viability was calculated in percentage using **Equation 3**.

Equation 3.

$$Cell\ Viability\ (\%) = \frac{Abs\ (Compound) - Abs\ (Vestigial\ Compound)}{Abs\ (DMSO) - Abs\ (Medium)} \times 100$$

2.9. Visible light irradiation

Visible light irradiation was performed in MCF-7 and PC-3 cancer cells and in normal primary Fibroblasts using a continuous 532 nm green diode-pumped solid-state laser (Changchun New Industries Optoelectronics Tech. Co., LTD, Changchun, China) coupled to an optical fibre (76). Cells were seeded on a 96-well plate with a density of $0.75X10^4$ cells/well and incubated for 24 h at 37 °C in a 99% humidified atmosphere and 5% (v/v) CO_2. After 24h, the medium was replaced by fresh phenol red free media supplemented with 25 µM of compound, 0.25% (v/v) DMSO (vector control), or 0.4 µM of doxorubicin (positive control) and incubated for 6 h in same conditions of incubation mentioned before. Then, the medium was replaced by fresh media without phenol red and cells irradiated with green laser for 60 s using a laser diode intensity (LDI) of 2.45 W/cm^2 (controls without irradiation) (76). After laser irradiation, cells were incubated 24 h at 37 °C in a 99% humidified atmosphere and 5% (v/v) CO_2. The effect of visible irradiation on cell viability was evaluated by MTS assay as described in section 2.8.

2.10. Statiscal Analysis

Statistical analysis of data was performed using GraphPad Prism program (version 6.0). The one-way ANOVA test with multiple comparisons was performed to compare the different experimental groups of data.

3. Results and Discussion

3.1. Expression of steroid receptors by Western-Blot

Before assessing the internalization and intracellular tracking of steroid-BODIPY conjugates in normal and cancer cell lines it is important to fully characterize the expression of the respective receptors in each type of cell. For that reason, we quantified, by Western-Blot (see section 2.3), the expression of estrogen α receptor in ER-positive (MCF-7 and PC-3) and in ER-negative (MDA-MB-231 and LNCaP) cancer cell lines, and the expression of the androgen receptor in AR-positive (MCF-7 and LNCaP) and in AR-negative (MDA-MB-231 and PC-3) cancer cell lines and of both hormone receptors in healthy cells (fibroblasts).

3.1.1. Estrogen Receptor α expression

In mammals there are three ERα isoforms: full-length ERα with a molecular weight of 66 kDa and the two truncated isoforms, ERα36 and ERα46 with molecular weights of 36 and 46 kDa, respectively (77). Representative images for ERα protein expression are shown in **Figure 3.1 (A)** and the relative intensity of ERα expression is demonstrated in **Figure 3.1 (B)** (calculated from the quantification of ERα band marked within red squares in **Figure 3.1 (A)**). ER-positive cell line MCF-7 expressed a ~66 kDa protein that corresponds to full-length ERα. Smaller and higher molecular weight bands (~46 kDa and >66 kDa, respectively) were visualized in some ER-positive and ER-negative cell lines. PC-3 cell line, ER-positive, expressed one of the isoforms with a molecular weight of ~46 kDa (ERα46). Uncharacterized bands can be seen at a molecular weight of ~73 kDa, ~90 kDa and ~100 kDa in MCF-7 and MDA-MB-231 cell lysates. The results presented are in agreement with the information available in the literature regarding the studied receptors and cell lines (77,78) - ER-positive cell lines studied, MCF-7 and PC-3, expressed ERα.

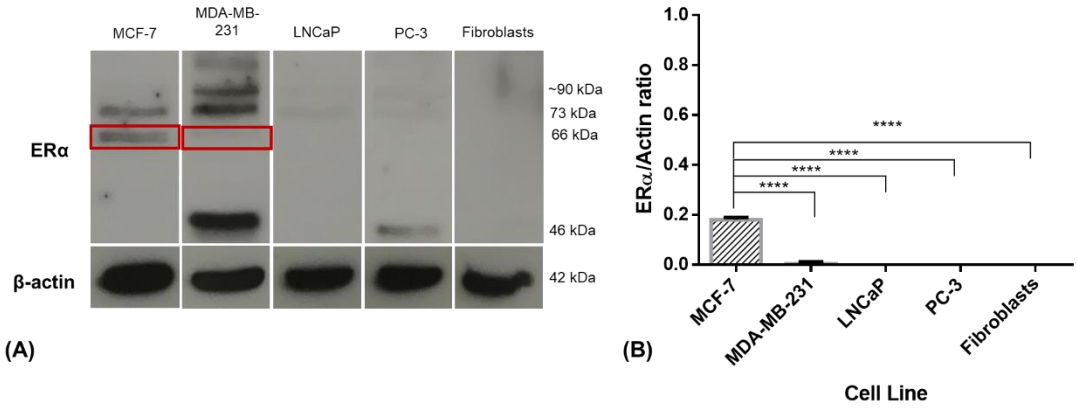

Figure 3.1 - Estrogen α Receptor (ERα) expression in MCF-7, MDA-MB-231, LNCaP, PC-3 cell lines and Fibroblasts. (A) Representative images of western blot results. β-actin was used as control. (B) Relative intensity values (normalized to the β-actin) of ERα66 -in MCF-7, MDA-MB-231, LNCaP, PC-3 cell lines and Fibroblasts. Relative intensity values are expressed as mean ± SEM of two independent experiments each one in duplicate and the statistical significance was evaluated by one-way ANOVA method (**** $P < 0.0001$).

3.1.2.. Androgen Receptor (AR) expression

In addition to ER, several cancer cells also express AR. AR-positive cell lines express an AR protein with a molecular weight of 98 kDa (25). Representative images of AR protein expression are shown in **Figure 3.2 (A)** demonstrating that AR-positive cell lines (MCF-7 and LNCaP) expressed a ~98 kDa protein that corresponds to AR. Relative intensity of AR expression is shown in **Figure 3.2 (B).**

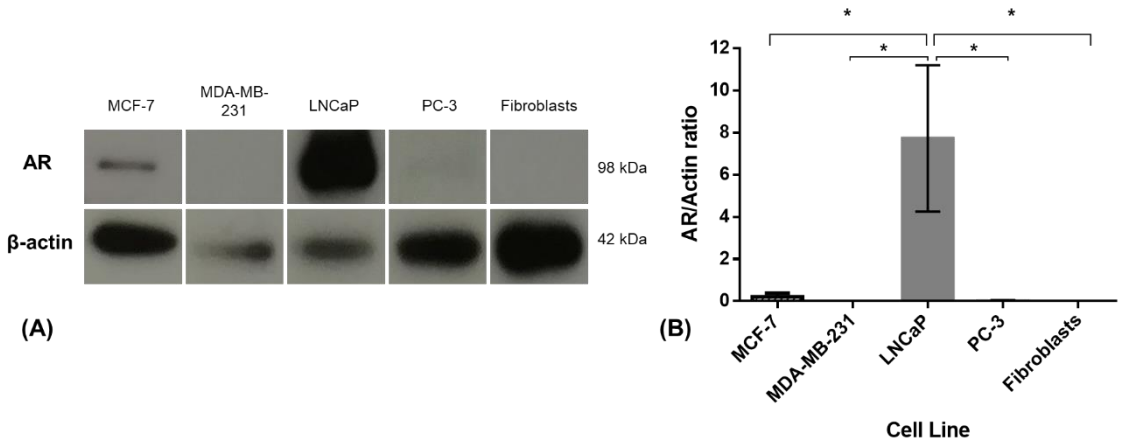

Figure 3.2 - Androgen Receptor (AR) expression in MCF-7, MDA-MB-231, LNCaP, PC-3 cell lines and Fibroblasts. (A) Representative images of western blot results. β-actin was used as control. (B) Relative intensity values (normalized to the β-actin) of AR in MCF-7, MDA-MB-231, LNCaP, PC-3 cell lines and Fibroblasts. Relative intensity values are expressed as mean ± SEM of two independent experiments each one in duplicate and the statistical significance was evaluated by one-way ANOVA method (*P ≤ 0.050).

3.2. Intracellular tracking of steroid-BODIPY conjugates in cancer and normal cells

Estradiol- and androgen analogues conjugated to BODIPY are potential multimodal imaging probes (optical and PET imaging) as well as theranostics (PET and PDT). The intracellular tracking of the studied conjugates in human cells is essential to understand their interactions with biological systems. The conjugates has an UV/Vis absorption spectra that range from 500 to 710 nm and their fluorescence emission properties with a range from 520 to 700 nm (16). Taking advantage of the fluorescence of BODIPY probes, intracellular tracking of the steroid-BODIPY conjugates were studied by fluorescence microscopy.

The six estradiol- and androgen analogues conjugated to BODIPY compounds were tested in four different cancer cell lines and normal cells (fibroblasts) to understand the capability of the conjugates to internalize (dependent or not of the steroid receptors) and their localization inside cancer cells. Each cell line was incubated with 50 μM of steroid-BODIPY conjugates for 0.75h, 2h and 6h and after cells were visualized by fluorescence microscopy in order to quantify the cellular uptake.

3.2.1. Steroid-BODIPY conjugates in breast cancer cells

Most breast cancers over-express hormone receptors in tumor cells. MCF-7 breast cancer cell line is an ER-positive (section 3.1), making it an ideal in vitro model to study hormone response in cancer treatment.

Figure 3.3 shows the fluorescence images of estradiol-BODIPY conjugates in MCF-7 breast cancer cell line and **Figure 3.4** represents the normalized fluorescence intensity values of all steroid-BODIPY conjugates. For simplicity, only the fluorescence images related to estradiol conjugates are represented while the fluorescence images of androgen-BODIPY conjugates in each cell type is shown in **Figure 6.1 of Annex A**.

Generally, the fluorescence of all BODIPY conjugates in cells increased during the 6h of incubations at different rates (**Figure 6.5 (A) of Annex A**). After 6h of incubation, HA-4187 androgen-BODIPY conjugate shows a higher fluorescence intensity compared to the other conjugates. In contrast, androgen-BODIPY conjugate with the lowest fluorescence intensity is HA-4200, a testosterone derivate which typically has low receptor binding affinity for AR compared to 19-nortestosterone analogues (68,77,79).

Despite not having the highest fluorescence intensity, estrogen-derived conjugates internalization rate in the first 2h of incubation is higher compared to androgen conjugates (**Figure 3.4 (A)** and **(B)**; **Figure 6.5 (A) of Annex A**). This might be due to an increased cellular permeability or affinity to estrogen molecules combined with BODIPY dye (31,80). Estradiol-BODIPY conjugate 11β-OMe, a derivate of EE2-C8-BODIPY conjugate, shows a higher cellular uptake than EE2-C8. This derivate, in addition of a long spacer chain introduction that may improve ER-binding, presents a polar methoxy group that may facilitate *in vitro* localization in target cells, and increase the target/non-target ratio of E2 as observed by others *in vivo* (16,67) .

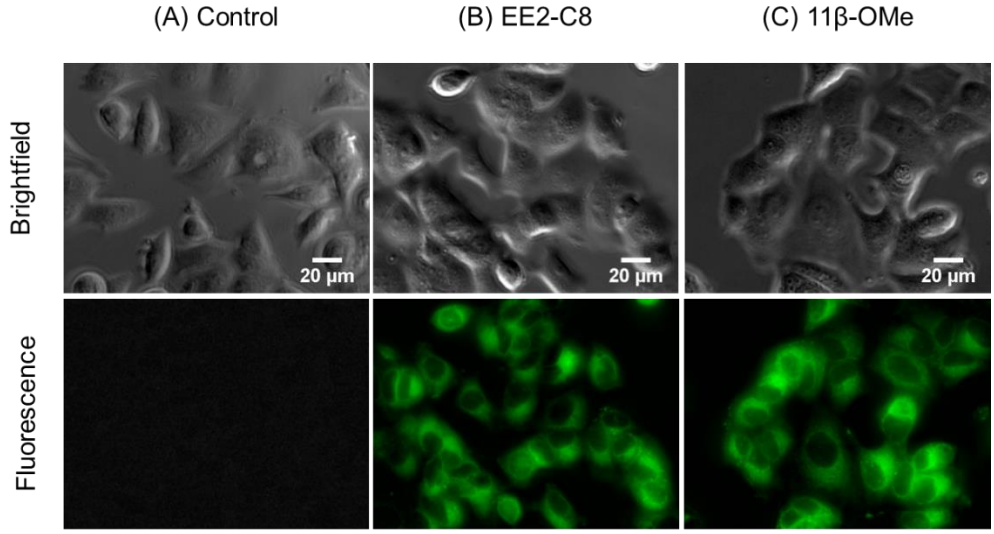

Figure 3.3 - Brighfield and Fluorescence images of steroid-BODIPY conjugates in MCF-7 breast cancer cell line at 6h. MCF-7 cells were seeded for 24h in complete DMEM medium (with Phenol red) supplemented with MEM and then medium was replaced with DMEM without phenol red and (A) 0.5% (v/v) DMSO (control) or 50 µM of (B) EE2-C8 and (C) 11β-OMe.

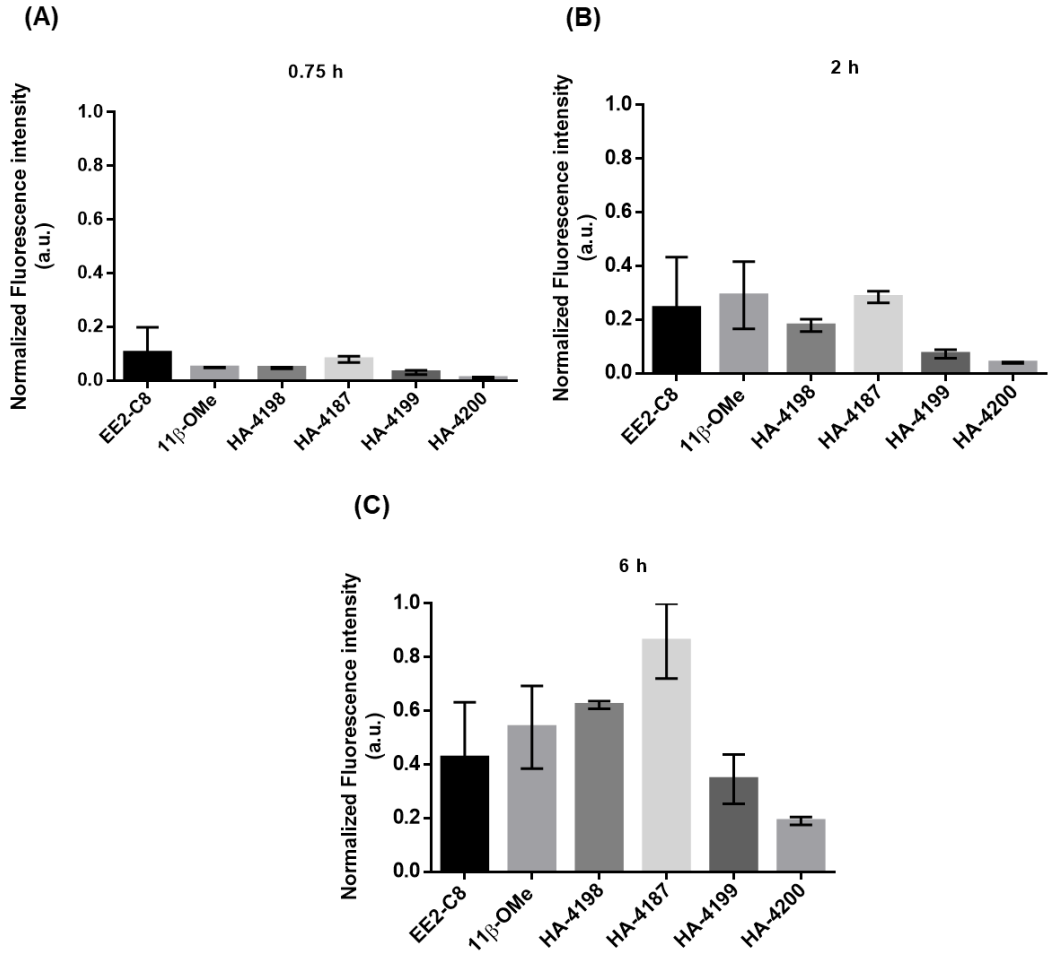

Figure 3.4 - Normalized Fluorescence intensity of MCF-7 cells incubated for (A) 0.75 h, (B) 2 h and (C) 6 h with steroid-BODIPY conjugates. The fluorescence intensity of the cells was corrected for background fluorescence and normalized with vehicle (DMSO), in arbitrary units (a.u.). Results are expressed as mean ± SEM of two independent experiments each one in duplicate.

A specific breast cancer subtype lacking ER, PR and HER2R expression has been defined as triple-negative breast cancer (TNBC) and accounts for10-20% of all breast cancers. MDA-MB-231 is a TNBC cell line that despite some researchers indicate that it expresses AR and others not (81,82), the western-blot results (section 3.1) do not show any AR expression indicating that this cell line may be a good model to compare with MCF7 results concerning all BODIPY conjugates internalization.

Fluorescence microscopy images of steroid-BODIPY conjugates in MDA-MB-231 cells are represented in **Figure 6.2 of Annex A** and the respective normalized fluorescence quantification data of all conjugates are shown in **Figure 3.5**. As stated before, BODIPY is a cell-permeable dye and generally, cellular uptake of these molecules increases with time (**Figure 6.5 (B) of Annex A**) (80,83). As shown in **Figure 6.2 of Annex A** and **Figure 3.5**, all steroid-BODIPY derivates show fluorescence in MDA-MB-231 cells. After 6h of exposure to the conjugates, androgen derivate HA-4187 presented the highest level of fluorescence while the other androgen-BODIPY

conjugate, HA-4200, a testosterone derivate, exhibited the lowest fluorescence level. It is interesting to note that HA-4187 conjugate, a 19-nortestosterone derivate, besides the 17α-ethynyl group also has a 7α-methyl group introduced in steroid skeleton, increasing the binding affinity of the conjugate for AR (68). Concerning the estradiol-BODIPY conjugates, 11β-OMe derivate shows higher fluorescence levels compared to EE2-C8. Due to the introduction of the polar methoxy group, which increase the polarity and water solubility of the 11β-OMe derivate, cellular uptake also seems to increase (83). Altogether, these results may indicate non-specific cellular uptake of the conjugates and the presence of fluorescence in intracellular vesicles suggest an endocytic pathway as the cellular uptake route of the conjugates (37,72,84,85). However, we cannot discharge that some low levels of AR expression (not detect in the western blot, section 3.1) might be associated with some internalization.

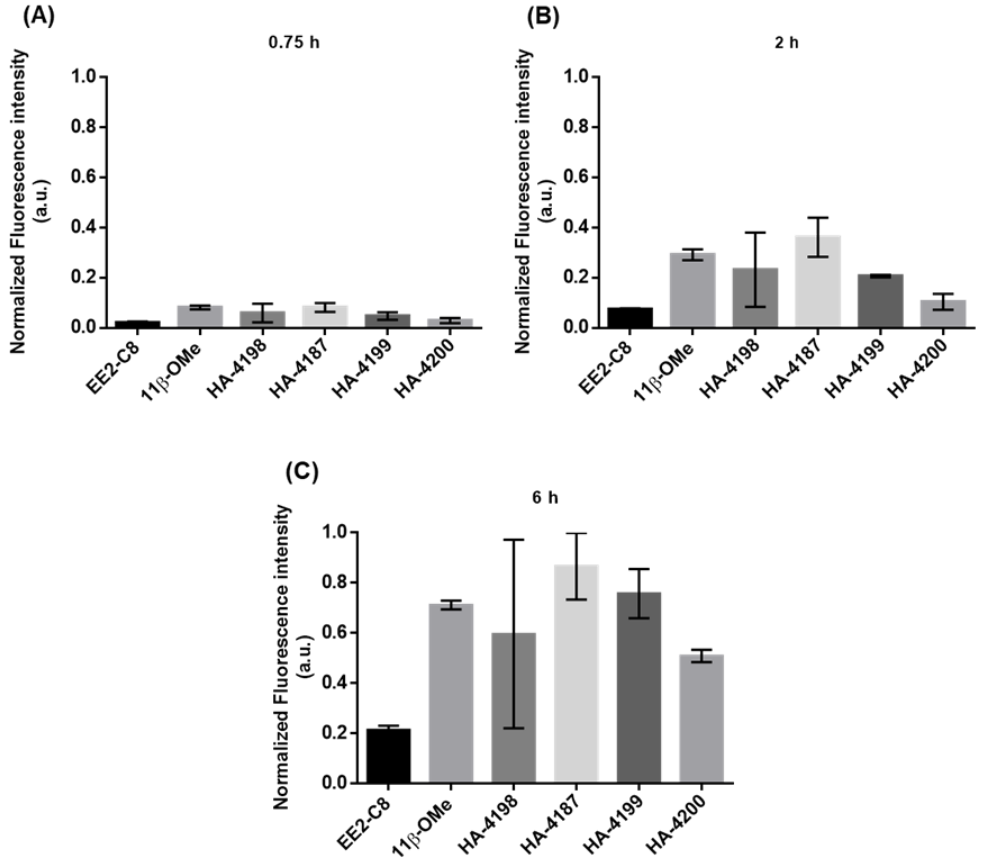

Figure 3.5 - Normalized fluorescence intensity of MDA-MB-231 cells incubated for (A) 0.75 h, (B) 2 h and (C) 6 h with steroid-BODIPY conjugates. The fluorescence intensity of the cells was corrected for background fluorescence and normalized with vehicle (DMSO), in arbitrary units (a.u.). Results are expressed as mean ± SEM of two independent experiments each one in duplicate.

3.2.2. Steroid-BODIPY conjugates in prostate cancer cells

PC-3 cell line is one of the best models to the study androgen-independent prostate cancer, due to its very low or lack of the AR expression (86). This prostate cancer cell line is an ER-positive

model, as mentioned before. Nevertheless, the expression of the classical ER (ERα and ERβ) in this cell line is still under discussion in the literature (78).

Although this cell line is androgen-independent cancer, androgen conjugates do internalize in these cancer cells (**Figure 3.6** and **Figure 6.3 in Annex A**) as well as estradiol conjugates (**Figure 6.3 in Annex A**). The normalized green fluorescence is shown in **Figure 3.6**. As observed with breast cancer cell lines, cellular fluorescence levels of all steroid-BODIPY conjugates increases with the exposure time (**Figure 6.5 (C) of Annex A**). Regarding the estradiol-BODIPY analogues, 11β-OMe derivate shows a much higher cellular fluorescence compared to EE2-C8. These marked differences may be due to the structural differences in the conjugated steroid molecules mentioned before in section 2.1. Despite PC-3 cell line is an AR-negative, cellular uptake of androgen-BODIPY analogues is higher than the fluorescence levels of the EE2-C8 estradiol-BODIPY conjugate. HA-4187 conjugate has higher cellular uptake than the other androgen conjugates possibly because of structural alterations of the steroid skeleton (section 2.1). As in MDA-MB-231 cells, fluorescence images of PC-3 cells also shows the accumulation of conjugates in intracellular vesicles indicating once again that internalization of BODIPY conjugates independently of the receptors might be occurring (**Figure 3.5, 3.6** and section 3.2.1).

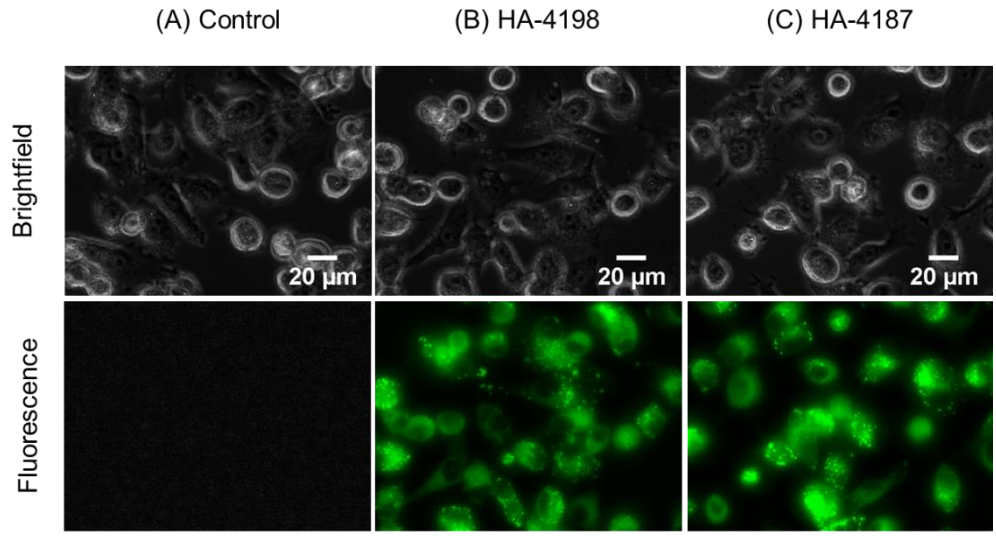

Figure 3.6 - Brighfield and Fluorescence images of estradiol-BODIPY conjugates in PC-3 cells at 6h. PC-3 cells were seeded for 24h in complete RPMI medium (with Phenol red) and then medium was replaced with RPMI without phenol red and (A) 0.5% (v/v) DMSO (control) or 50 µM of (B) EE2-C8 and (C) 11β-OMe

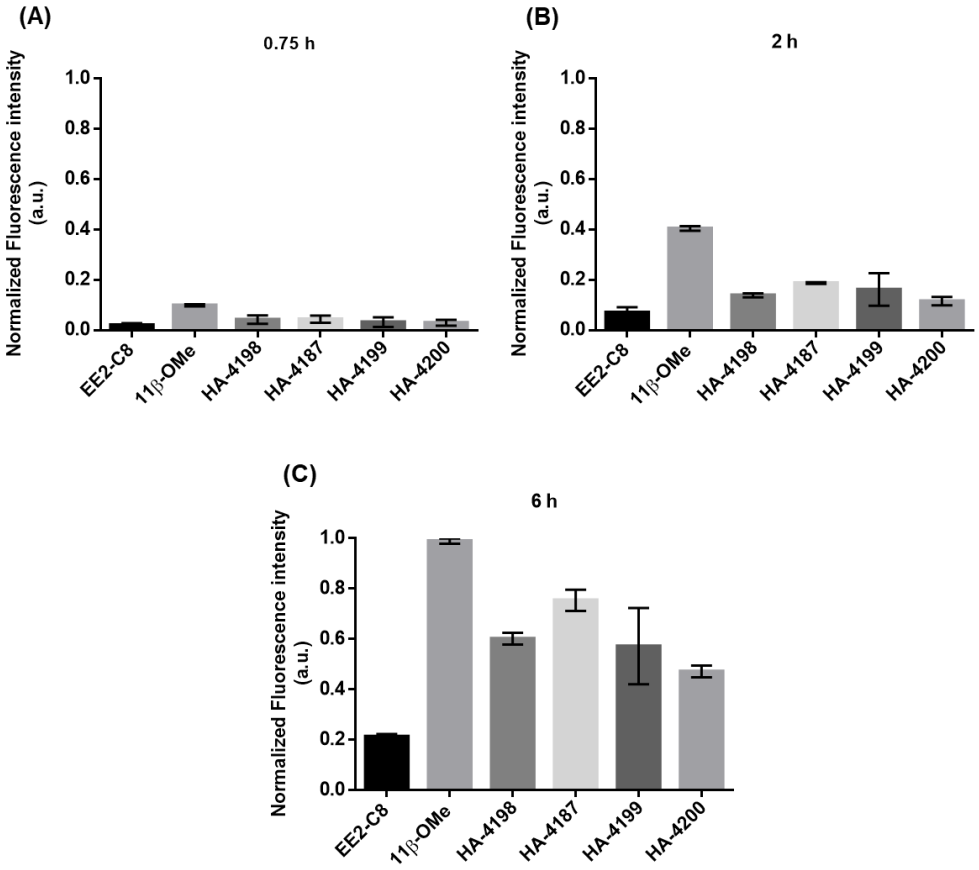

Figure 3.7 - Normalized fluorescence intensity of PC-3 cells incubated for (A) 0.75 h, (B) 2 h and (C) 6 h with steroid-BODIPY conjugates. The fluorescence intensity of the cells was corrected for background fluorescence and normalized with vehicle (DMSO). Results are expressed as mean ± SEM of two independent experiments each one in duplicate.

LNCaP prostate cancer cell line is also used in this study as *in vitro* model of androgen dependent prostate cancer. LNCaP is the most widely used AR-positive cell line due to significant expression levels of AR (87) and is ER-negative. Fluorescence images of cellular uptake of steroid-BODIPY derivates in LNCaP cells are shown in **Figure 6.4 of Annex A** and fluorescence intensity quantification are represented in **Figure 3.8**. As observed with the other studied cell lines, the intensity of green fluorescence increases with the exposure time in LNCaP cells for all steroid-BODIPY conjugates (**Figure 3.8** and **Figure 6.5 (D) in Annex A**). Androgen-BODIPY conjugates, HA-4198 and HA-4187, as well as estradiol-BODIPY derivate 11β-OMe show a high cellular fluorescence levels compared to the EE2-C8 conjugate (**Figure 3.8** and **Figure 6.4 in Annex A**). Once again, because this cell line is ER-negative, we were not expecting to see such a high level of fluorescence for the estradiol-BODIPY derivate 11β-OMe, which indicates some independent cellular uptake mechanism. However, the high level of fluorescence in **Figure 3.8** with this cell line may indicate that the concentration used for the assays (50 μM) is very high leading to a saturation of the fluorescence signal.

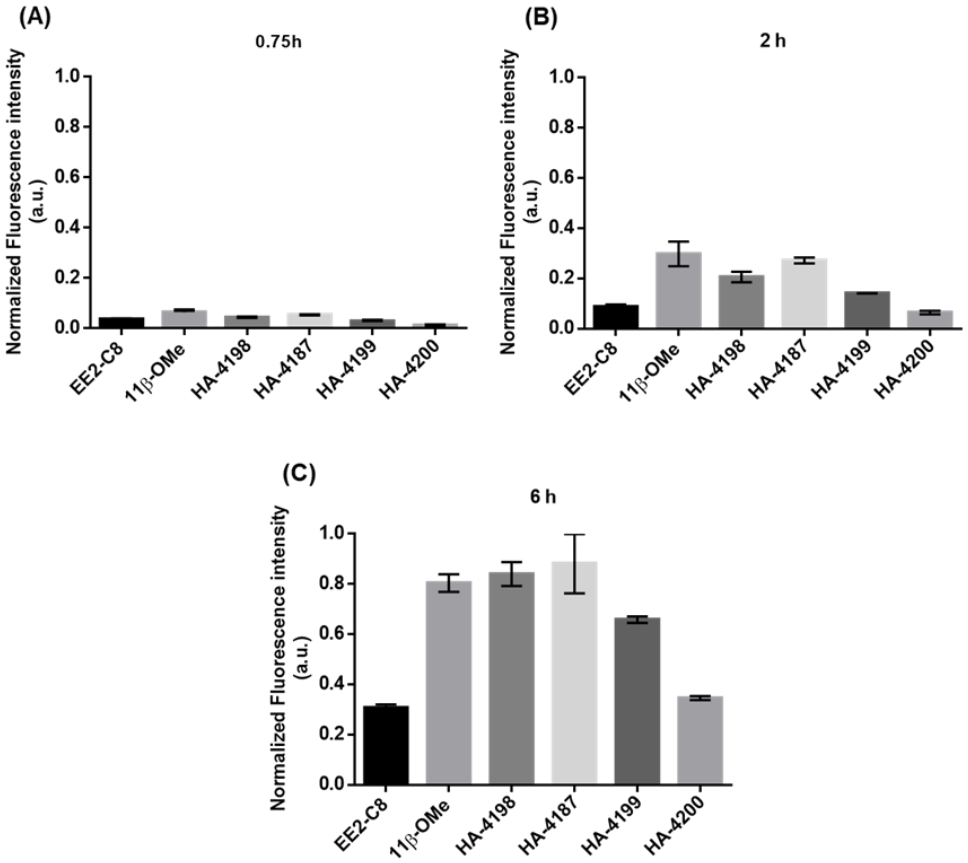

Figure 3.8 - Normalized fluorescence intensity of LNCaP cells incubated for (A) 0.75 h, (B) 2 h and (C) 6 h with steroid-BODIPY conjugates. The fluorescence intensity of the cells was corrected for background fluorescence and normalized with vehicle (DMSO), in arbitrary units (a.u.). Results are expressed as mean ± SEM of two independent experiments each one in duplicate.

Considering all these non-specific internalizations of the BODIPY conjugates observed in all the different cancer cell lines tested so far, we decided also to study the internalization of these conjugates in a non-tumor cell type of different origin, primary dermal fibroblasts, a mesenchymal cell line.

3.2.3. Steroid-BODIPY conjugates in primary normal Fibroblasts

All the internalization studies in fibroblasts were evaluated after 6 h of incubation with the conjugates (maximum level of fluorescence attained with the other tumor cell models) and the results are shown in **Figure 3.9** and **Figure 6.6 of Annex A** and the normalized fluorescence intensity in **Figure 3.10**. As demonstrated in green fluorescence images, EE2-C8-BODIPY (estradiol derivate) conjugate has a higher intensity compared to HA-4198 (androgen derivate). However, when analyzing the normalized fluorescence intensity (**Figure 3.10**) a different result is observed. Except the EE2-C8 and HA-4200 (testosterone derivate), with the lower fluorescence intensity, all conjugates show similar fluorescence levels in in fibroblasts (**Figure 3.10**). Similar to the results in the cancer cell models, a green fluorescence is observed for all the BODIPY conjugates in fibroblasts (**Figures3. 9 and 3.10** and **Figure 6.6 in Annex A**), that might be due

to some cell permeability to BODIPY conjugates (80) or endocytosis (discussed further in section 3.4).

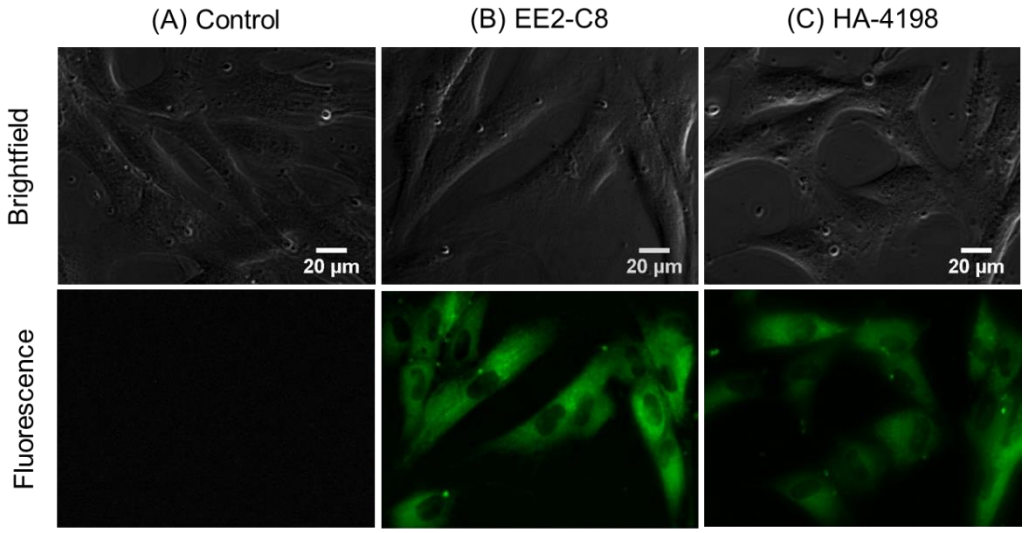

Figure 3.9 - Brightfield and fluorescence of steroid-BODIPY conjugates in Fibroblasts (normal cells) at 6h. Fibroblasts were seeded for 24h in complete DMEM medium (with Phenol red) and then medium was replaced with DMEM without phenol red and (A) 0.5% (v/v) DMSO (control) or 50 µM of (B) EE2-C8 and (C) HA-4198.

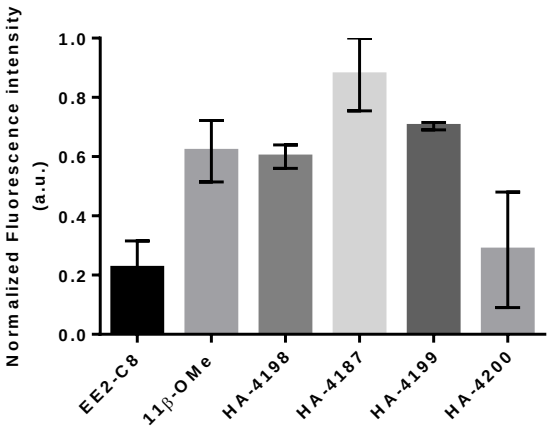

Figure 3.10 - Normalized fluorescence intensity of Fibroblasts incubated for 6 h with steroid-BODIPY conjugates. The fluorescence intensity of the cells was corrected for background fluorescence and normalized with vehicle (DMSO). Results are expressed as mean ± SEM of two independent experiments each one in duplicate.

3.3. Internalization of Steroid-BODIPY with specific inhibitors

Considering all the previous non-specific interaction/internalization of steroid-BODIPY conjugates in breast and prostate tumor cell lines and also in fibroblasts and to further understand if some of the cellular fluorescence might be due to a specific interaction with the androgen and/or estrogen receptors the same analysis was performed but in this case cells were previously incubated with the specific inhibitors of the steroid receptors, such as estradiol (E2) and testosterone (T) in breast

cancer cells and prostate cancer cells, respectively. By blocking the receptors with molecules that have a higher binding affinity for them, this study is crucial to understand the affinity of our BODIPY conjugates for those receptors.

In order to quantify the fluoresce intensity of conjugates in breast and prostate cancer cells, cells were treated with and without 10 μM of specific inhibitor for 1 h and then with the steroid-BODIPY conjugates during 6h. After 6h of incubation, cells were visualized by fluorescence microscopy.

First, preliminary experiments were performed with a concentration of 50 μM of steroid-BODIPY conjugates (as in section 3.2). However, with this concentration and for some cells and conjugates a high saturation of fluorescence intensity was observed (absence or presence of the inhibitors) not allowing a good quantitative measure of the differences, if existent. For this reason, we decided to use half of the initial concentration (25 μM) to continue these studies.

Considering the previous results (section 3.2) we decided to perform the assay in breast cancer cell lines with the estradiol-BODIPY conjugates (EE2-C8 and 11β-OMe). The specific inhibitor used in this study was E2 which is a key regulator of growth, differentiation and function in a variety of target tissues and your principal biological effects are mediated through estrogen receptors. This estradiol molecule has 100% of relative affinity binding (RBA) for ERα, as demonstrated in (67). Thus, E2 was used as ERα blocking in order to study other estradiol analogues.

In MCF-7, an ER-positive cell line, both estradiol conjugates internalization decreases when the cells were incubated with E2 - **Figure 3.11 (A) and (B)**. Similar results were observed MDA-MD-231 (**Figure 3.12 (A) and (B)**). However, in MDA-MD-231, an ER-negative cell line, both estradiol conjugates internalization decreases with E2 pre-treatment (**Figure3.12**). In both breast cancer cell lines, the 11β-OMe conjugate has a higher fluorescence intensity than the EE2-C8 conjugate (**Figures 3.11 and 3.12**). Recently, was shown that EE2-C8-BODIPY conjugates have the highest RBA for the ERα among a diversity of EE2-BODIPY conjugates (67)due to the presence of a long spacer chain at the 17α-position (16). Besides this addition that improve ER-binding, a methoxy group was also introduced to the structure skeleton of EE2-BODIPY conjugate. Therefore, 11β-OMe derivate of conjugate EE2-BODIPY has peculiar interest since such substitution could facilitate in vivo localization in target tissues (16,67).

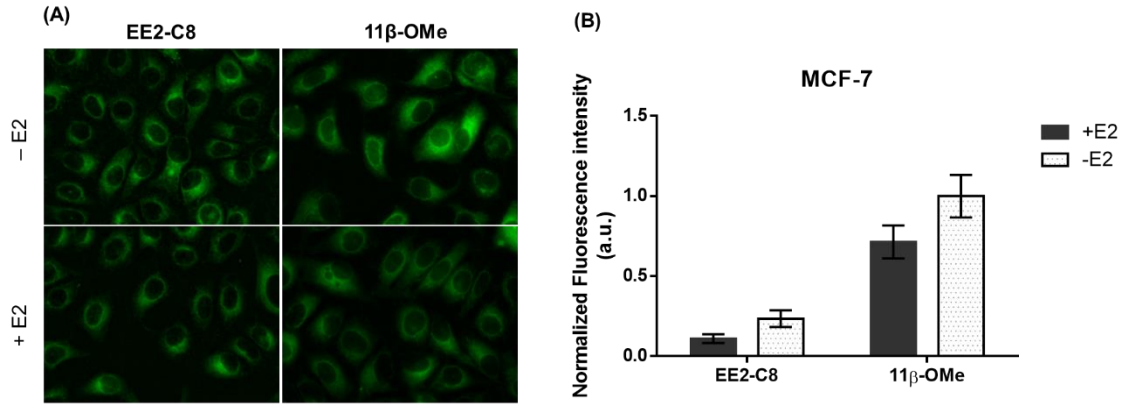

Figure 3.11 - Internalization of estradiol-BODIPY derivates (EE2-C8 and 11β-OMe) in MCF-7 breast cancer cell line with or without E2. MCF-7 cells were incubated 1h with specific inhibitor (+E2) or without inhibitor (-E2). After 6h of EE2-C8 and 11β-OMe incubation, (A) cells were visualized using an inverted microscope and (B) fluorescence intensity was quantified. Fluorescence intensity of the cells was corrected for background fluorescence and normalized with vehicle (DMSO). Higher fluorescence intensity was set as 1 and cellular uptake was determined as function of that. Results are expressed as the mean ± SEM of two independent experiment in duplicate.

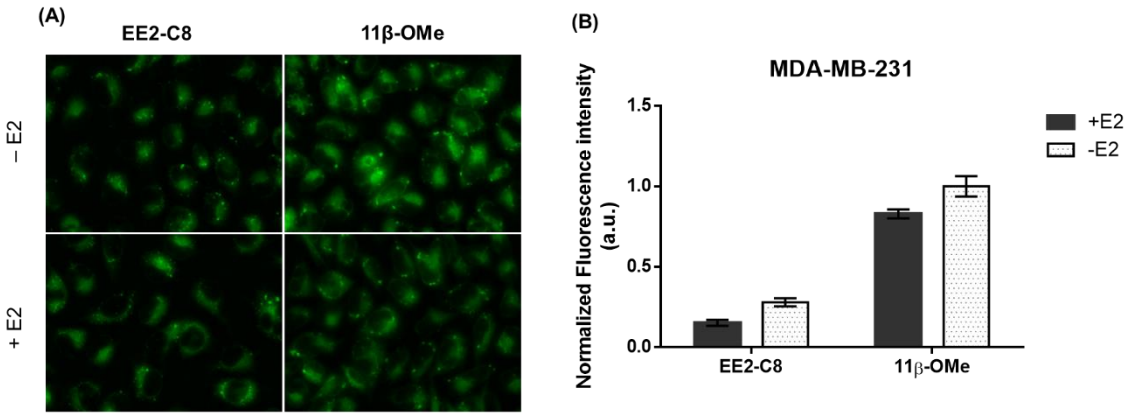

Figure 3.12 - Internalization of estradiol-BODIPY derivates (EE2-C8 and 11β-OMe) in MDA-MB-231 breast cancer cell line with or without E2. MDA-MB-231 cells were incubated 1h with specific inhibitor (+E2) or without inhibitor (-E2). After 6h of EE2-C8 and 11β-OMe incubation, (A) cells were visualized using an inverted microscope and (B) fluorescence intensity was quantified. Fluorescence intensity of the cells was corrected for background fluorescence and normalized with vehicle (DMSO). Higher fluorescence intensity was set as 1 and cellular uptake was determined as function of that. Results are expressed as the mean ± SEM of two independent experiment in duplicate.

In prostate cancer cell lines, we have performed similar experiments with the androgen-BODIPY conjugates (HA-4198 and HA-4187) and using as the specific inhibitor testosterone (T). These androgen-BODIPY conjugates are parent compounds of 17α-ethynyl-nortestosterone (17α-ENT) that showed a significant binding affinity for AR and PgR (68). In general, 19-nortestosterone derivates exhibit higher binding affinity than corresponding testosterone analogs. Thus, two 19-nortestosterone derivates were chosen to perform this study in prostate cancer cells, HA-4198 (-19-nortestosterone) and HA-4187 (-7α-methyl-19-nortestosterone).

In PC-3 cells, an AR-negative, both androgen conjugates internalization decreases when the cells were incubated with T as shown in **Figure 3.13 (A) and (B)**. In LNCaP cells, similar results were demonstrated (**Figure 3.14 (A) and (B)**). In these AR-positive cells, both androgen conjugates fluorescence also decreased with T treatment. Previous studies demonstrated that receptor binding data expose a systematic pattern in RBA values caused by structural modifications of the steroid skeleton. An introduction of a 7α-methyl group to 19-nortestosterone increased binding affinity to the AR (68). Consequently, in LNCaP cells, with elevated AR expression, HA-4187 internalization was higher than HA-4198, since the first has 7α-methyl group.

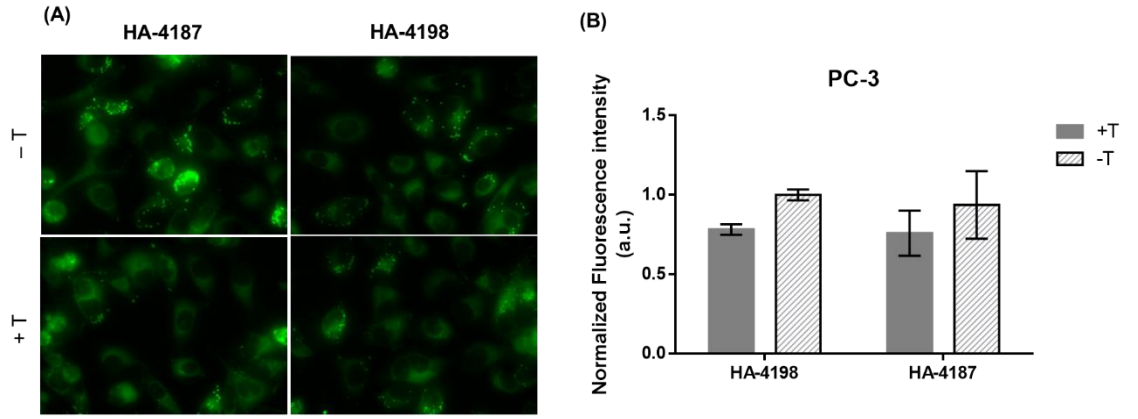

Figure 3.13 - Internalization of androgen-BODIPY derivates (HA-4198 and HA-4187) in PC-3 prostate cancer cell line with and without T. PC-3 cells were incubated 1h with specific inhibitor (+T) or without inhibitor (-T). After 6h of HA-4198 and HA-4187 incubation, (A) cells were visualized using an inverted microscope and (B) fluorescence intensity was quantified. Fluorescence intensity of the cells was corrected for background fluorescence and normalized with vehicle (DMSO). Higher fluorescence intensity was set as 1 and cellular uptake was determined as function of that. Results are expressed as the mean ± SEM of two independent experiment in duplicate.

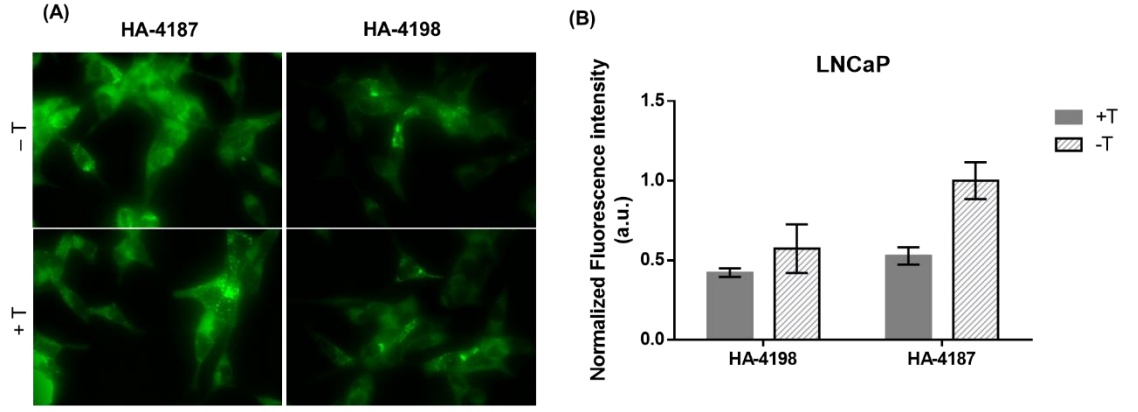

Figure 3.14 - Internalization of androgen-BODIPY derivates (HA-4198 and HA-4197) in LNCaP prostate cancer cell line with or without T. LNCaP cells were incubated 1h with specific inhibitor (+T) or without inhibitor (-T). After 6h of HA-4198 and HA-4187 incubation, (A) cells were visualized using an inverted microscope and (B) fluorescence intensity was quantified. Fluorescence intensity of the cells was corrected for background fluorescence and normalized with vehicle (DMSO). Higher fluorescence intensity was set as 1 and cellular uptake was determined as function of that. Results are expressed as the mean ± SEM of two independent experiment in duplicate.

To conclude, in the presence of specific inhibitors a decreased of the fluorescence intensity of steroid-BODIPY conjugates in all cancer cell lines is observed. This result suggest that the steroid-BODIPY conjugates have some degree of affinity for the respective hormone receptors. However, for a better quantification of this affinity other type of tests such as RBA assays with different cell lines and all studied conjugates would be needed.

All the data so far clearly indicates that the BODIPY conjugates are entering cells by androgen or estrogen receptors independent mechanisms. Considering this, we decided to further explore energy dependent or independent cellular uptake and trafficking of steroid-BODIPY conjugates.

3.4. Assessment of cell uptake and trafficking of steroid-BODIPY conjugates

3.4.1. Active vs. passive transport

As demonstrated in previous results, all steroid-BODIPY conjugates are able to enter cells. Thus, in order to better understand the energy dependence of the transport mechanism of the conjugates through the cell membrane, the internalization of conjugates at two temperatures (4 and 37 °C) was studied. Low temperature can reduce cell metabolism and consequently block the ATP production by interfering with the metabolic pathways of the cells (88). It is known that the active transport process is minimal at 0-4 °C, and optimal at 37 °C. Therefore, when cellular uptake of a compound occurs at 37 °C but not at 4 °C, it has been usually assumed that the transport is carrier mediated (89).

As shown in **Figure 3.15**, cellular uptake of all conjugates by PC-3 cells, at a low temperature, was reduced relative to the cellular uptake at 37 °C (see **Figure 6.7 in Annex B**). These results indicate that the internalization of steroid-BODIPY conjugates is an energy-dependent process.

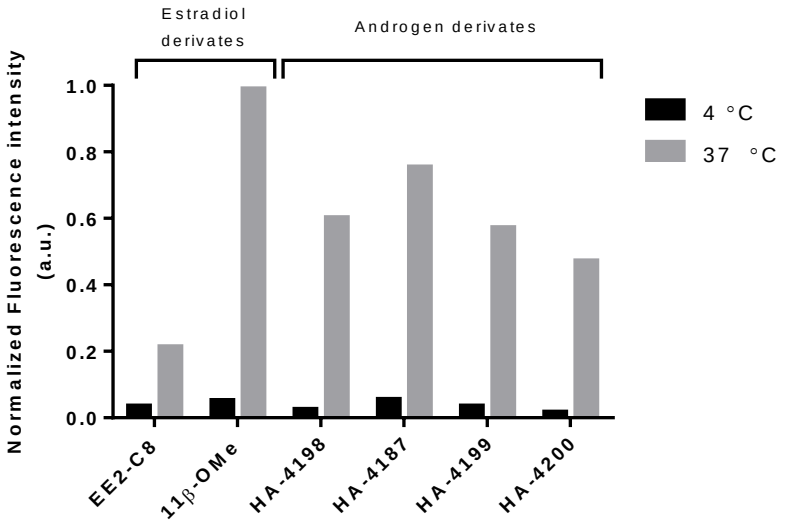

Figure 3.15 - Internalization of steroid-BODIPY conjugates in PC-3 cells at 4 °C or 37 °C during 6 h. PC-3 cells were seeded for 24h in complete RPMI medium (with Phenol red) and then medium was replaced with RPMI without phenol red and 50 µM of estradiol derivates (EE-C8 and 11β-OMe) or androgen derivates (HA-4198, HA-4187, HA-4199 and HA-4200) incubated at 4 °C or 37 °C. After 6 h of conjugates incubation, cells were visualized an inverted microscope and fluoresce intensity was quantified. Fluorescence intensity of the cells was corrected for background fluorescence and normalized with vehicle (DMSO). Results are expressed as mean of one independent experiment in duplicate.

3.4.2. Inhibition of endocytosis of steroid-BODIPY conjugates in the triple-negative breast cell line (MDA-MB-231)

Considering that endocytic processes do not occur efficiently with temperatures below 10 °C (90), results from section 3.4.1 conclude that the internalization of the steroid-BODIPY conjugates is an energy-dependent process, and, as such, the mechanism of internalization of these conjugates might be performed by endocytic pathways. In order to demonstrate that BODIPY conjugates are internalized by endocytosis and which endocytosis pathway is involved (caveolae-mediated endocytosis, clathrin-mediated endocytosis and macropinocytosis), different pharmacologic inhibitors of endocytosis (amiloride (EIPA), wortmannin, chlorpromazine and filipin) were used (36,88).

MDA-MD-231 cells, were pre-treated for 2 h with four endocytic inhibitors, 12.5 µM of amiloride and 0.3 µM of wortmannin (inhibitors of macropinocytosis), 30 µM chlorpromazine (inhibitor of clathrin-mediated endocytosis) and 5 µM of Filipin (inhibitor of caveolae-mediated endocytosis), prior to the incubation of estradiol conjugate EE2-C8. MDA-MB-231 cells were used due to their lack of estrogen receptors thus allowing for a better understanding of the results. After EE2-C8 incubation, the cells were visualized by an inverted microscope and the green fluorescence intensity was quantified. **Figure 3.16** shows the results of EE2-C8 endocytosis inhibition in MDA-MB-231 breast cancer cells. EE2-C8 internalization in the absence of any inhibitor (control) was set as 1 and the cellular uptake of EE2-C8 in presence of each endocytosis inhibitor was determined as function of the control.

Amiloride blocks macropinocytosis, which acts as an inhibitor of the NA+/H+ pump at the surface of the cell (38,88). The effect of amiloride on the cellular uptake of EE2-C8 (**Figure 3.16**) had no impact on the internalization of EE2-C8 conjugate. Wortmannin is also a macropinocytosis inhibitor but with a different blocking mechanism of the endocytic pathway. Wortmannin is a potent inhibitor of phosphoinositide 3-kinases (PI3KS) and it is widely used in trafficking studies (91). Hence, cellular uptake with this inhibitor decreased compared with the amiloride inhibitor, as shown in **Figure 3.16**. Interestingly, the green fluorescence intensity decreased with both clathrin- and caveolae-mediated endocytosis inhibitors, chlorpromazine and filipin, respectively (**Figure 3.16**). Chlorpromazine is a cationic amphipathic drug that interacts with clathrin from the coated pits that causes assembly on endosomal membranes, leading to clathrin-mediated endocytosis inhibition in some cells (38). However, Filipin, a cholesterol-binding agent inhibiting caveolae-mediated endocytosis (38), has a greater decrease in the uptake of EE2-C8 BODIPY conjugate suggesting that the endocytic pathway of the conjugates might be in part also mediated by caveolae.

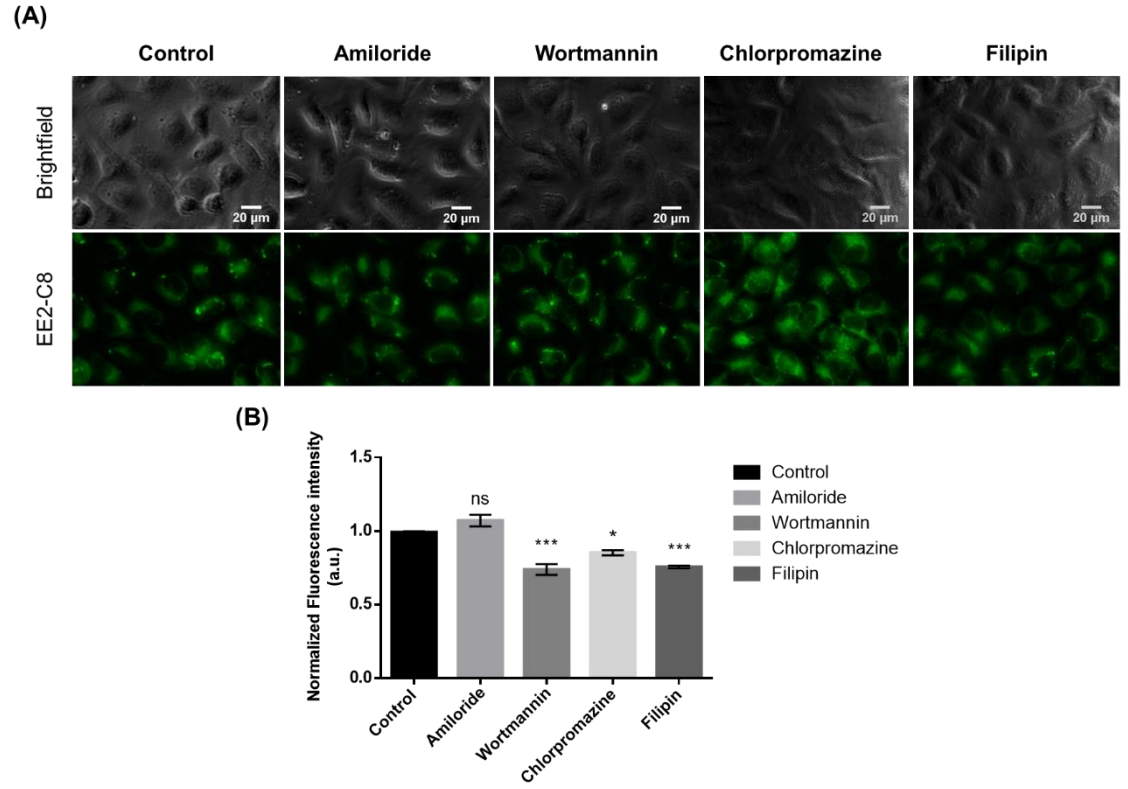

Figure 3.16 - Inhibition of endocytosis of EE2-C8 estradiol-BODIPY conjugates in MDA-MB-231 cell line. MDA-MB-231 cells were incubated 2 h without endocytosis inhibitor (control) or with four different endocytosis inhibitors (Amiloride, Wortmannin, Chlorpromazine and Filipin. Then, cells were incubated for 6 h with 0.5% (v/v) DMSO or 50 µM of EE2-C8. Cells were visualized on inverted microscope and images of conjugate channel with blue excitation (green) (A) and fluorescence intensity was quantified (B). The presented fluorescence images were treated using Image J software. Fluorescence intensity of the cells was corrected for background fluorescence and normalized with vehicle (DMSO). Results are expressed as the mean ± standard deviation of one independent experiment each one in duplicate. The statistical significance was evaluated by one-way ANOVA method (ns – not significant, * $P \leq 0.05$, *** $P \leq 0.001$).

Most steroid receptors are situated in nucleus of the cells. However, new data reported that a small proportion (approximately 5%) of different steroid receptors localized to the cell membrane, namely ERs, PR and AR, and in cytosol (92) .In addition, it has been reported that receptors for estrogen, androgen and progesterone forms complexes at the plasma membrane and in the nucleus in breast and prostate cancer cells, influencing tumor cell biology. In previous reports it was demonstrated that membrane pools of steroid receptors are associated with a caveolin-1 (CAV1) structural coat protein of caveolae (92). A relevant example, Oestradiol is highly concentrated in isolated caveolae. Consequently, it immediately engages ERα bound to caveolin-1, which serves as a scaffold for membrane-localized signalling molecules (92). Although lacking ER expression, caveolae-mediated endocytosis is a possible endocytic pathway for cellular uptake of the studied conjugates in this cell line as well as for the other cell lines. However, more tests should be carried out to check cellular trafficking of these conjugates, such as the use of different endocytic inhibitors concentrations (88).

3.4.3. Intracellular localization of Steroid-BODIPY in Breast and Prostate cancer cell lines

As demonstrated in section 3.4.2, one of the possible mechanism of BODIPY conjugates uptake is via endocytosis. In this mechanism, the cells internalize the cell membrane along with cell surface receptors and soluble molecules. Lysosomes constitute the final stage for the degradative endocytic pathway. The involvement of these functional organelles in cancer in the last decades have become marked, allowing new developments for cancer therapy (84).

Lysosome-associated membrane glycoprotein 2 (LAMP-2), which is located at the lysosomal membrane, maintains lysosomal stability, participates in autophagy and is crucial for lysosomal function. The efficiency of lysosomal function regulates cancer cells. These cellular compartments digest and recycle extracellular and intracellular materials. A decrease of LAMP-2 protein levels provokes the permeabilization of the lysosomal membrane and disturbs the cells leading to the lysosomal cell death pathway. With the tumour progression, a variety of cancer cell lines are associated with enhanced LAMP-2 levels (72,93,94). Previous evidence suggests that steroid receptors can exist in different subcellular locations and therefore required for complete action of steroid hormones (92).

In order to understand the intracellular localization of steroid-BODIPY after cellular uptake, cancer cells were stained with a dye selective for the nucleus (Hoechst 33258, blue) and a lysosomes-selective dye (LAMP-2, red), respectively. Breast and prostate cancer cell lines mentioned before were stained and visualized by fluorescence microscopy. Estradiol-BODIPY conjugates (EE2-C8 and 11β-OMe) were tested in breast cancer cell lines and androgen-BODIPY conjugates (HA-4198 and HA-4187) were investigated in prostate cancer cell lines.

Figure 3.17 shows the co-localization of EE2-C8 and 11β-OMe estradiol-BODIPY conjugates with lysosomes in MCF-7 cells after LAMP-2 incubation. Co-localization of estradiol conjugates with lysosomes dye is also demonstrated in MDA-MB-231 cells (**Figure 6.8 in Annex B**). In breast cancer cells, cellular distribution of estradiol-BODIPY conjugates is not uniform. However, cellular distribution in MCF-7 cells appears to be more uniform than in MDA-MB-231 TNBC cells. Although non-uniform cytosolic distribution, these conjugates show an apparent exclusion from the nucleus, with an accentuated accumulation around nuclear membrane (increased fluorescence intensity). Furthermore, co-localization in breast cancer cells are displayed green conjugates fluorescence overlapped with the red LAMP-2 fluorescence, suggesting that the estradiol conjugates aggregated in the lysosomal vesicles. In contrast to MCF-7 cells, MDA-MB-231 cells showed a greater accumulation in lysosomal vesicles due to the formation of the aggregates demonstrated in **Figure 6.8 of Annex B**. Additionally, the difference in co-localization is also noted between EE2-BODIPY conjugate and its 11β-OMe derivate which exhibit a marked co-localization in both breast cancer cells. As shown in cellular uptake studies (**Section 3.2.1**), has a higher cellular uptake than EE2-C8.

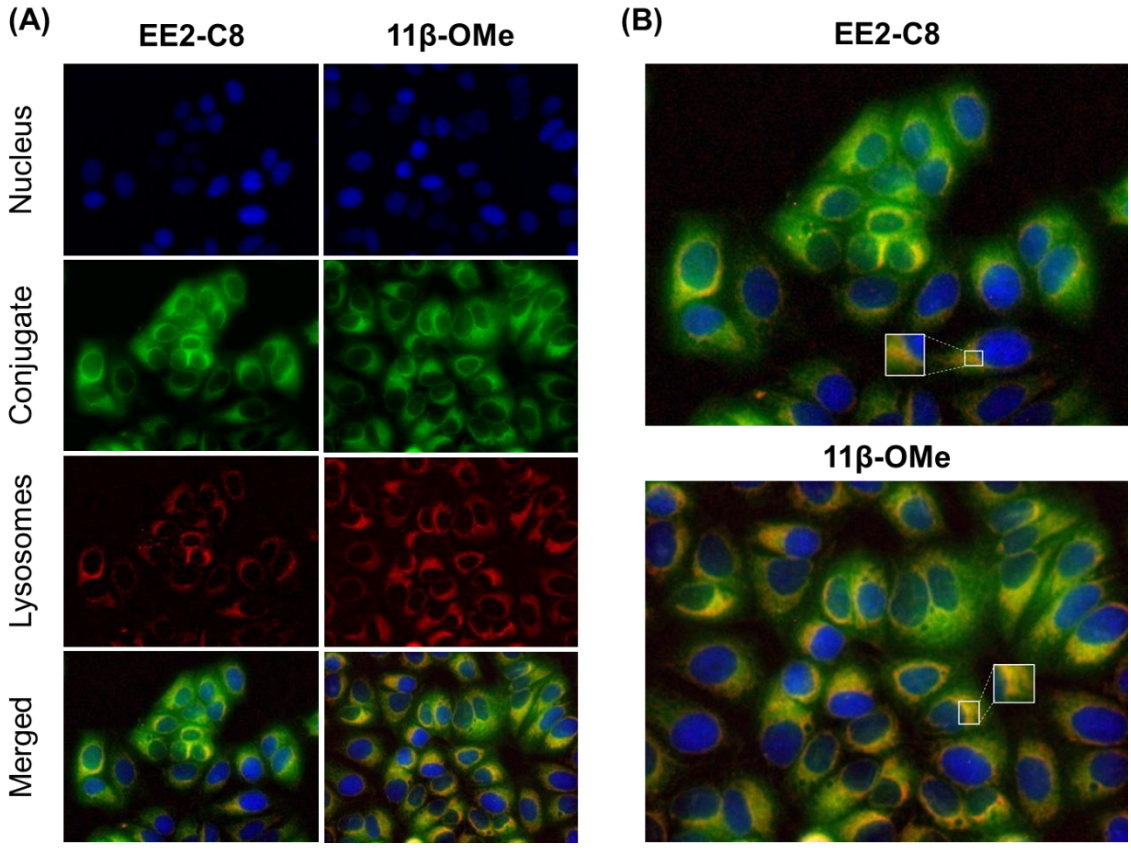

Figure 3.17 - Internalization and localization of estradiol-BODIPY conjugates (EE2-C8 and 11β-OMe) in MCF-7 breast cancer cell line at 6h. Cells were stained with Hoechst 33258 (nucleus marker) and LAMP-2 (lysosome marker). Cells were visualized on inverted microscope and images of Hoechst channel were acquired with UV excitation (blue), LAMP-2 channel with green excitation (red) and conjugate channel with blue excitation (green). The presented fluorescence images were treated using Image J software.

The co-localization of androgen-BODIPY conjugates (HA-4198 and HA-4187) with lysosomes in PC-3 prostate cancer cells are displayed in **Figure 3.18**. Additionally, co-localization of these androgen conjugates with lysosomes is also shown in LNCaP cells (**Figure 6.9 of Annex B**). The results for androgen-BODIPY conjugates in prostate cancer cells are similar to the results presented before for estradiol conjugates in breast cancer cells. However, androgen conjugates accumulation around nuclear membrane is much lower in prostate cancer cells than in breast cancer cells, presenting also an uneven cytosolic distribution. In androgen-dependent prostate cancer cells (LNCaP), the conjugates cellular uptake is saturated and so there is some difficulty in visualizing the overlap of green conjugate fluorescence with red LAMP-2 fluorescence. Nevertheless, the presence of conjugate aggregates that may be lysosomal vesicles is notorious.

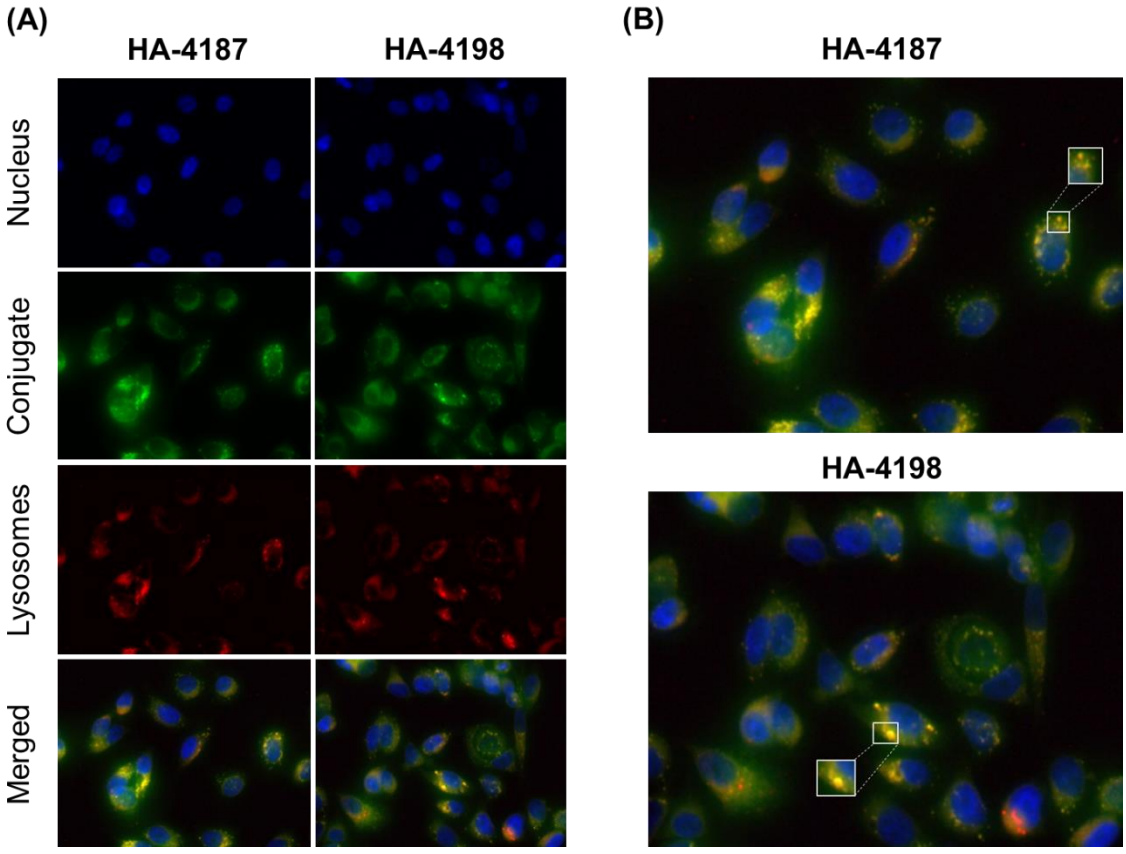

Figure 3.18 - Internalization and localization of androgen-BODIPY conjugates (HA-4198 and HA-4187) in PC-3 prostate cancer cell line at 6h. Cells were stained with Hoechst 33258 (nucleus marker) and LAMP-2 (lysosome marker). Cells were visualized on inverted microscope and images of Hoechst channel were acquired with UV excitation (blue), LAMP-2 channel with green excitation (red) and conjugate channel with blue excitation (green). The presented fluorescence images were treated using Image J software.

With this study, there may be an idea of the intracellular location of the conjugates in cancer cells. However, in order to fully understand the localization of these conjugates, it would be necessary

to perform confocal microscopy and additional co-localization assays (isolation of different sub-cellular fractions and quantification of the conjugates in those fractions).

In conclusion, these conjugates could be internalized through claveolae-mediate endocytic routes, as demonstrated in section 3.4.2, and shuttle to a specific intracellular compartment, such as lysosomes (72). Release of lysosomal enzymes can result in lysosomal death, apoptosis and extensive lysosomal rupture can result in necrosis. Compounds that target the lysosomes and contribute to lysosome-mediated cell death can also be induced by a diversity of stimuli, such as UV irradiation and oxidative stress. Thus, in the last decades, the function of lysosomes as cell death mediators have a great potential in cancer therapy (84,94).

3.5. Internalization of steroid-BODIPY conjugates in a 2D Co-culture

Co-culture systems are often applied to elicit some of the *in vivo* conditions, allowing a diversity of cell types cultured together in order to investigate the influence of one type of culture system on another (95,96). In present work, a co-culture of cancer cells (MDA-MB-231 or PC-3) and Fibroblasts (normal cells) were done in a proportion of 1:1. Two different concentrations (5 and 25 μM) of steroid-BODIPY conjugates were used. An estradiol-BODIPY conjugate (EE2-C8) was used for MDA-MB-231 cancer cells and fibroblasts co-culture and an androgen-BODIPY conjugate (HA-4198) was used for PC-3 prostate cancer cells and fibroblasts co-culture. This study was performed to correlate the levels of conjugates in cancer and normal cells and to elucidate conjugates specificity for the respective steroid receptors.

Figure 3.19 (A) shows fluorescence microscopy images of the internalization of EE2-C8 in MDA-MB-231 cells and Fibroblasts co-culture and **Figure 3.19 (B)** presents the fluorescence intensity quantification of EE2-C8 in each cell type. The internalization of EE2-C8 is higher in MDA-MB-231 compared to fibroblasts and increases with EE2-C8 concentration (25 μM) (**Figure 3.19**). Fluorescence images also demonstrate that EE2-C8 internalization is much lower in MDA-MB-231 cancer cells and almost absent with EE2-C8 concentration of 5 μM (**Figure 3.19**). As previously mentioned, MDA-MB-231 cells are an ER-negative and, therefore, internalization of estradiol derivates might not be mediated by estrogen receptors.

Figure 3.20 (A) and (B) demonstrate fluorescence microscopy images of the internalization of HA-4198 in PC-3 cells and fibroblasts as well as fluorescence intensity quantification of HA-4198 in each cell type, respectively. The results presented in **Figure 3.20** are similar to previous results described for MDA-MB-231 and fibroblasts co-cultures. The internalization of HA-4198 is increased with a higher concentration of androgen derivate for both cell types. With lower concentration, the internalization of HA-4198 in fibroblasts is almost absent, as visualized in green fluorescence images indicating that this androgen derivate is more specific for cancer cells than for normal cells (**Figure 3.20**).

Fibroblasts had a different behavior when co-cultured with cancer cells in comparison with the cellular uptake study done in section 2.3. Internalization of steroid-BODIPY conjugates in a culture of fibroblasts demonstrated that all conjugates are cell permeable. However, fibroblasts in co-culture with cancer cells exhibited a significant decreased or absence of fluorescence intensity. This study allows to conclude that steroid-BODIPY conjugates are more specific for cancer cells than for healthy cells when both type of cells co-exist together.

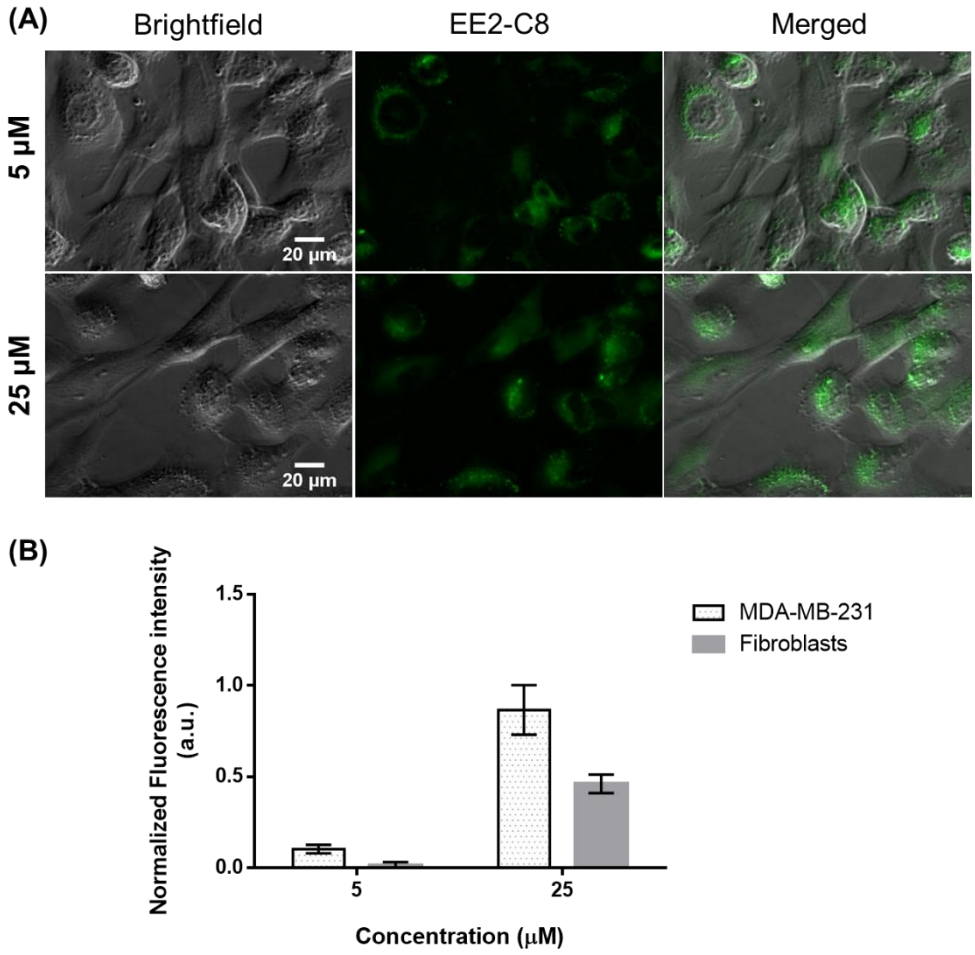

Figure 3.19 - Internalization of EE2-C8 estradiol-BODIPY conjugate in a co-culture of MDA-MB-231 cells and fibroblasts. MDA-MB-231 cells and fibroblasts were seeded in a 1:1 proportion. Co-culture was incubated 6h with 0.25% (v/v) DMSO (control) or **5 µM and 25 µM** of estradiol derivate EE2-C8. Cells were visualized by an inverted microscope (A) and fluorescence intensity was quantified (B). Fluorescence intensity of the cells was corrected for background fluorescence and normalized with vehicle (DMSO). Results are expressed as mean ± standard deviation of one independent experiment in duplicate.

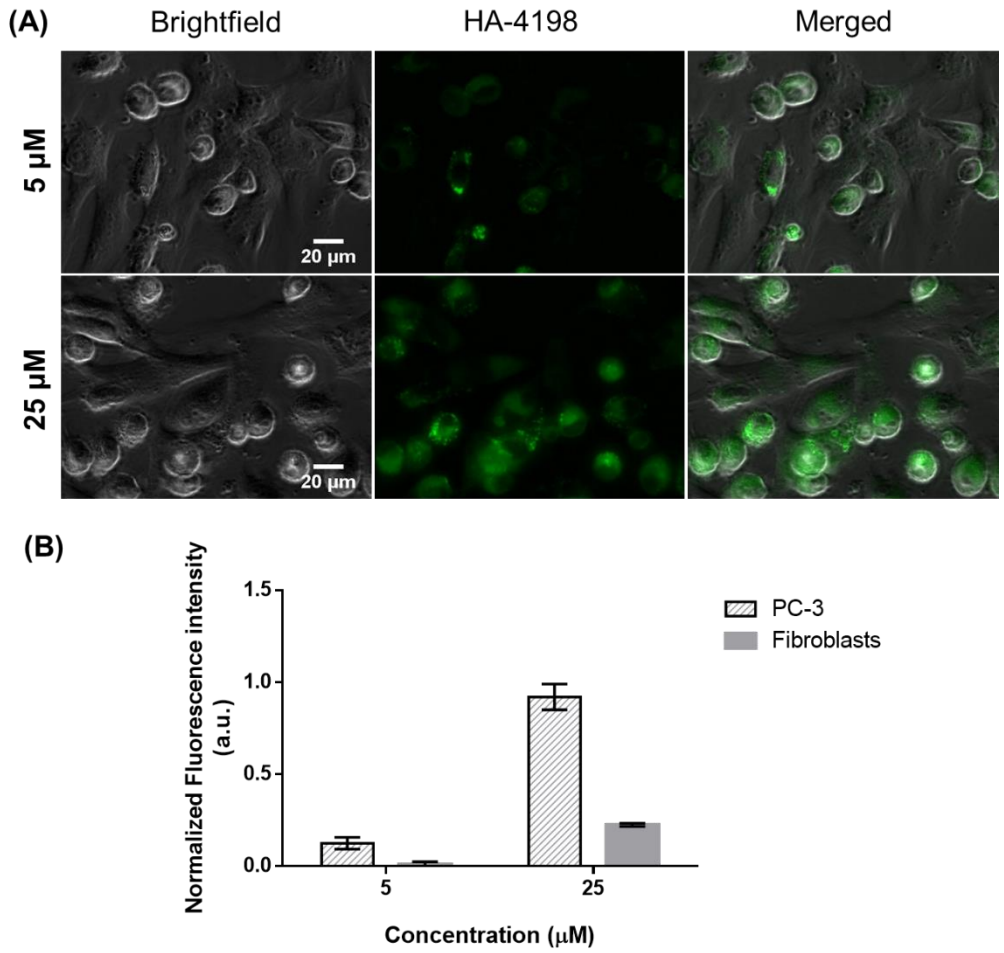

Figure 3.20 - Internalization of HA-4198 androgen-BODIPY conjugate in a co-culture of PC-3 cells and Fibroblasts. PC-3 cells and fibroblasts were seeded in a 1:1 proportion. Co-culture was incubated 6h with 0.25% (v/v) DMSO (control) or **5 µM and 25 µM** of androgen derivate HA-4198. Cells were visualized by an inverted microscope (A) and fluorescence intensity was quantified (B). Fluorescence intensity of the cells was corrected for background fluorescence and normalized with vehicle (DMSO). Results are expressed as mean ± standard deviation of one independent experiment in duplicate.

3.6. Cell Viability Assays

Cytotoxicity potential of the conjugates was determined by means of the MTS assay against a series of human cancer cell lines and a normal cell line. As mention previously, the MTS colorimetric assay is based on MTS reagent bioreduction into a soluble product (formazan) by intracellular dehydrogenase enzymes in metabolically active cells. Thus, the determination of the viable cell number is achievable, since the amount of formazan measured is directly proportional to the number of viable cells (74,75).

In previous studies (unpublished data), the antiproliferative activity of the estradiol-BODIPY analogue EE2-C8 was tested in MCF-7 cells in a range of concentrations between 0.01 to 50 µM with an exposure period of 3h and 24h at 37°C.In that study, no decrease of cell viability was

observed for both time points (results not shown). Considering these results in the present study we used to higher concentration of conjugates (50 μM) and MTS assay was performed after 6h and 24h exposition, in the cancer cell lines as well as in normal human fibroblasts.

Estradiol-BODIPY analogues (EE2-C8 and 11β-OMe) were tested in breast cancer cell lines, MCF-7 (**Figure 3.21 (A)**) and MDA-MB-231 (**Figure 3.21 (B)**). The results allowed to confirm that no antiproliferative effect was observed for both estradiol-BODIPY conjugates and both exposure periods in breast cancer cell lines.

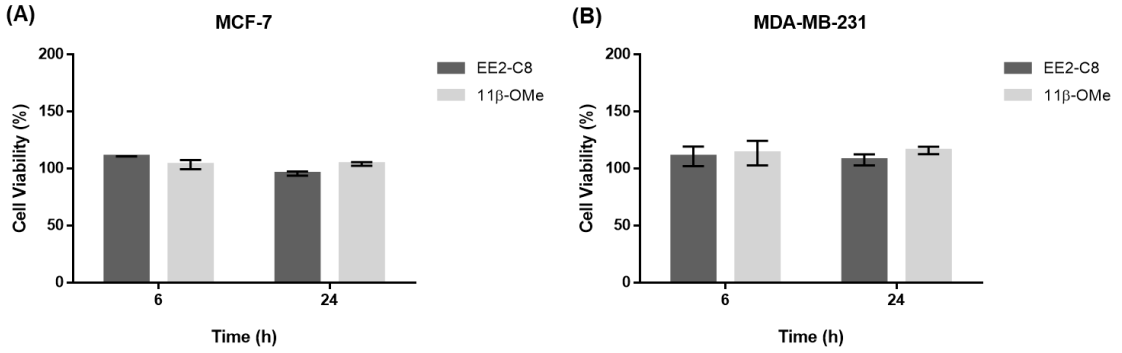

Figure 3.21- Cell viability of estradiol-BODIPY conjugates determined by means of the MTS assay. Breast cancer cell lines (A) MCF-7 and (B) MDA-MB-231 were incubated with 50μM of EE2-C8 or 11β-OMe for 6h and 24h. Data normalized against the control (0.5% (v/v) DMSO) and expressed as the mean ± SEM of two independent assays.

Androgen-BODIPY analogues were tested in prostate cancer cell lines, PC-3 (**Figure 6.10 (A) in Annex C**) and LNCaP (**Figure 6.10 (A) in Annex C**). In PC-3 cell line, all androgen-BODIPY analogues also demonstrated no cytotoxic effect. Except for HA-4199 and HA-4200 androgen-BODIPY conjugates, that presents a very slight decrease of viability in LNCaP cells, the remaining conjugates show no cytotoxic effect on this cell line. Interestingly, a slight increase of viability is observed for HA-4198 and HA-4187 (**Figure 6.10 (A) of Annex C**).

Cell viability of all steroid-BODIPY conjugates was also determined in primary human fibroblasts. According to results, no loss of cell viability on human healthy fibroblasts is observed (**Figure 6.11 in Annex C**).

In general, these results showed that all conjugates were non-toxic to cancer and normal cells, enabling their application for certain cancer therapies, namely PDT.

3.7. Visible Light Irradiation

BODIPY derivates are a class of new photosensitizers with a variety of characteristics such as high fluorescence, excellent optical properties and synthetic versatility. These small molecules could be a potential photosensitizer used in PDT for cancer treatment (16,80,97). The conjugation

of BODIPY dyes to different ligands, namely steroids, could improve the conjugate properties as target selectivity. These PS is covalently attached to steroids that are recognized by respective receptors having a significant potential in diagnostic and therapy of cancer (11).

Preliminary tests were performed to choose the conditions of this study: conjugate concentration, laser diode intensity and the exposition time (see **Figure 6.12 in Annex D**). PC-3 cells were incubated with 50 μM of androgen-BODIPY conjugate (HA-4187) and irradiated with three different laser diode intensities (2.45, 3.12 and 3.78 W/cm^2) during 60 seconds. These results demonstrated that cell viability decreases approximately 70% after irradiation for all tested LDI. Nevertheless, despite these results, the lowest LDI (2.45 W/cm^2) was chosen. The concentration of conjugates used in the next studies was 25 μM because of conjugate saturation with highest concentration of 50 μM.

Thus, MCF-7 and PC-3 cancer cells and normal primary fibroblasts were incubated with steroid-BODIPY conjugates (25 μM) for 6 h, and then the medium was replaced by fresh phenol red free media without conjugates in order to prevent optical interference because of the absorption band of phenol red overlapping. Cells were irradiated for 60 seconds using a LDI of 2.45 W/cm^2. The effect of visible irradiation on cell viability was evaluated by MTS assay, 24 h after green laser irradiation.

MCF-7 breast cancer and normal cells were incubated with estradiol-BODIPY conjugates (EE2-C8 and 11β-OMe) and irradiated with a green laser. **Figure 3.22 (A) and (B)** shows cell viability after laser irradiation. As also demonstrated in the previous section, cell viability without irradiation in both cell types is 100% for EE2-C8 conjugate and approximately 80/90% for 11β-OMe conjugate. However, after visible irradiation, cell viability decreases approximately 80% for both estradiol derivates. For EE2-C8 conjugate, cell viability decreased is more accentuated in MCF-7 cancer cells than in normal cells (approximately 40%), while for 11β-OMe conjugate, cell viability in fibroblasts decreases by about 80%.

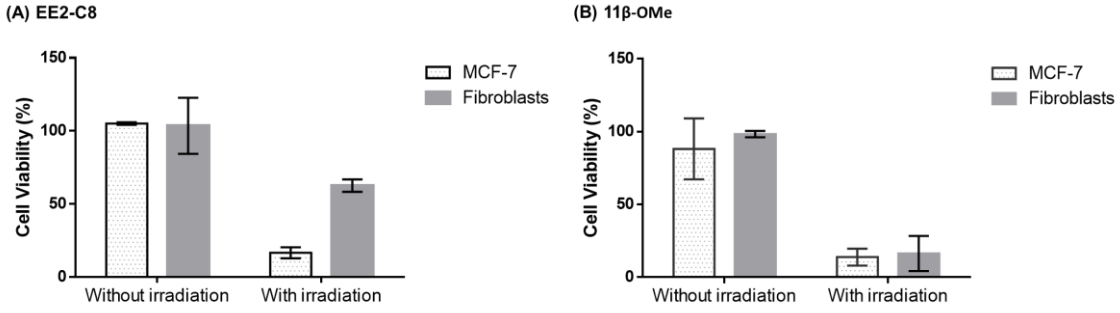

Figure 3.22 - Breast cancer cell and normal cell (Fibroblasts) death following PDT induced by visible light and (A) EE2-C8 or (B) 11β-OMe estradiol-BODIPY conjugates as photosensitizers. Cell viability via the MTS assay in MCF-7 cell line and fibroblasts 24 h after visible irradiation. Data normalized against the control (0.25% (v/v) DMSO) and expressed as the mean ± SEM of two independent assays in triplicate.

Figure 3.23 (A) and (B) presents cell viability of PC-3 prostate cancer cells and fibroblasts incubated with androgen-BODIPY conjugates (HA-4198 and HA-4187) after visible irradiation. Both conjugates, such as for MFC-7 cells, without irradiation, do not affect cell viability. In contrast, irradiation of these prostate cancer cells incubated with androgen derivates causes a severe increase in cell death similar to MCF-7 cells. HA-4198 conjugate decreases cell viability in fibroblasts approximately 20% and HA-4187 also decreases around 40-50% (not statistically significantly due to the large standard deviation).

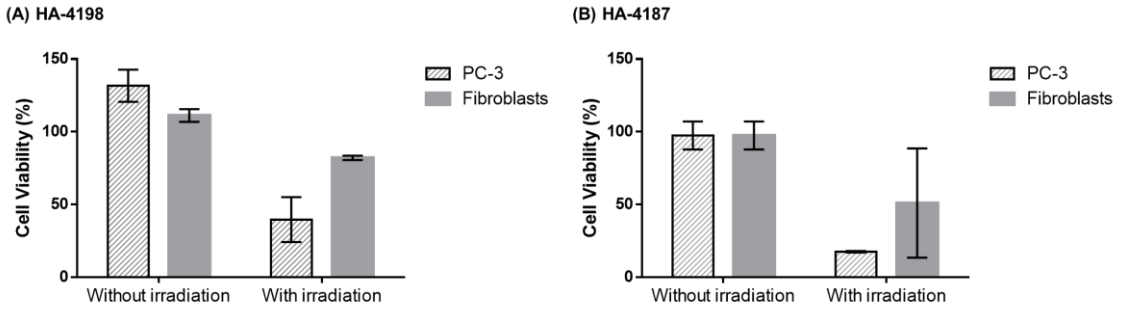

Figure 3.23 - Prostate cancer cell and normal (Fibroblasts) death following PDT induced by visible light and (A) HA-4198 or (B) HA-4187 androgen-BODIPY conjugates as photosensitizers. Cell viability via the MTS assay in PC-3 cell line and fibroblasts 24 h after visible irradiation. Data normalized against the control (0.25% (v/v) DMSO) and expressed as the mean ± SEM of two independent assays in triplicate.

PDT is an alternative method for cancer treatment that possesses three important elements for its effective activity: a photosensitizer, light irradiation and oxygen to induce cell death. Each of these components, individually, do not produce a biological response. However, a mixture of the three components promotes the formation of reactive oxygen species (ROS) triggering irreversible damage (52–55). These results indicate that these steroid-BODIPY conjugates, namely, EE2-C8 and HA-4198, are potential photosensitizers for PDT against breast and prostate cancer cells, respectively. As demonstrated, these conjugates without irradiation do not affect cell viability.

4. Conclusions and Future Perspectives

Cancer remains one of the leading causes of death worldwide. Over recent years, the research for cancer treatment has been intensive in order to increase the therapeutic efficacy without affecting healthy cells and tissues and to reduce the resistance of cancer cells to treatment. In order to mitigate these current concerns it is important to develop new diagnostic and treatment strategies that could be more selective and with less side effects. Cancer theranostics combines diagnosis and therapy having a great potential for personalized cancer treatment. This new approach requires agents that simultaneously have the ability of targeting, imaging, and also to treat.

Hormone-dependent cancers, as breast and prostate cancers, mostly express steroid receptors. Thus, the first line of treatment for these cancer types is generally hormone therapy with drugs that target and block steroid receptors.

The present work addressed the study of receptor based fluorescence probes (estrogen-, testosterone- and nortestosterone derivates conjugated to BODIPY dye) as potential platforms for imaging, photosensitizers for photodynamic therapy, and also for PET.

Cellular uptake of steroid-BODIPY conjugates was assessed by fluorescence microscopy in order to evaluate the tracking of these conjugates in relevant breast and prostate cancer cells. These studies demonstrated non-specific internalization of BODIPY conjugates in all different cancer cell lines and also in normal fibroblasts. The presence of fluorescence in intracellular vesicles suggested that endocytic pathway is the cellular uptake mechanism of the conjugates. In addition, receptors blocking studies indicated that the steroid-BODIPY conjugates enter the cells by steroid receptors independent mechanisms. For this reason, energy-dependent cellular uptake and trafficking pathway of steroid-BODIPY conjugates were also evaluated by fluorescence microscopy.

Cellular uptake of BODIPY conjugates by cancer cells, at low temperature, was reduced compared to the cellular uptake at 37 °C, indicating that these conjugates entering in cancer cells through an energy-dependent process, and, as such, this mechanism might carried out by endocytic pathways. For that purpose, different pharmacologic inhibitors of endocytosis were pre-incubated in an ER-negative cell line (MDA-MB-231). Although lacking ER expression, caveolae-mediated endocytosis (inhibited by filipin) is a possible endocytic pathway for all studied cell lines. To support this trafficking mechanism, the co-localization of steroid-BODIPY conjugates with lysosomes was also demonstrated with a selective lysosomes marker (LAMP-2). However, confocal microscopy and additional assays, would be necessary to completely understand the location of these conjugates.

2D Co-culture assays with cancer cells and normal fibroblasts were also done to elucidate conjugates specificity for cancer cells and for their respective steroid receptors. These results

allowed to conclude that steroid-BODIPY conjugates are more specific for cancer cells due to a significant decrease or absence of fluorescence in fibroblast in co-culture.

To assess the conjugates potential for PDT, visible irradiation studies were also performed. Cell viability assays demonstrated that the conjugates without irradiation are non-toxic for cancer and normal cells. In contrast, light irradiation causes a severe cell death. The results demonstrated that steroid-BODIPY conjugates, especially EE2-C8 and HA-4198, are potential photosensitizers for PDT against breast and prostate cancer cells. Future studies will be necessary to evaluate the mechanisms associated to the effect of light irradiation with these conjugates, including the generation of ROS as well as the cell death mechanisms.

5. References

1. Alberts B. Cellular Communities: Tissues, Stem Cells, and Cancer. In: Science G, editor. Essential Cell Biology. 3rd ed. 2010. p. 689–731.

2. Bertram JS. The molecular biology of cancer. Vol. 21, Molecular Aspects of Medicine. Elsevier Ltd; 2000. p. 167–223.

3. Hanahan D, Weinberg RA. Hallmarks of cancer: The next generation. Cell. 2011 Mar 4;144(5):646–74.

4. WHO | Cancer [Internet]. Available from: https://www.who.int/topics/cancer/en/ (Accessed February 2020).

5. Ruddon RW. Cancer Biology. Fourth. Oxford University Press U, editor. 2007.

6. Bray F, Ferlay J, Soerjomataram I, Siegel RL, Torre LA, Jemal A. Global Cancer Statistics 2018 : GLOBOCAN Estimates of Incidence and Mortality Worldwide for 36 Cancers in 185 Countries. CA A Cancer J Clin. 2018;68:394–424.

7. Dados do cancro em Portugal – SNS [Internet]. 2018. Available from: https://www.sns.gov.pt/noticias/2018/02/02/dados-do-cancro-em-portugal/ (Accessed February 2020).

8. Phung DC, Nguyen HT, Phuong Tran TT, Jin SG, Yong CS, Truong DH, et al. Combined hyperthermia and chemotherapy as a synergistic anticancer treatment. J Pharm Investig. 2019;0(0):0.

9. Haider M, Lange PH. Breast and Prostate Cancers: A Comparison of Two Endocrinologic Malignancies. In: Prostate Cancer: Science and Clinical Practice: Second Edition. Elsevier Inc.; 2016. p. 157–65.

10. Hamed S, Zahra J, Arash S, Momeni F, Mokhtari M, Sadri J, et al. Breast cancer diagnosis : Imaging techniques and biochemical markers. J Cell Physiol. 2017;233(7):5200–13.

11. Osati S, Ali H, Guérin B, Lier JE Van. Steroid-photosensitizer conjugates : Syntheses and applications. J Porphyrins. 2017;21(11):1–30.

12. Whirledge S, Cidlowski JA. Steroid Hormone Action. In: Yen & Jaffe's Reproductive Endocrinology: Physiology, Pathophysiology, and Clinical Management: Eighth Edition. Elsevier Inc.; 2019. p. 115-131.e4.

13. Ahmad N, Kumar R. Steroid hormone receptors in cancer development: A target for cancer therapeutics. Vol. 300, Cancer Letters. Elsevier; 2011. p. 1–9.

14. Fuentes N, Silveyra P. Estrogen receptor signaling mechanisms. In: Advances in Protein Chemistry and Structural Biology. Academic Press Inc.; 2019. p. 135–70.

15. Nagai MA, Brentani MM. Gene Expression Profiles in Breast Cancer to Identify Estrogen Receptor Target Genes. In: Recent Advances in Medicinal Chemistry. Elsevier Inc.; 2014. p. 381–403.

16. Osati S, Ali H, Guerin B, Lier JE Van. Synthesis and spectral properties of estrogen- and androgen-BODIPY conjugates. Steroids. 2017;123(January):27–36.

17. Jameera Begam A, Jubie S, Nanjan MJ. Estrogen receptor agonists/antagonists in breast cancer therapy: A critical review. Vol. 71, Bioorganic Chemistry. Academic Press Inc.; 2017. p. 257–74.

18. Holschbach MA, Handa RJ. Androgen Action and Stress. Vol. 2, Stress: Neuroendocrinology and Neurobiology. Elsevier Inc.; 2017. 227–235 p.

19. Levine PM, Garabedian MJ, Kirshenbaum K. Targeting the androgen receptor with steroid conjugates. J Med Chem. 2014 Oct 23;57(20):8224–37.

20. Latil A, Bie I, Vidaud D, Lidereau R, Berthon P, Cussenot O, et al. Evaluation of Androgen , Estrogen (ERalpha and ERbeta), and Progesterone Receptor Expression in Human Prostate Cancer by Real-Time Quantitative Reverse Transcription-Polymerase Chain Reaction Assays. Cancer Res. 2001;61(5):1919–26.

21. Androgen receptor antagonists for prostate cancer therapy. Endocr Relat Cancer. 2014;21(4):105–18.

22. Cronauer M V, Klocker H, Maly K, Hobisch A, Bartsch G, Culig Z. Androgen receptor protein is down-regulated by basic fibroblast growth factor in prostate cancer cells. Br J Cancer. 2000;82(1):39–45.

23. Alimirah F, Chen J, Basrawala Z, Xin H, Choubey D. DU-145 and PC-3 human prostate cancer cell lines express androgen receptor : Implications for the androgen receptor functions and regulation. 2006;580:2294–300.

24. Elshan NGRD, Rettig MB, Jung ME. Molecules targeting the androgen receptor (AR) signaling axis beyond the AR-Ligand binding domain. Med Res Rev. 2019;39(3):910–60.

25. Meehan KL, Sadar MD. Androgens and androgen receptor in prostate and ovarian malignancies. Vol. 8, Frontiers in Bioscience. 2003.

26. Ogino Y, Miyagawa S, Iguchi T. Testosterone/Dihydrotestosterone. In: Handbook of Hormones. Elsevier; 2016. p. 515-e94E-3.

27. Davey RA, Grossmann M. Androgen Receptor Structure, Function and Biology: From

Bench to Bedside. Clin Biochem Rev. 2016;37(1):3–15.

28. Schwartz N, Verma A, Bivens CB, Schwartz Z, Boyan BD. Rapid steroid hormone actions via membrane receptors. Vol. 1863, Biochimica et Biophysica Acta - Molecular Cell Research. Elsevier B.V.; 2016. p. 2289–98.

29. Moraga-Amaro R, van Waarde A, Doorduin J, de Vries EFJ. Sex steroid hormones and brain function: PET imaging as a tool for research. J Neuroendocrinol. 2018;30(2):e12565.

30. De Amicis F, Chimento A, Montalto FI, Casaburi I, Sirianni R, Pezzi V. Steroid receptor signallings as targets for resveratrol actions in breast and prostate cancer. Vol. 20, International Journal of Molecular Sciences. MDPI AG; 2019.

31. Ec ET. Novel 17 a -Etinylestradiol-Substituted BODIPY Dyes : Synthesis , Photophysical Properties and Fluorescence Imaging Studies in Breast Cancer Cell Lines. Chem Sel. 2018;3(11):2962–7.

32. Zhang R, Qin X, Kong F, Chen P, Pan G. Improving cellular uptake of therapeutic entities through interaction with components of cell membrane. Vol. 26, Drug Delivery. Taylor and Francis Ltd; 2019. p. 328–42.

33. Parsons TK, Pratt RN, Tang L, Wu Y. An active and selective molecular mechanism mediating the uptake of sex steroids by prostate cancer cells. Mol Cell Endocrinol. 2018 Dec 5;477:121–31.

34. Pal S. Membrane structure and function. In: Fundamentals of Molecular Structural Biology. Elsevier; 2020. p. 405–20.

35. Scita G, Di Fiore PP. The endocytic matrix. Nature. 2010 Jan 28;463(7280):464–73.

36. Sahay G, Alakhova DY, Kabanov A V. Endocytosis of nanomedicines. J Control Release. 2010 Aug 3;145(3):182–95.

37. Canton I, Battaglia G. Endocytosis at the nanoscale. Chem Soc Rev. 2012 Apr 7;41(7):2718–39.

38. Dutta D, Donaldson JG. Search for inhibitors of endocytosis. Cell Logist. 2012;2(4):203–8.

39. Platt N, Fineran P. Measuring the phagocytic activity of cells. Methods Cell Biol. 2015 Jan 1;126:287–304.

40. Alliegro M. Endocytosis. In: xPharm: The Comprehensive Pharmacology Reference. Elsevier Inc.; 2007. p. 1–5.

41. Mellman I, Yarden Y. Endocytosis and cancer. Cold Spring Harb Perspect Biol. 2013

Dec;5(12).

42. Parton RG, McMahon KA, Wu Y. Caveolae: Formation, dynamics, and function. Vol. 65, Current Opinion in Cell Biology. Elsevier Ltd; 2020. p. 8–16.

43. Kumari S, Mg S, Mayor S. Endocytosis unplugged: Multiple ways to enter the cell. Cell Res. 2010 Mar 2;20(3):256–75.

44. Cabral RM, Baptista P V. Anti-cancer precision theranostics : a focus on multifunctional gold nanoparticles. Expert Rev Mol Diagn. 2014;14(08):1041–52.

45. Zhang J, Jiang C, Figueiró Longo JP, Bentes Azevedo R, Zhang H, Alexandre Muehlmann L. An updated overview on the development of new photosensitizers for anticancer photodynamic therapy. Acta Pharm Sin B. 2018;8(2):137–46.

46. Chen XS, Wong S. Cancer Theranostics. 1st ed. Academic Press; 2014. 544 p.

47. Beik J, Abed Z, Ghoreishi FS, Hosseini-nami S, Mehrzadi S, Shakeri-zadeh A, et al. Nanotechnology in hyperthermia cancer therapy : From fundamental principles to advanced applications ☆. J Control Release. 2016;235:205–21.

48. Zhang J, Ning L, Huang J, Zhang C, Pu K. Activatable molecular agents for cancer theranostics. Vol. 11, Chemical Science. Royal Society of Chemistry; 2020. p. 618–30.

49. Alcantara D, Leal MP, García-Bocanegra I, García-Martín ML. Molecular imaging of breast cancer: Present and future directions. Front Chem. 2014;2.

50. Cabral RM, Baptista P V. The Chemistry and Biology of Gold Nanoparticle-Mediated Photothermal Therapy: Promises and Challenges. Nano Life. 2013;3(3):1–18.

51. Zhang Q, Li L. Photodynamic combinational therapy in cancer treatment. J BUON. 2018;23(3):561–7.

52. Li X, Lee S, Yoon J. Supramolecular photosensitizers rejuvenate photodynamic therapy. Chem Soc Rev. 2018;47:1174–88.

53. Cai Y, Si W, Huang W, Chen P, Shao J, Dong X. Organic Dye Based Nanoparticles for Cancer Phototheranostics. Small. 2018;14(25):1–17.

54. Singh P, Pandit S, Mokkapati VRSS, Garg A, Ravikumar V, Mijakovic I. Gold Nanoparticles in Diagnostics and Therapeutics for Human Cancer. Int J Mol Sci. 2018;19(7).

55. Banerjee SM, Macrobert AJ, Mosse CA, Periera B, Bown SG, Keshtgar MRS. Photodynamic therapy : Inception to application in breast cancer. The Breast. 2017;31:105–13.

56. Vankayala R, Hwang KC. Near-Infrared-Light-Activatable Nanomaterial-Mediated Phototheranostic Nanomedicines : An Emerging Paradigm for Cancer Treatment. Adv Mater. 2018;30(20):1–27.

57. Avendaño C, Menéndez JC. Medicinal Chemistry of Anticancer Drugs. 2015. 768 p.

58. Hou X, Tao Y, Pang Y, Li X, Jiang G, Liu Y. Nanoparticle-based photothermal and photodynamic immunotherapy for tumor treatment. Int J Cancer. 2018;143(12):3050–60.

59. Denkova AG, Kruijff RM De, Serra-crespo P. Nanocarrier-Mediated Photochemotherapy and Photoradiotherapy. Adv Healthc Mater. 2018;7(8):1–21.

60. Lan G, Ni K, Lin W. Nanoscale metal – organic frameworks for phototherapy of cancer. Coord Chem Rev. 2019;379:65–81.

61. Gift MM, Ann KC, Ivan M, Heidi A. A Review of Nanoparticle Photosensitizer Drug Delivery Uptake Systems for Photodynamic Treatment of Lung Cancer. Photodiagnosis Photodyn Ther. 2018;22:147–54.

62. Srivatsan A, Missert JR, Upadhyay SK. Porphyrin-based photosensitizers and the corresponding multifunctional nanoplatforms for cancer-imaging and phototherapy. J Porphyr Phthalocyanines. 2015;19:109–34.

63. Chen XS, Nibib B, Huang SP, Chen X. Overcoming the Achilles' heel of photodynamic thrapy. Chem Soc Rev. 2016;45:6488–519.

64. Josefsen LB, Boyle RW. Photodynamic Therapy and the Development of Metal-Based Photosensitisers. Met Based Drugs. 2008;2008.

65. Osati S, Ali H, Lier JE Van. BODIPY-steroid conjugates: Synthesis and Biological applications. J Porphyr Phthalocyanines. 2016;20(1):61–75.

66. Kowada T, Maeda H, Kikuchi K. BODIPY-based probes for the fluorescence imaging of biomolecules in living cells. Vol. 44, Chemical Society Reviews. Royal Society of Chemistry; 2015. p. 4953–72.

67. Osati S, Ali H, Marques F, Paquette M, Beaudoin S, Guerin B, et al. BODIPY-17α-ethynylestradiol conjugates: Synthesis, fluorescence properties and receptor binding affinities. Bioorganic Med Chem Lett. 2017 Feb 1;27(3):443–6.

68. Ali H, Rousseau J, van Lier JE. Synthesis of (17α, 20E/Z)Iodovinyl testosterone and 19-nortestosterone derivatives as potential radioligands for androgen and progesterone receptors. J Steroid Biochem Mol Biol. 1994;49(1):15–29.

69. Galvao J, Davis B, Tilley M, Normando E, Duchen MR, Cordeiro MF. Unexpected low-dose toxicity of the universal solvent DMSO. FASEB J. 2014;28(3):1317–30.

70. Probes M. Hoechst Stains. 2005. (Technical Bulletin).

71. Abcam. Goat Anti-Rabbit IgG H&L (TRITC) ab6718. (Technical Bulletin).

72. Totta P, Pesiri V, Marino M, Acconcia F. Lysosomal Function Is Involved in 17β-Estradiol-Induced Estrogen Receptor α Degradation and Cell Proliferation. Migliaccio A, editor. PLoS One. 2014;9(4).

73. Promega. CellTiter 96 ® AQueous One Solution Cell Proliferation Assay. 2012. (Technical Bulletin)

74. Kuete V, Karaosmanoğlu O, Sivas H. Anticancer Activities of African Medicinal Spices and Vegetables. In: Medicinal Spices and Vegetables from Africa: Therapeutic Potential Against Metabolic, Inflammatory, Infectious and Systemic Diseases. Elsevier Inc.; 2017. p. 271–97.

75. Riss TL, Moravec RA, Niles AL, Duellman S, Benink HA, Worzella TJ, et al. Cell Viability Assays. Assay Guidance Manual. Eli Lilly & Company and the National Center for Advancing Translational Sciences; 2004

76. Mendes R, Pedrosa P, Lima JC, Fernandes AR, Baptista P V. Photothermal enhancement of chemotherapy in breast cancer by visible irradiation of Gold Nanoparticles. Sci Rep. 2017;7(1).

77. Girgert R, Emons G, Gründker C. Estrogen signaling in ERα-negative breast cancer: ERβ and GPER. Vol. 10, Frontiers in Endocrinology. Frontiers Media S.A.; 2019.

78. Pisolato R, Lombardi APG, Vicente CM, Lucas TFG, Lazari MFM, Porto CS. Expression and regulation of the estrogen receptors in PC-3 human prostate cancer cells. Steroids. 2016;107:74–86.

79. Giovannelli P, Di Donato M, Galasso G, Di Zazzo E, Bilancio A, Migliaccio A. The androgen receptor in breast cancer. Vol. 9, Frontiers in Endocrinology. Frontiers Media S.A.; 2018.

80. Awuah SG, You Y. Boron dipyrromethene (BODIPY)-based photosensitizers for photodynamic therapy. Vol. 2, RSC Advances. The Royal Society of Chemistry; 2012. p. 11169–83.

81. Chavez KJ, Garimella S V., Lipkowitz S. Triple negative breast cancer cell lines: One tool in the search for better treatment of triple negative breast cancer. Breast Dis. 2010;32(1–2):35–48.

82. Giovannelli P, Di Donato M, Auricchio F, Castoria G, Migliaccio A. Androgens Induce Invasiveness of Triple Negative Breast Cancer Cells Through AR/Src/PI3-K Complex

Assembly. Sci Rep. 2019;9(1):1–14.

83. Xuan S, Zhao N, Ke X, Zhou Z, Fronczek FR, Kadish KM, et al. Synthesis and Spectroscopic Investigation of a Series of Push-Pull Boron Dipyrromethenes (BODIPYs). J Org Chem. 2017;82(5):2545–57.

84. Appelqvist H, Wäster P, Kågedal K, Öllinger K. The lysosome: from waste bag to potential therapeutic target. J Mol Cell Biol. 2013;5(4):214–26.

85. Sandvig K, Kavaliauskiene S, Skotland T. Clathrin-independent endocytosis: an increasing degree of complexity. Vol. 150, Histochemistry and Cell Biology. Springer Verlag; 2018. p. 107–18.

86. Dominska K, Kowalski A, Ochedalski T, Rebas E. Effects of testosterone and 17ß-estradiol on angiotensin-induced changes in tyrosine kinase activity in the androgen-independent human prostate cancer cell line, DU145. Int J Mol Med. 2017;40(5):1573–81.

87. Sampson N, Neuwirt H, Puhr M, Klocker H, Eder IE. In vitro model systems to study androgen receptor signaling in prostate cancer. Endocr Relat Cancer. 2013;20(2):49–64.

88. Zhang J, Liu D, Zhang M, Sun Y, Zhang X, Guan G, et al. The cellular uptake mechanism, intracellular transportation, and exocytosis of polyamidoamine dendrimers in multidrug-resistant breast cancer cells. Int J Nanomedicine. 2016;11:3677–90.

89. Sugano K, Kansy M, Artursson P, Avdeef A, Bendels S, Di L, et al. Coexistence of passive and carrier-mediated processes in drug transport. Vol. 9, Nature Reviews Drug Discovery. Nature Publishing Group; 2010. p. 597–614.

90. Mota AAR, Carvalho PHPR, Guido BC, De Oliveira HCB, Soares TA, Corrêa JR, et al. Bioimaging, cellular uptake and dynamics in living cells of a lipophilic fluorescent benzothiadiazole at low temperature (4 °c). Chem Sci. 2014 Aug 26;5(10):3995–4003.

91. Ying S, Du S, Dong J, Ng BX, Zhang C, Li L, et al. Intracellular effects of prodrug-like wortmannin probes. Chinese Chem Lett. 2019 Jan 1;30(1):67–70.

92. Levin ER, Hammes SR. Nuclear receptors outside the nucleus: extranuclear signalling by steroid receptors. Vol. 17, Nature Reviews Molecular Cell Biology. Nature Publishing Group; 2016. p. 783–97.

93. Morell C, Bort A, Vara-Ciruelos D, Ramos-Torres Á, Altamirano-Dimas M, Díaz-Laviada I, et al. Up-regulated expression of LAMP2 and autophagy activity during neuroendocrine differentiation of prostate cancer LNCaP cells. PLoS One. 2016;11(9).

94. Piao S, Amaravadi RK. Targeting the lysosome in cancer. Vol. 1371, Annals of the New York Academy of Sciences. Blackwell Publishing Inc.; 2016. p. 45–54.

95. Carter M, Shieh J. Chapter 14 - Cell Culture Techniques. Guide to Research Techniques in Neuroscience. Elsevier Inc.; 2015. 295–310 p.

96. Goers L, Freemont P, Polizzi KM. Co-culture systems and technologies: Taking synthetic biology to the next level. Vol. 11, Journal of the Royal Society Interface. Royal Society; 2014.

97. Gibbs JH, Zhou Z, Kessel D, Fronczek FR, Pakhomova S, Vicente MGH. Synthesis, spectroscopic, and in vitro investigations of 2,6-diiodo-BODIPYs with PDT and bioimaging applications. J Photochem Photobiol B Biol. 2015;145:35–47.

6. Annexes

6.1. Annex A

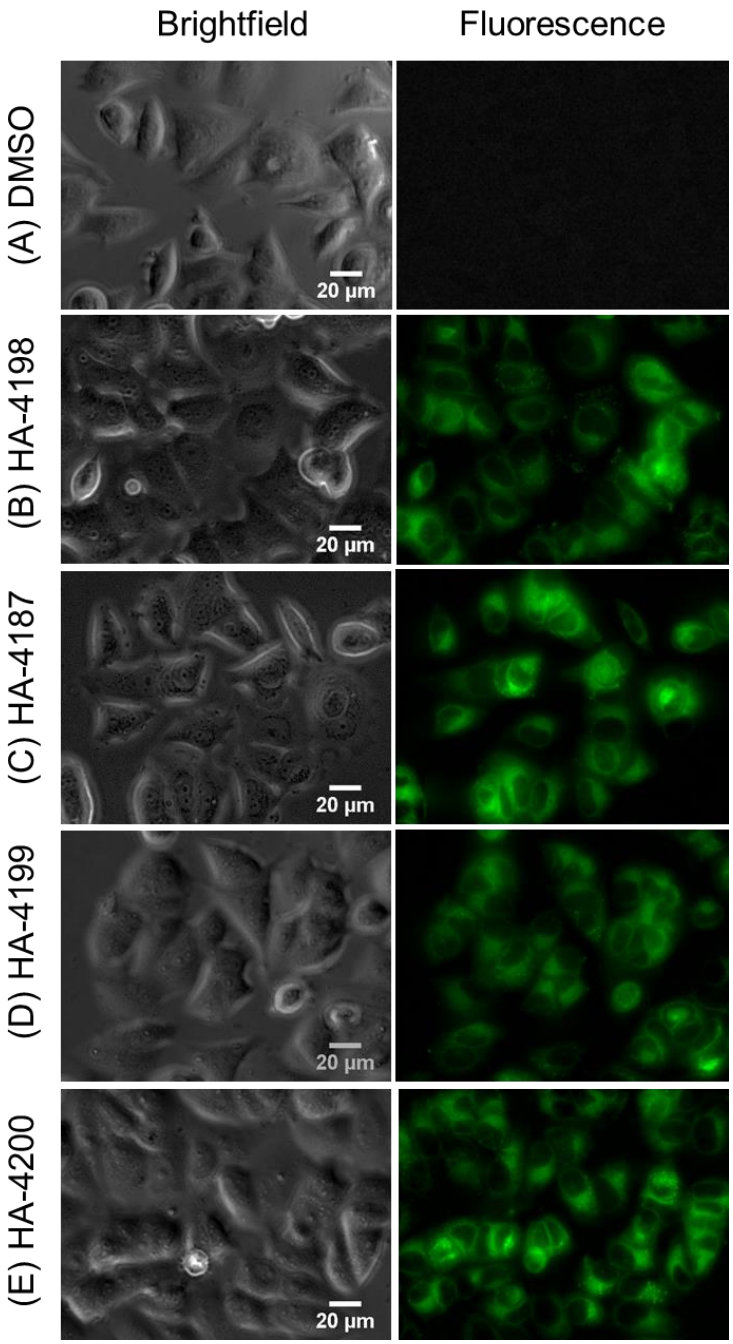

Figure 6.1 - Brighfield and fluorescence images of androgen-BODIPY conjugates in MCF-7 breast cancer cell line at 6h. MCF-7 cells were seeded for 24h in complete DMEM medium (with Phenol red) supplemented with MEM and then medium was replaced with DMEM without phenol red and (A) 0.5% (v/v) DMSO (control) or 50 µM of (B) HA-4198, (C) HA-4187, (D) HA-4199 and (E) HA-4200.

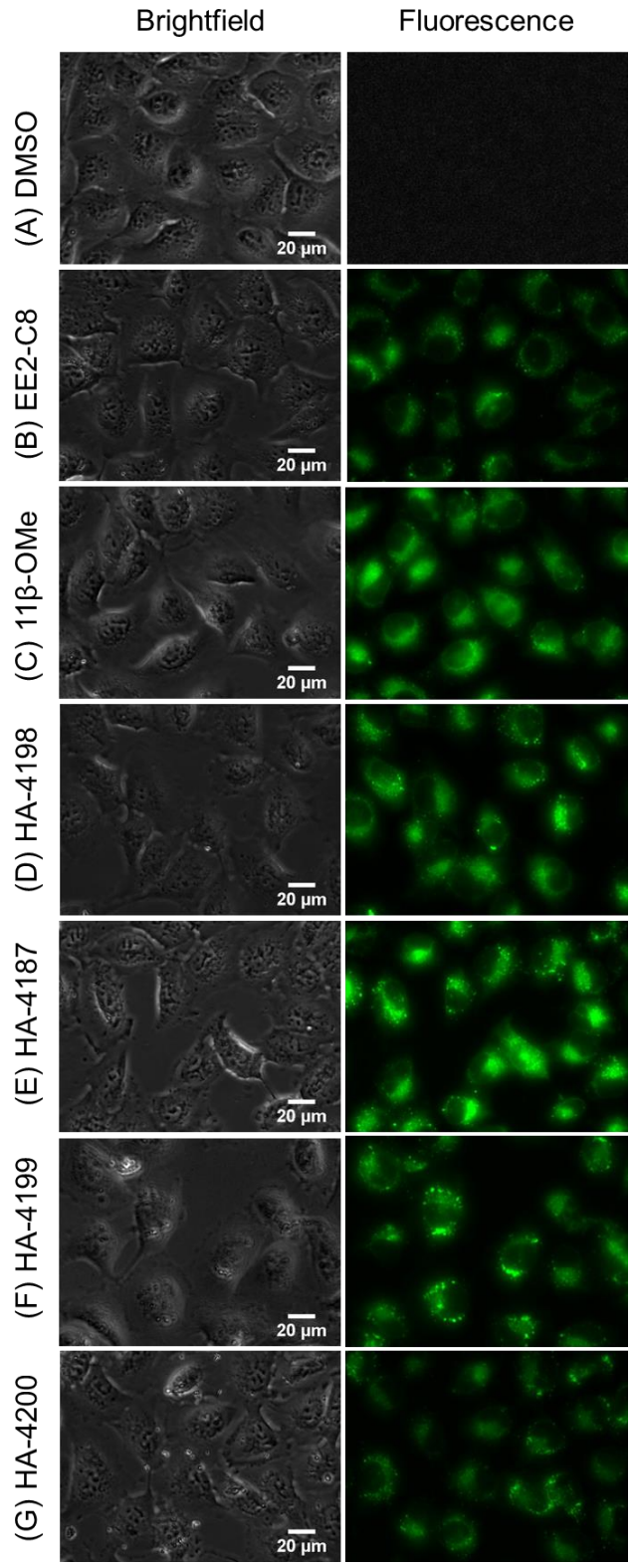

Figure 6.2 - Brighfield and fluorescence images of steroid-BODIPY conjugates in MDA-MB-231 breast cancer cell line at 6h. MDA-MB-231 cells were seeded for 24h in complete DMEM medium (with Phenol red) supplemented with MEM and then medium was replaced with DMEM without phenol red and (A) 0.5% (v/v) DMSO (control) or 50 µM of (B) EE2-C8, (C) 11β-OMe, (D) HA-4198, (E) HA-4187, (F) HA-4199 and (G) HA-4200.

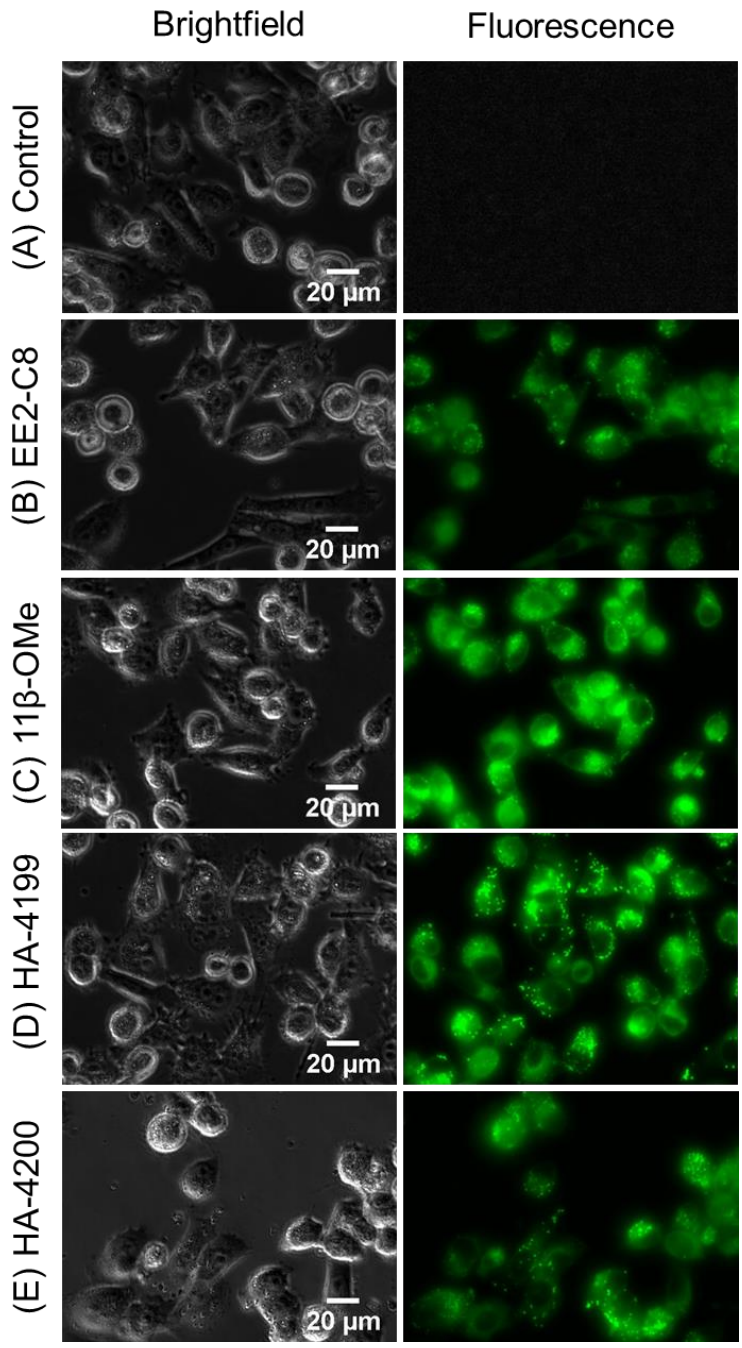

Figure 6.3 - Brightfield and fluorescence images of androgen-BODIPY conjugates in PC-3 prostate cancer cell line at 6h. PC-3 cells were seeded for 24h in complete RPMI medium (with Phenol red) and then medium was replaced with RPMI without phenol red supplemented with (A) 0.5% (v/v) DMSO (control) or 50 µM of (B) EE2-C8, (C) 11β-OMe, (D) HA-4199 and (E) HA-4200.

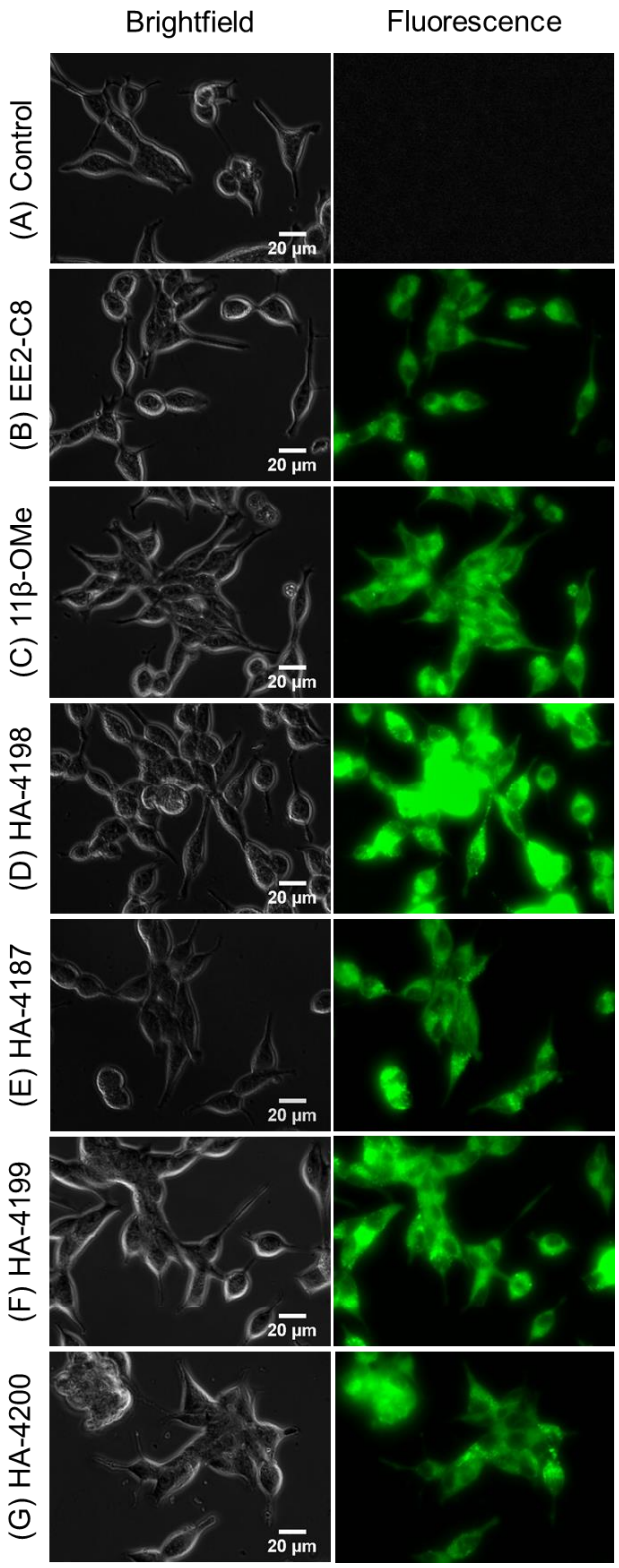

Figure 6.4 - Brightfield and fluorescence images of steroid-BODIPY conjugates in LNCaP prostate cancer cell line at 6h. LNCaP cells were seeded for 24h in complete RPMI medium (with Phenol red) and then medium was replaced with RPMI without phenol red supplemented with (A) 0.5% (v/v) DMSO (control) or 50 µM of (B) EE2-C8, (C) 11β-OMe, (D) HA-4198, (E) HA-4187, (F) HA-4199 and (G) HA-4200.

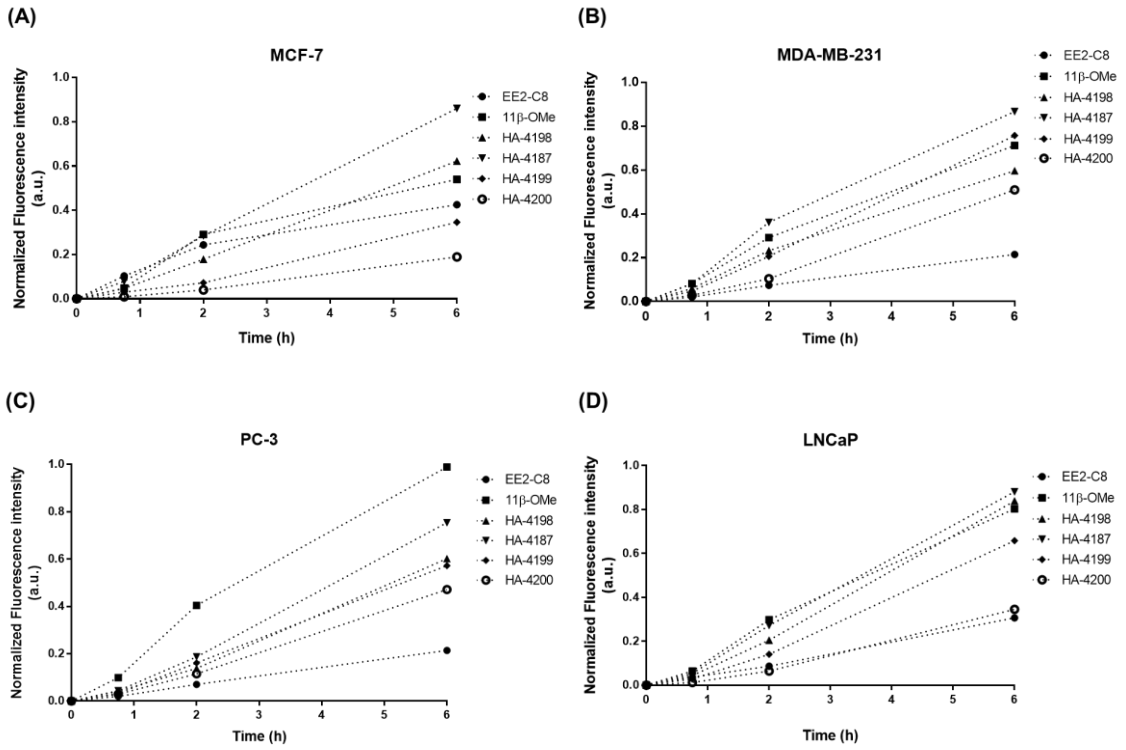

Figure 6.5 - Normalized fluorescence intensity of the (A) MCF-7, (B) MDA-MB-231, (C) PC-3 and (D) LNCaP cells incubated for 0, 0.75, 2 and 6 h with steroid-BODIPY conjugates. The fluorescence intensity of the cells was corrected for background fluorescence and normalized with vehicle (DMSO) and in arbitrary units (a.u.).

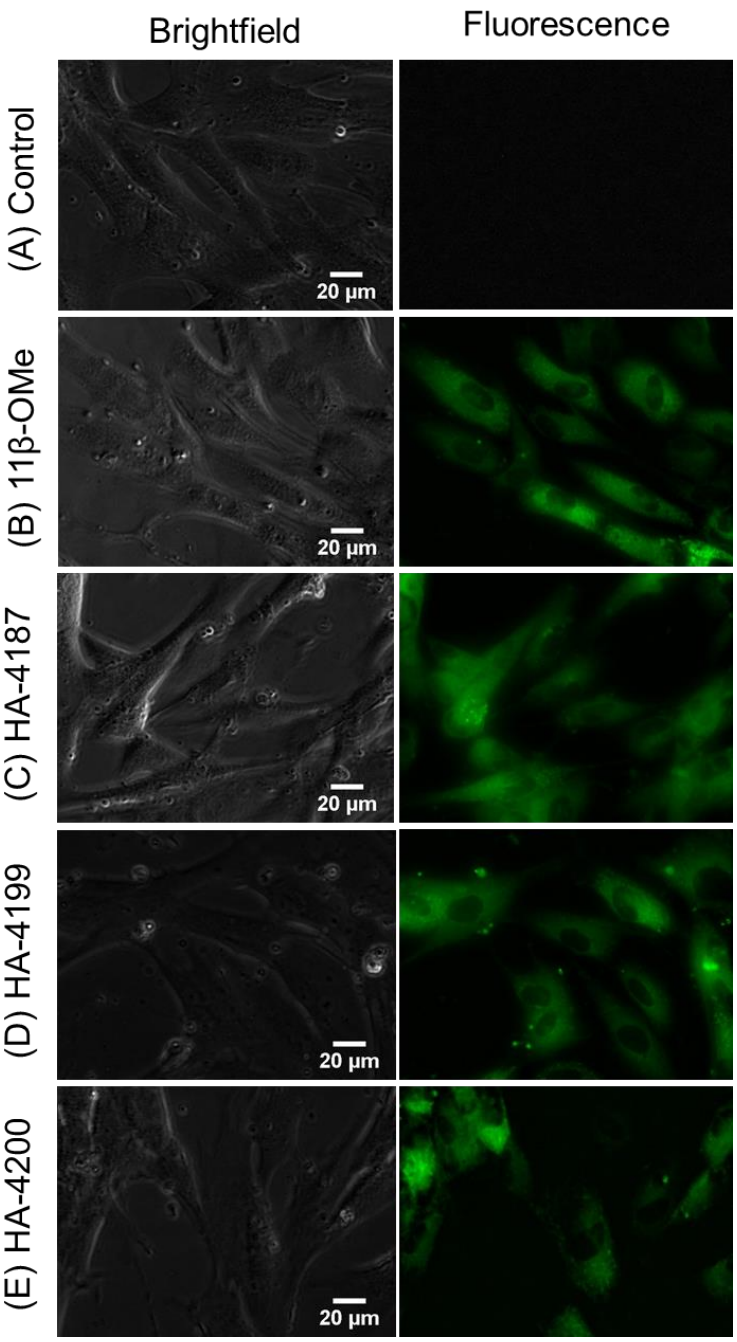

Figure 6.6 - Brightfield and fluorescence images of steroid-BODIPY conjugates in Fibroblasts at 6h. Fibroblasts were seeded for 24h in complete DMEM medium (with Phenol red) and then medium was replaced with DMEM without phenol red supplemented with (A) 0.5% (v/v) DMSO (control) or 50 µM of (B) 11β-OMe, (C) HA-4187, (D) HA-4199 and (E) HA-4200.

6.2. Annex B

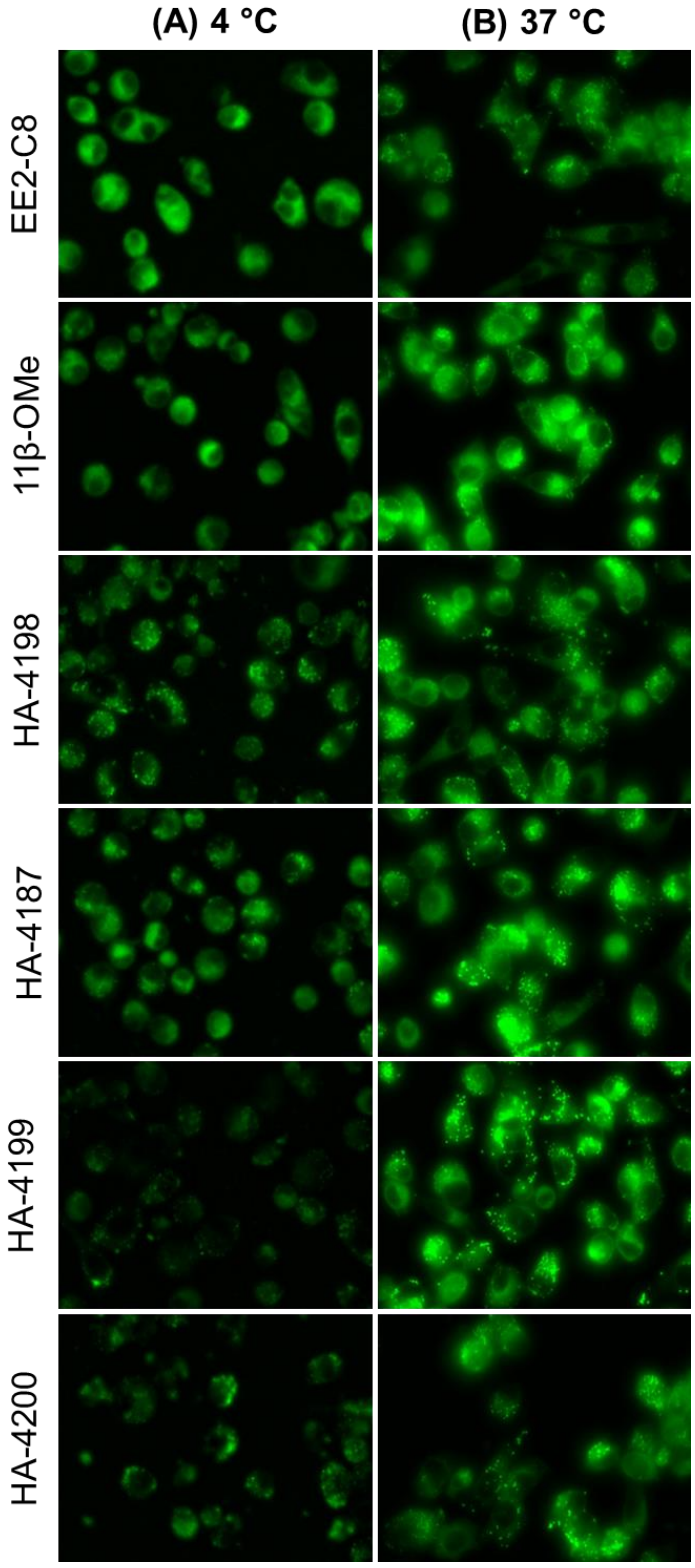

Figure 6.7 - Brightfield and fluorescence images of steroid-BODIPY conjugates in PC-3 cells at 6h. PC-3 cells were seeded for 24h in complete RPMI medium (with Phenol red) and then medium was replaced with RPMI without phenol red and 50 μM of compound incubated at (A) 4 °C or (B) 37 °C.

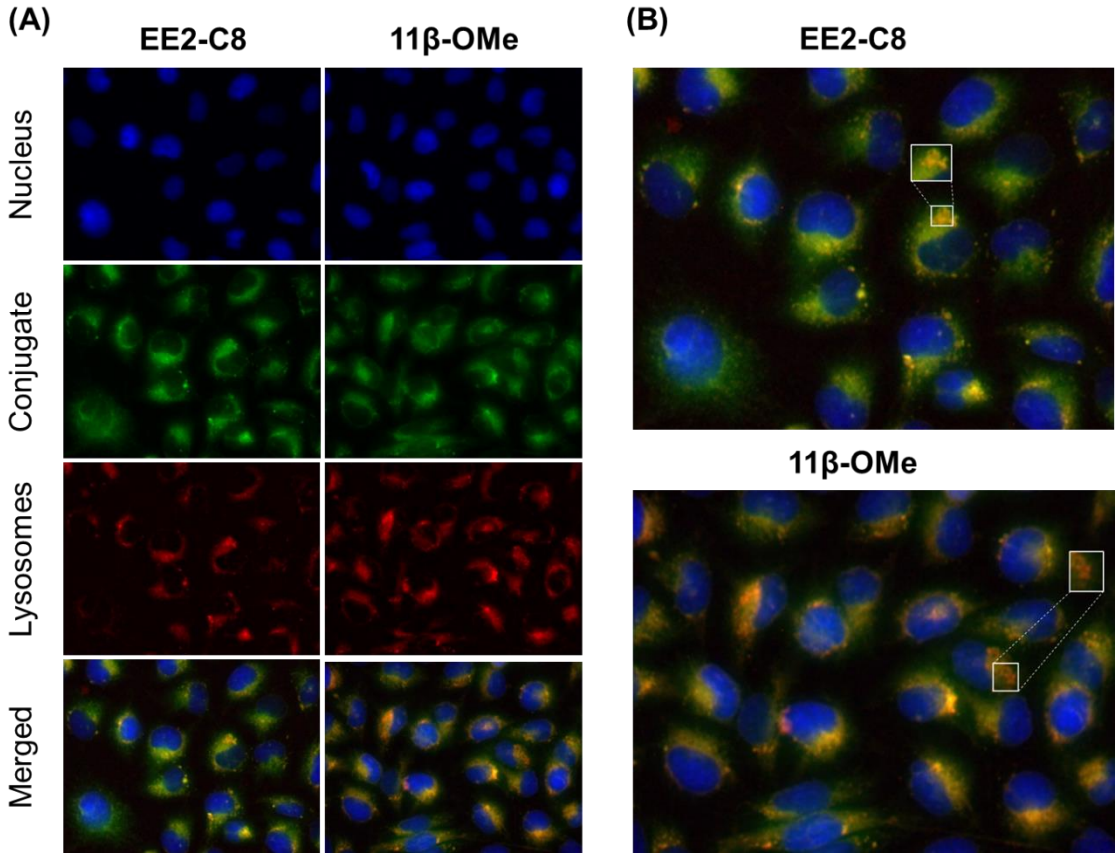

Figure 6.8 - Internalization and localization of estradiol-BODIPY conjugates (EE2-C8 and 11β-OMe) in MDA-MB-231 triple negative breast cancer cell line. Cells were stained with Hoechst 33258 (nucleus marker) and LAMP-2 (lysosome marker). Cells were visualized on inverted microscope and (A) images of Hoechst channel were acquired with UV excitation (blue), LAMP-2 channel with green excitation (red) and conjugate channel with blue excitation (green). The presented fluorescence images were treated using Image J software.

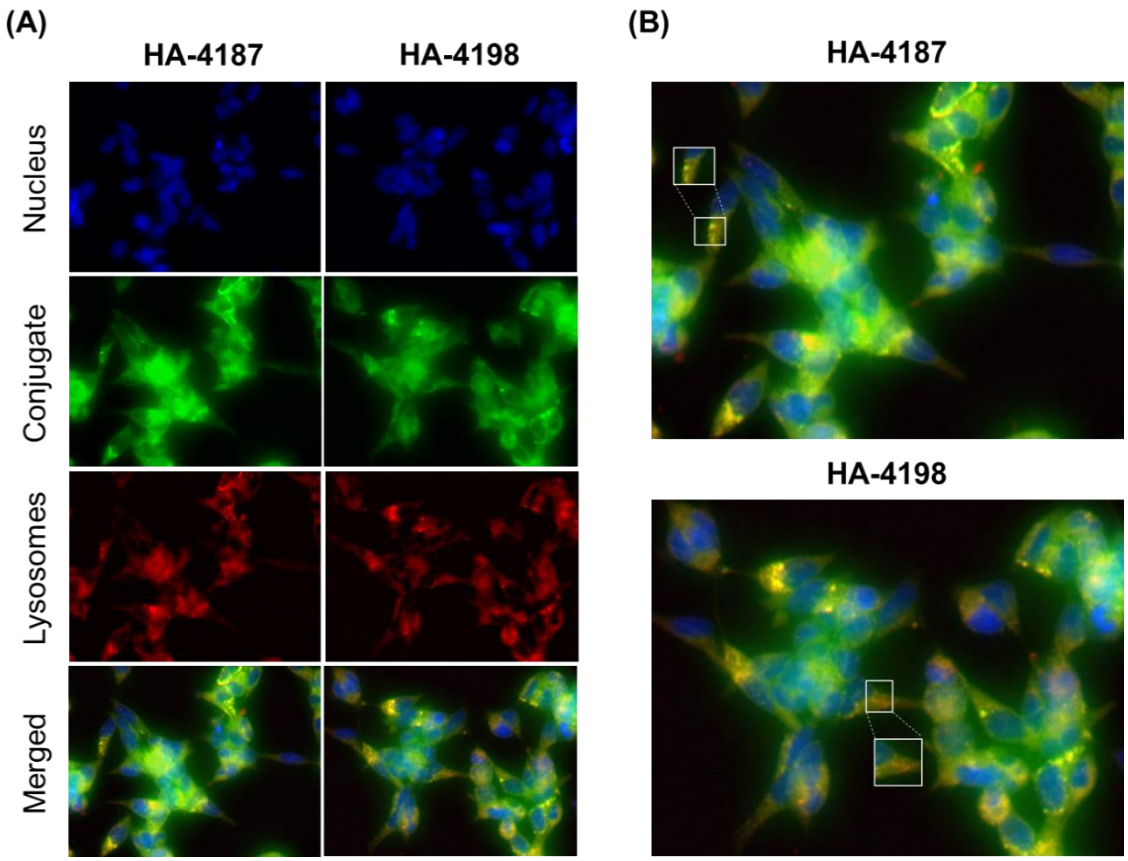

Figure 6.9 - Internalization and localization of androgen-BODIPY conjugates (HA-4198 and HA-4187) in LNCaP prostate cancer cell line. Cells were stained with Hoechst 33258 (nucleus marker) and LAMP-2 (lysosome marker). Cells were visualized on inverted microscope and (A) images of Hoechst channel were acquired with UV excitation (blue), LAMP-2 channel with green excitation (red) and conjugate channel with blue excitation (green). The presented fluorescence images were treated using Image J software.

6.3. Annex C

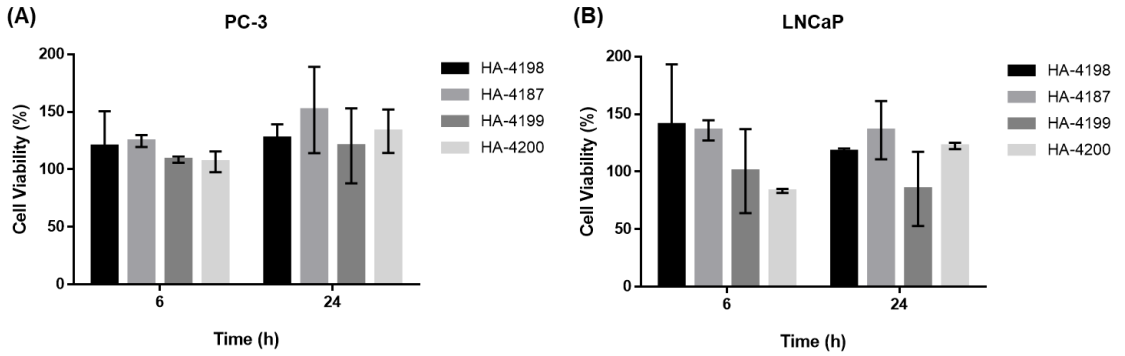

Figure 6.10 - Cell viability of androgen-BODIPY conjugates determined by means of the MTS assay. Prostate cancer cell lines (A) PC-3 and (B) LNCaP were incubated with 50μM of HA-4198, HA-4187, HA-4199 or HA-4200 for 6h and 24h. Data normalized against the control (0.5% (v/v) DMSO) and expressed as the mean ± SEM of two independent assays.

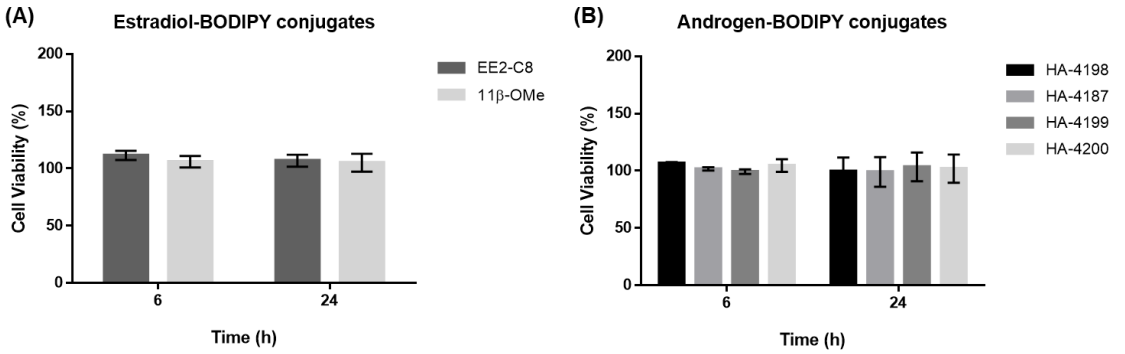

Figure 6.11 - **Cell viability of steroid-BODIPY conjugates determined by means of the MTS assay.** Human normal fibroblasts were incubated with 50μM of (A) estradiol-BODIPY conjugates or (B) androgen-BODIPY conjugates for 6h and 24h. Data normalized against the control (0.5% (v/v) DMSO) and expressed as the mean ± SEM of two independent assays.

6.4. Annex D

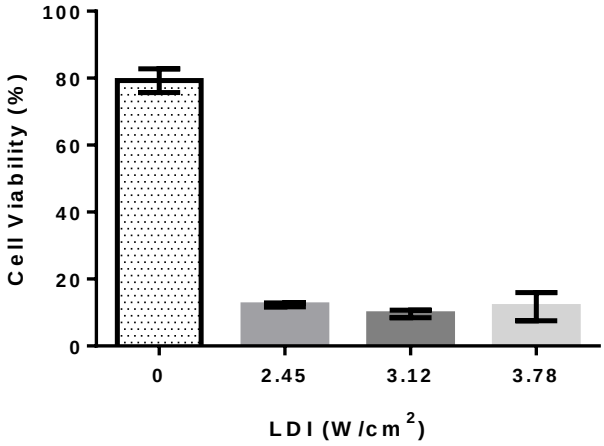

Figure 6.12 - Prostate cancer cell death following PDT induced by visible light and 50 µM of HA-4187 androgen-BODIPY conjugate as photosensitizer. Cell viability via MTS assay in PC-3 cell line 24 h after visible irradiation with three different LDI (2.45, 3.12 and 3.78 W/cm^2) during 60 seconds. Data normalized against the control (0.5% (v/v) DMSO) and expressed as the mean ± SEM of two independent assays in triplicate

6.5. Annex E

Publication

PROGRESS REPORT

ADVANCED THERAPEUTICS
www.advtherap.com

Light Irradiation of Gold Nanoparticles Toward Advanced Cancer Therapeutics

*Ana Amendoeira, Lorenzo Rivas Garcia, Alexandra R. Fernandes, and Pedro V. Baptista**

Cancer is one of the leading causes of death in the world. To challenge this epidemic, there are growing demands for the development of new advanced and targeted therapeutics capable of effectively tackling cancer cells with improved selectivity. Nanomedicine has put forward several innovative therapeutics toward improving therapeutic efficacy while decreasing the deleterious side effects of current chemotherapy. Multifunctional gold nanoparticles (AuNPs) have been at the core of a plethora of advanced therapeutic strategies that provide selective targeting with their unique optical properties, capable to interact with the light of specific wavelength to deliver therapy with tremendous spatiotemporal precision. AuNPs have been exploited as photodynamic and photothermal therapeutic agents alone or in combination with other cancer treatment modalities with other cancer applications. Due to their exceptional physicochemical properties, they have been proven efficacious allies for photodynamic therapy and for photothermal therapy regimens. Herein, the rapidly progressing literature related to the use of these promising strategies against cancer is discussed, highlighting their possible future clinical translation.

1. Introduction

Cancer is a major public health problem worldwide and the second leading cause of mortality. According to the World Health Organization, cancer is responsible for an estimated 9.6 million deaths in 2018. Strikingly, about one in six deaths worldwide is thought to be due to cancer.[1] The increasing knowledge into the molecular and cellular events that lead to cancer have allowed the development of new strategies to tackle this disease.[2] Still, at the forefront of cancer treatment are the most common and conventional therapies—surgery for the removal of tumor tissue followed by chemo and radiotherapy, either alone and/or in combination, which is mostly dependent on the type and stage of cancer. There is no unanimous approach to tackle all types of cancer, let alone therapy strategies not showing 100% effectiveness for every patient. Not only is cancer a complex set of diseases congregated together, but the disease is extremely heterogeneous in presentation and development, resulting from the intricate interplay between molecular and cellular events involved in tumorigenesis, the surrounding environment that allows growth, development and spreading, which is then modulated differently by the immune system according to each individual's profile.[3,4] Conventional cancer therapies have shown some limitations due to the lack of selectivity toward the malignant cells that lead to a series of deleterious side effects. Also, these more conventional therapies are incapable of total tumor eradication, causing variable clinical evolution and tumor response to treatment. These conventional strategies can also originate a powerful selective pressure leading to increased resistance to treatment.[5–7] The standard approach relies on the surgical removal of the tumor, which is efficient for primary tumors. However, incomplete resection may leave (pre-)malignant cells at the tumor site, which then are prone to cancer recurrence.[8] Chemotherapy uses chemical drugs to eradicate proliferating cancer cells, whose limited effectiveness, severe toxic side effects, and the possibility of drug resistance have stimulated the development of new compounds.[9–11] Chemotherapy is usually used in combination with surgery, radiotherapy, or immunotherapy.[7] Radiotherapy uses ionizing radiation of high energy (X-rays, gamma rays, or electrons) to kill cancer cells. This therapy generally is a complementary method of surgery or chemotherapy to improve the eradication of cancer cells.[12,13]

The understanding of the drawbacks of these standard therapeutic solutions has led to new strategies, from combinatory therapies relying on standard drugs to radial innovative approaches that make use of new technologies.[14] Among these new therapies, which could clinically be advantageous, nanomedicine has prompted innovative approaches that include selective and specific delivery of agents to the tumor, the possibility of utilizing new structures to combine several therapeutic modules, such as photothermal capability and photodynamic therapy, alone or in combination. Indeed, nanomedicine may offer numerous exciting possibilities for the development of new methods for diagnostics, and cancer treatment and improve the efficacy of available therapeutics.[5,7,8,15,16]

A. Amendoeira, Dr. L. R. García, Prof. A. R. Fernandes, Prof. P. V. Baptista
UCIBIO
DCV
Faculdade de Ciências e Tecnologia
Universidade NOVA de Lisboa
Campus de Caparica, 2829-516 Caparica, Portugal
E-mail: pmvb@fct.unl.pt

The ORCID identification number(s) for the author(s) of this article can be found under https://doi.org/10.1002/adtp.201900153

DOI: 10.1002/adtp.201900153